NASA CR-170504

GE-BO-78-034
15 July 1978

1878-1978

MSS STANDARD INTERFACE DOCUMENT

Contract NAS5-24167

(NASA-CR-170504) MSS STANDARD INTERFACE DOCUMENT (General Electric Co.) 120 p

N83-74202

Unclas
00/15 09826

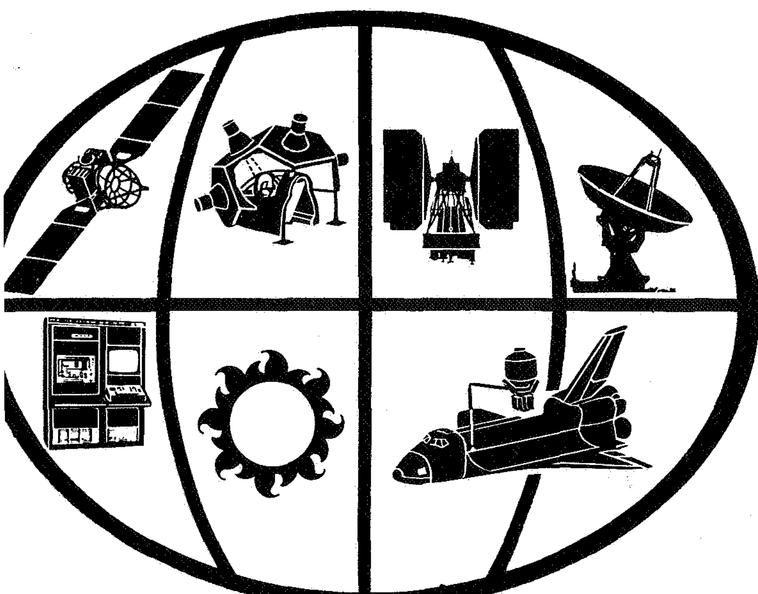

Prepared for
GODDARD SPACE FLIGHT CENTER
Greenbelt, MD

space division

Prepared by
General Electric Company
Space Division
Beltsville, MD

GENERAL ELECTRIC

GE-BO-78-034
15 July 1978

MSS STANDARD INTERFACE DOCUMENT

Contract NAS5-24167

Prepared for
GODDARD SPACE FLIGHT CENTER
Greenbelt, MD

Prepared by
General Electric Company
Space Division
Beltsville, MD

TABLE OF CONTENTS

TABLE OF CONTENTS (Cont)

TABLE OF CONTENTS (Cont)

LIST OF ILLUSTRATIONS

LIST OF TABLES

SECTION 1
LANDSAT SPACECRAFT

SECTION 1
LANDSAT SPACECRAFT

The Landsat observatories are earth-pointing stabilized spacecraft consisting of integrated subsystems that provide the power, environment, data recording, data transmission and information flow required to support the payloads. The Landsat 3 spacecraft is shown in Figure 1-1 which annotates the major subsystems.

Three payloads are carried. The RBV (return-beam vidicon) camera system, the MSS (multispectral scanner), and the DCS (data collection system).

On Landsats 1 and 2, a three-camera RBV system is used. The three cameras each image the same area simultaneously in a different spectral range. The Landsat 3 RBV consists of two panchromatic cameras which produce side-by-side images of approximately 98 Km square.

The MSS is a line scanning device that uses an oscillating mirror to continuously scan perpendicular to the spacecraft velocity. Six lines (six detectors) are scanned simultaneously in each of four spectral bands for each mirror sweep. In addition, two lines (two detectors) are scanned in a fifth band on Landsat 3. Spacecraft motion provides the along-track progression of the scan lines. Radiation from the ground scene is rapidly interrogated serially from the detectors and either transmitted directly to ground stations (the usual case) or recorded on on-board recorders for subsequent playback.

The DCS (data collection system) obtains data from remote, automatic data collection platforms and can relay the data to ground stations whenever a Landsat spacecraft can simultaneously view any platform and any ground station.

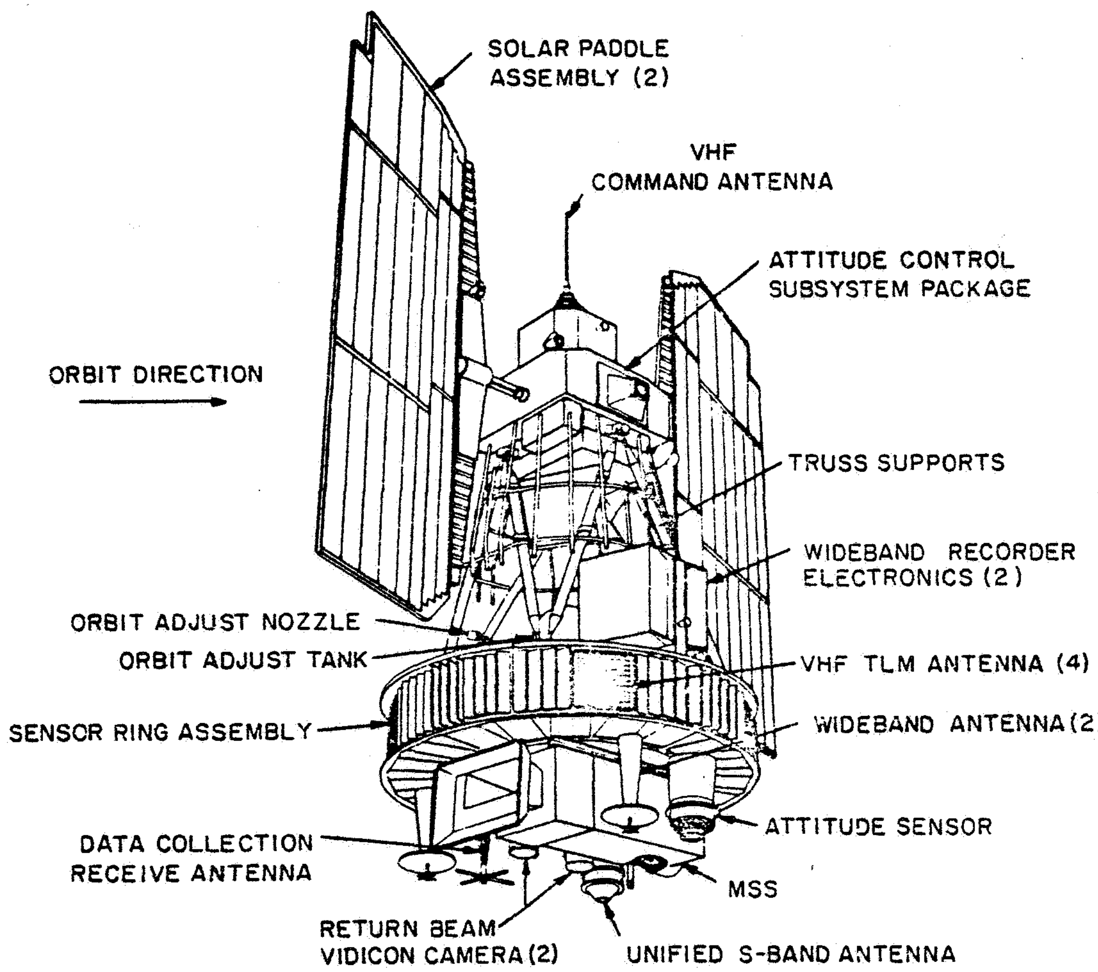

Figure 1-1. Landsat 3 Spacecraft

The spacecraft orbit is nearly polar (inclination $\sim$ 99.0°), circular at 920 Km and sun synchronous. Daytime passes over the U.S. occur in the morning and each Landsat orbit repeats itself every 18 days. By staggering the orbits of Landsat 2 and 3, repeat coverage is available every nine days.

Landsat 1 was launched on 23 July 1972 and data acquisition terminated on 7 January 1978. Landsat 2 was launched on 22 January 1975 and Landsat 3 on 5 March 1978.

SECTION 2
MULTISPECTRAL SCANNER DESCRIPTION

SECTION 2

MULTISPECTRAL SCANNER DESCRIPTION

An internal view of the five-band scanner is illustrated in Figure 2-1. The scanner consists of two major assemblies - the main housing and the radiometer assemblies. The sun calibrate mirror, sun shade, scan monitor, scan mirror, and the electronic housing comprise the major elements of the main housing assembly. The telescope, rotating shutter, fiber optics, PMT and photodiode sensors and preamplifiers, and calibration lamps and lamp drivers are the major assemblies comprising the radiometer assembly. Additionally, on the five-band scanner are two radiation cooled mercury-cadmium-telluride detectors and an optical relay to transfer the fifth band energy from the imaging plane of the primary telescope to these detectors. In flight, the radiation cooler door, which is shown in the closed position would be open, allowing the radiative transfer of thermal energy to space and also functioning as an earth radiation shield. The MSS block diagram, Figure 2-2, presents an overview of the scanner.

Tables 2-1 and 2-2 list the main parameters of the scanner and multiplexer.

2.1 SPECTRAL RESPONSE

The MSS responds to radiant energy, reflected and emitted, from the earth terrain near the spacecraft nadir. This energy is detected in five spectral bands (four for Landsats 1 and 2).

For the Landsats 1 and 2 missions, the four-band scanner detects radiant energy in the solar reflected spectral region from 0.5 to 1.1 microns. Landsat 3 contains the same four bands but in addition has a fifth band that detects radiant

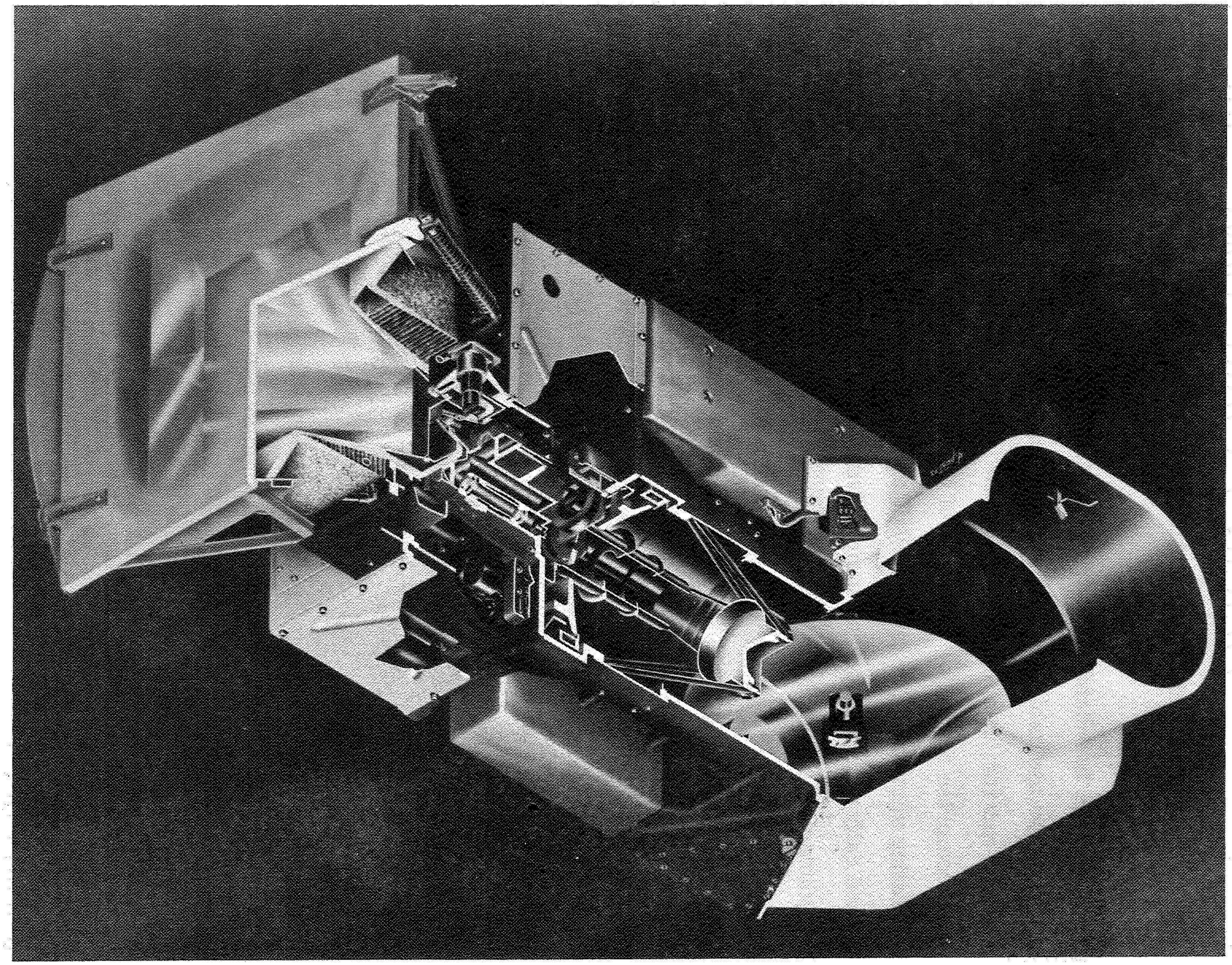

Figure 2-1. Five-Band MSS

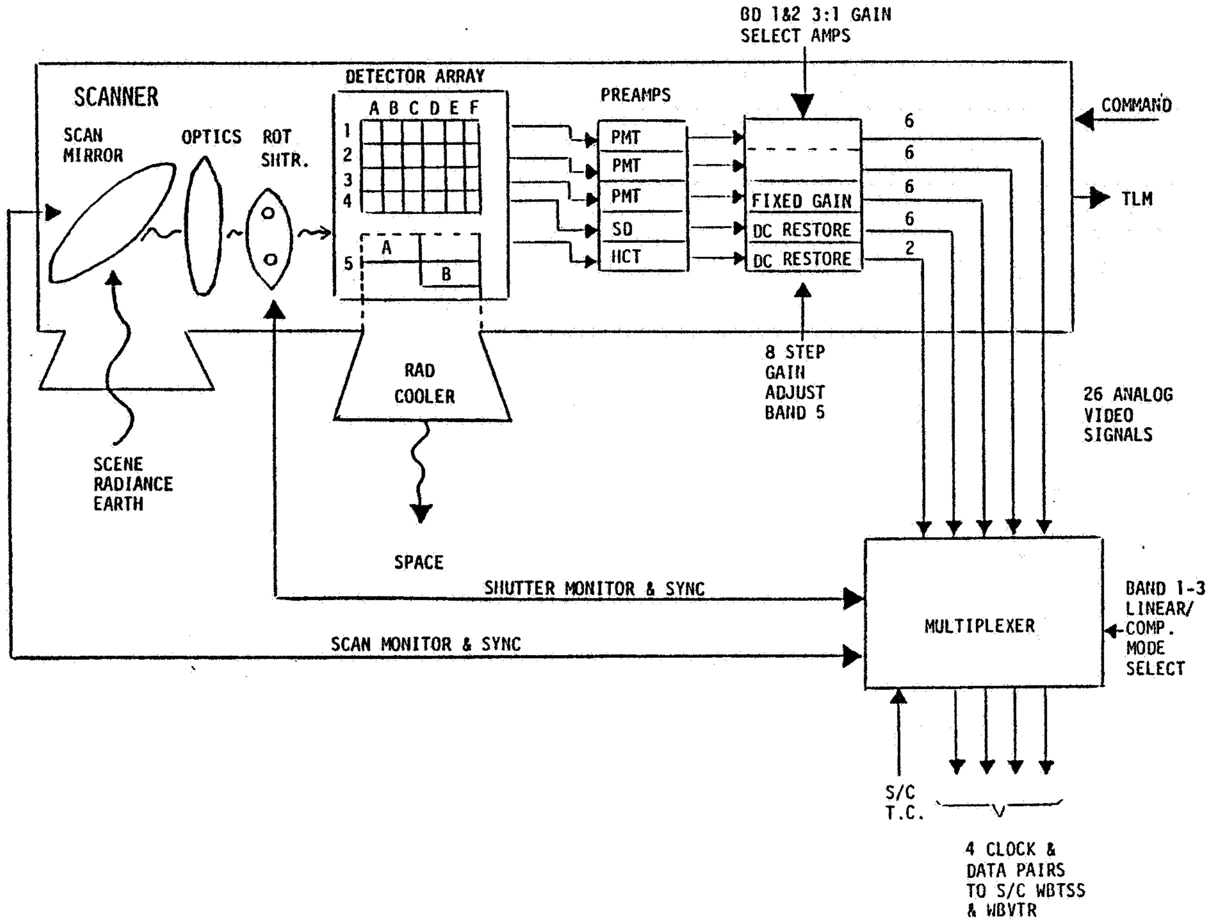

Figure 2-2. MSS Block Diagram

emitted (thermal) energy in the spectral region from 10.4 to 12.6 microns. The relative spectral response curves of each detector in bands 4 through 7 for Landsats 1, 2 and 3 are given in Appendices A, B and C.

2.2 OPTICS

The optics system of the scanner consists primarily of a scan mirror, a telescope, a rotating shutter, an array of 24 optical fibers and the band 8 relay optics. An optical schematic showing both the primary and band 8 optics is shown in Figure 2-3. Not shown in this schematic is the fiber optics array whose input face lies

Table 2-1. Scanner Characteristics

Item	Characteristics
OPTICAL	
Telescope Optics	9-inch Ritchey-Chretien type with 3. 5-inch secondary mirror, f/3. 6
Focal Length	32. 5 inches (0. 8255 meters)
Mirror Reflectivity	95 percent minimum
Scanning Method	Flat mirror oscillating ±3. 25 degrees at 13. 62 Hz ±0. 01 percent
Scan (Swath) Width at 496 nmi (919 km) Altitude	100 nautical miles (185 kilometers)
Scan Duty Cycle	31. 5 to 34. 0 milliseconds of 73. 42 milli-seconds cycle (2. 9 degree active scan)
Field of View (FOV)	11. 5 degrees
Instantaneous Field of View (IFOV)	0. 086 milliradian (259 feet or 79 meters scene) Bands 1-4 and 0. 26 milliradians (778 feet or 237 meters scene) Band 5
Number of Lines Scanned per Band	Six, Bands 1-4 Two, Band 5
Line Length variation	±36 feet (10. 9 meters) maximum
Optical Centerline Variation	±1 percent of swath width
Limiting Resolution from 496 nmi (919 km) Altitude	119. 1 feet (36. 3 meters) Bands 1-4 540 feet (165 meters) Band 5
Sampling Distance	183. 3 feet (55. 9 meters)
Optical Fiber Core	2. 791 milli-inches (0. 071 micrometers square

Table 2-1. Scanner Characteristics (Cont'd)

Item	Characteristics			
OPTICAL (cont'd)				
Spectral Band Wavelength:				
Band 1	0. 5 to 0. 6 micrometers			
Band 2	0. 6 to 0. 7 micrometers			
Band 3	0. 7 to 0. 8 micrometers			
Band 4	0. 8 to 1. 1 micrometers			
Band 5	10. 4 to 12. 6 micrometers			
Modulation Transfer Function	0. 29 minimum at spatial frequency corresponding to 225 foot bars, Bands 1-4 and 780 foot bars, Band 5			
Sensor Response:	Band 1	Band 2	Band 3	Band 4
Sensor	PMT	PMT	PMT	Photo-diode
High Light Level (10^{-4} w cm^{-2} $ster^{-1}$)	24. 8	20. 0	17. 6	46. 0
Signal to Noise Ratio	80	62	40	89
Low Light Level (10^{-4} w cm^{-2} $ster^{-1}$)	2. 5	2. 2	1. 8	4. 6
Signal to Noise Ratio	25	19	12	8
	Band 5			
Max NeΔt	1. 4°K at 300°K scene (Scanner) 1. 5°K at 300°K scene (System)			
Scene Temp. Range	260°K to 340°K			

Table 2-1. Scanner Characteristics (Cont'd)

Item	Characteristics
ELECTRICAL	
Input Voltages	-24.5 volts (+0.7 volt - 0.5 volt) regulated and -26 to -39 volts unregulated provided by spacecraft
Current:	
Regulated: SYSTEM	1.8 amp average
OUTGAS	1.1 amp
Unregulated: (Scan mirror)	0.5 amp average
Power: SYSTEM	59 watts average
OUTGAS	27 watts (70% duty cycle)
Video Data Signal:	
Number of Channels	26
Signal Range	0.00 to +4.00 volts
Scanner Source Impedance	100 ohms maximum
Overload Level	+6.4 volts, -0.7 volt
Overload Limit (applied to one output at a time)	±28 volts for 30 seconds; ±15 volts continuously
Bandwidth	DC to 42.3 ±2.5 KHz (-3 db) Bands 1-4 DC to 14.1 ±2.5 KHz (-3 kb) Bands 5
Scan Monitor Signal:	
Number per Scan	3
Amplitude (0 to peak)	1 volt minimum
Pulse Width (at 0.5 v)	2 μsec minimum
Scanner Source Impedance	50 ohms

Table 2-1. Scanner Characteristics (Cont'd)

Item	Characteristics
ELECTRICAL (cont'd)	
Rotating Shutter Sync Signal:	
Type	Complementary current source
Current Waveform	73.42 msec period; 2 μsec minimum; 2.4 to 5.4 ma pulses
Scan Mirror Drive:	
Waveform	73.42 msec ±0.01 percent period square-wave; ±11 volts amplitude
Scanner Load Impedance	50 K ohms minimum
Telemetry Excitation Voltage	-24.5 ± 0.5 volts
Telemetry Outputs:	
Analog -	
Range	0 to -6.375 volts
Output Impedance	10 K ohms maximum to maintain telemetry accuracy
Load Impedance	1 megohm sampling, 10 megohms non-sampling
Resolution	25 mvolts
Digital (single bit words) -	
Off condition	-0.5 ± 0.5 volt
On condition	-7.5 ± 2.5 volts
Output Impedance On	1 megohm maximum
Output Impedance Off	50 K ohms maximum

Table 2-1. Scanner Characteristics (Cont'd)

Item	Characteristics
ELECTRICAL (cont'd)	
Command Signal Inputs:	
Amplitude	-23.5 ±1.0 volts
Current	200 ma maximum
Pulse Width	40 ±5 msec
Impedance	30 ±5 ohms
Command Matrix A Output:	
De-energized State -	
Amplitude	-1.0 ±1 volt
Impedance	30 K ohms
Energized State -	
Amplitude	-23.5 ±1 volts
Impedance	30 ±5 ohms
Command Matrix B Output:	
De-enrgized State -	
Amplitude	-22.0 ±1 volts
Impedance	30 K ohms
Energized State -	
Amplitude	-1.0 ±1.0 volts
Impedance	30 ±5 ohms

Table 2-1. Scanner Characteristics (Cont'd)

Item	Characteristics
PHYSICAL	
Height (Spacecraft Z Axis)	23.38 inches, maximum
Width (Spacecraft Y Axis)	49.75 inches, maximum
Depth (Spacecraft X Axis)	21.25 inches, maximum
Weight	138.0 pounds, maximum

Table 2-2. MUX Characteristics

Item	Characteristics
ELECTRICAL	
Input Voltages	-24.5 volts, -0.7 volt, +0.5 volt regulated
Power	19.2 watts
Quantization	6 bits
Processing Modes	Linear and signal compression
Clock Stability	$\pm 1 \times 10^{-4}$/year
Initiation of Sampling	Scan monitor beginning of line pulse or interval timing
Number of Samples/Scan	3,314
Output Bit Rate	15 M bits per second ±0.5 percent
Sampling Rate	100.4175 kilo samples/second
Crosstalk	40 dB rejection
Video Data Input Signal:	
Number of Channels	24
Signal Range	0.00 to +4.00 volts

Table 2-2. MUX Characteristics (Cont'd)

Item	Characteristics
ELECTRICAL (cont'd)	
Overload Level	+4.1 volts -0.3 volts
Overload Limit, applied to no more than one input at a time	±28 volts for 30 sec maximum ±15 volts continuous
Scanner Source Impedance	100 ohms maximum
MUX Load Impedance	10 K ohms minimum in parallel with 100 pf maximum
Data Output Signal:	
Type	Complementary current source
Format	NRZ-L
Rate	15.06 Mbs
Bit Rate Clock Output Signal:	
Type	Complementary current source
Rate	15.06 Mbs
Spacecraft Clock Data Signal Input:	
Type	Complementary current source
Format	NRZ-L
Rate	2.51 Mbs
Scan Mirror Drive	Same as for scanner; see Table 2-1
Rotating Shutter Sync Signal	Same as for scanner; see Table 2-1
Scan Monitor Signal	Same as for scanner; see Table 2-1
Scan Monitor Detection Level	0.5 ±0.1 volt
Telemetry and Commands	Same as for scanner; see Table 2-1

Table 2-2. MUX Characteristics (Cont'd)

Item	Characteristics
PHYSICAL	
Height (Spacecraft Z axis)	6.810 inches, maximum
Width (Spacecraft Y axis)	9.092 inches, maximum
Depth (Spacecraft X axis)	4.004 inches, maximum
Weight	7.5 pounds, maximum

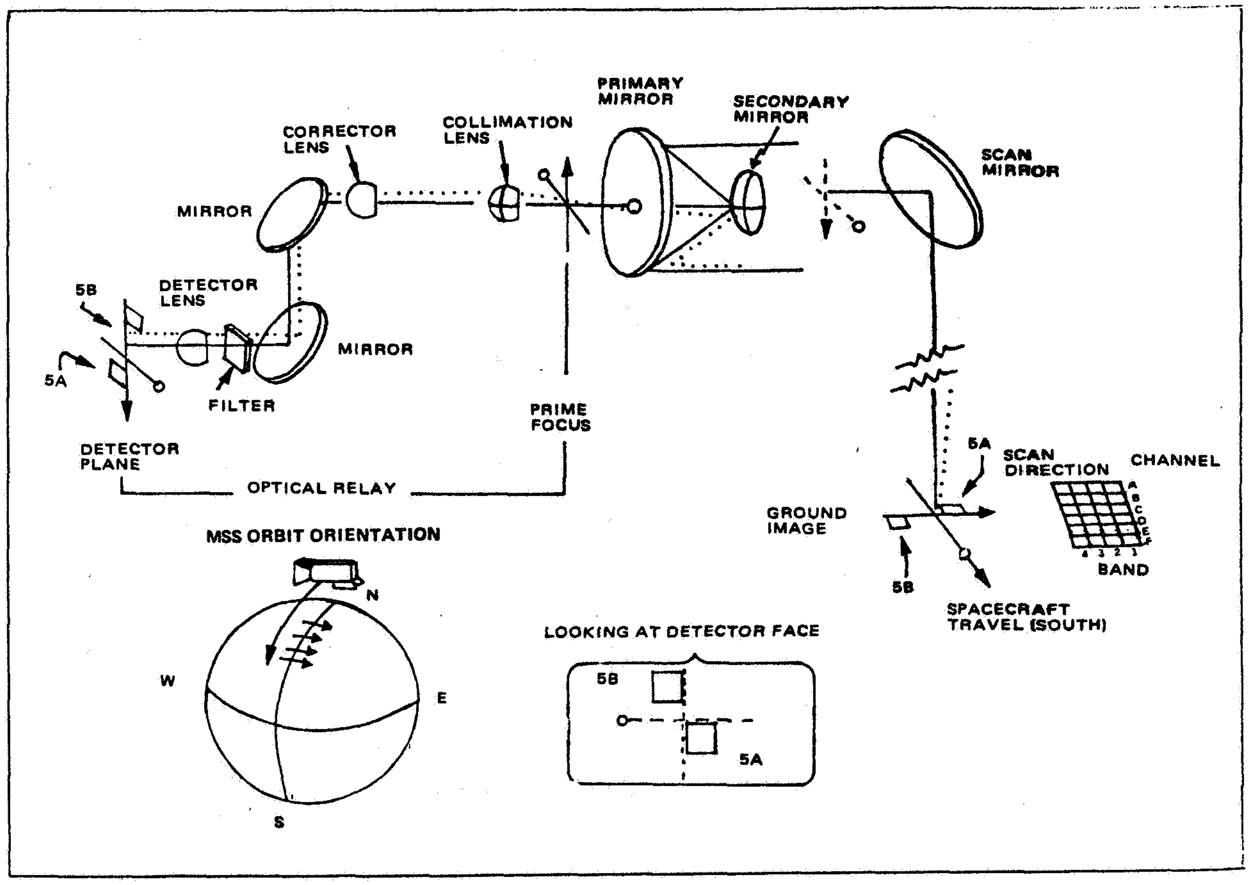

Figure 2-3. Primary and Relay Optics

in the primary focal plane, and the rotating shutter which is positioned between the fiber optics and the telescope.

Fiber optics are used for bands 4 through 7 to transmit the image spot intensities to the appropriate detectors. Twenty-four square fibers are arranged in the telescopes focal plane (see Figure 4-3 for the configuration) and carry the radiant energy to the 24 detectors.

Thermal infrared energy from the scene, is reflected from the scanning mirror, focused by the telescope, passes through a slot in the shutter wheel, continues through the relay optics and is refocused on the two band 8 detectors. The band 8 relay optics schematic is shown in Figure 2-4.

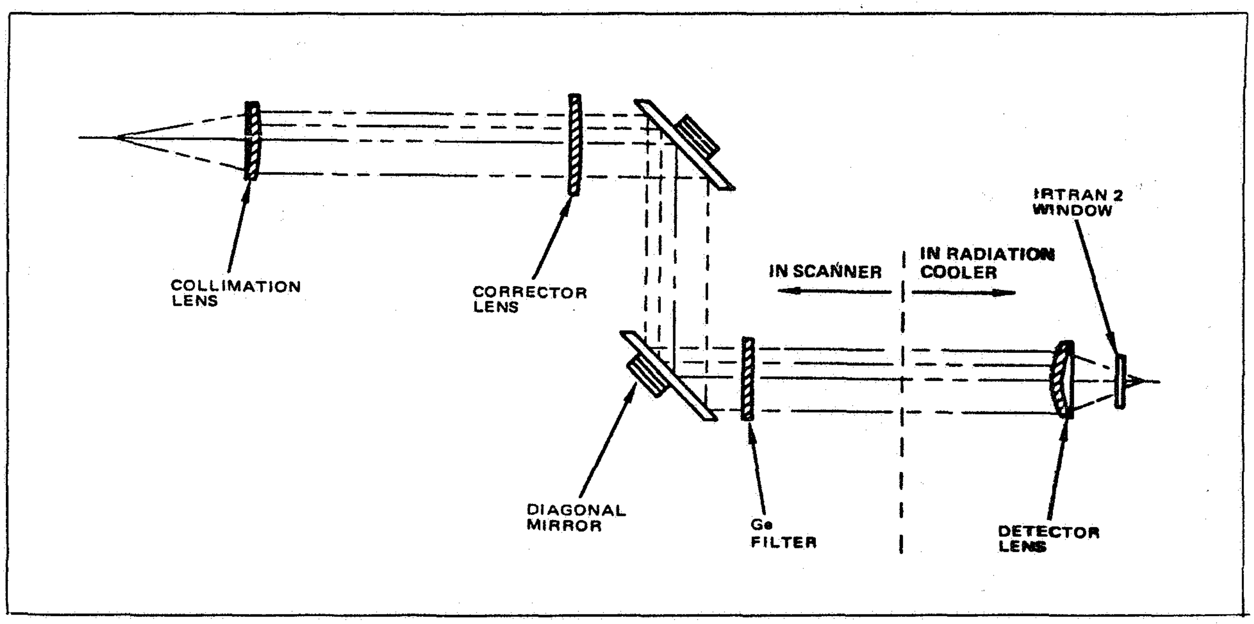

Figure 2-4. Band 8 Relay Optics Schematic

2.3 SCANNING MIRROR MOTION

The MSS scene is formed by two motions - the spacecraft velocity and the much faster crosstrack motion of the scan mirror. The ground scan pattern is shown in Figure 2-5. Successive mirror sweeps of six detectors per sweep per band are contiguously formed with one another due to the advancement in ground scene by the spacecraft forward motion.

The scan mirror, which images the scene through its movement, need only scan half the angle $\sim \pm 2.90$ of the full instantaneous field of view $\sim 11.6^{o}$, because of the angle doubling effect that occurs at reflection.

The scan mirror is suspended on its outer edges by two flexure pivots. Two impacting spring/damper mechanisms, located behind the mirror on opposite sides of the pivot axis, automatically reverse scan trace and retrace motion of the mirror upon impact. During the scan trace, the mirror motion is a free drifting motion at a virtually constant angular rate, except for the small sinusoidal component imposed by the flexure pivot and system losses. Retrace motion is accelerated by the drive coil to the velocity required to overcome losses and assure that the mirror velocity after the end-of-retrace impact occurs, will be the same as the previous scan velocity.

The scan mirror is synchronized by the torquing pulses. The synchronizing frequency is derived from the crystal clock operating at 15.0626 MHz and counted down to 13.62 Hz. This also synchronizes the mirror with the scanner shutter and other multiplexer functions.

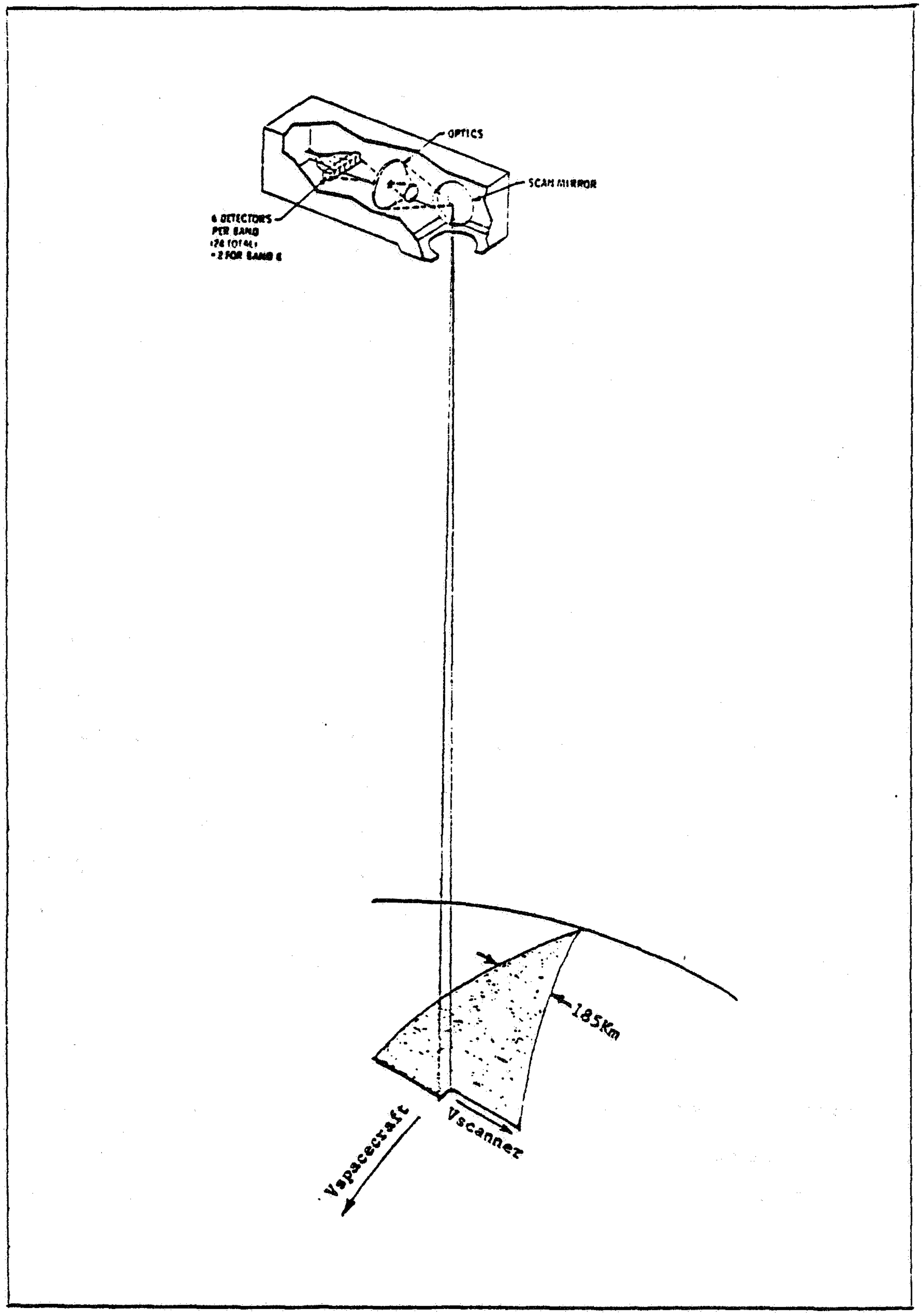

Figure 2-5. MSS Ground Scan

2.4 MULTIPLEXER

The multiplexer is a high speed PCM (pulse code modulated) encoder. The analog multiplexer function samples and commutates each video channel input from the scanner once every 10 microseconds and multiplexes the analog samples into a PAM (pulse amplitude modulated) serial data stream. The A/D (analog to digital) function then converts each analog data sample into a six-bit digital word. The channel sampling rate of the multiplexer is 25 channels every 10 microseconds resulting in a sampling rate of 2.5 million samples per second.

2.5 DATA FORMAT

The multiplexer major frame format is shown in Figure 2-6. A major frame consists of one complete scan/retrace cycle of the scan mirror which is driven by the multiplexer at its frequency of 13.62 Hz. Data is tagged throughout the sweep by the use of minor frame sync code (MFSC) and its complement ($\overline{\text{MFSC}}$).

2.6 CALIBRATION

2.6.1 BANDS 4 THROUGH 7 CALIBRATION

The shutter wheel is slotted so that the earth image projected through the telescope during the trace portion of each scan cycle reaches the fiber optics array. During retrace, the shutter blocks the earth image. During alternate scan retrace intervals (once each shutter revolution) the shutter performs the bands 4 through 7 calibration function. The light from the calibration lamp is attenuated from bright to dark as a continuously variable (white to black) wedge - shaped neutral density filter is moved past the fiber optics. This results in a wedge-shaped output waveform (calibration wedge) from each PMT and photodiode. The wedges appear every other scan line, as shown in Figure 2-6, in series with the earth image video data. The calibration wedge represents the PMT or photodiode response to the known characteristics of the calibration lamp.

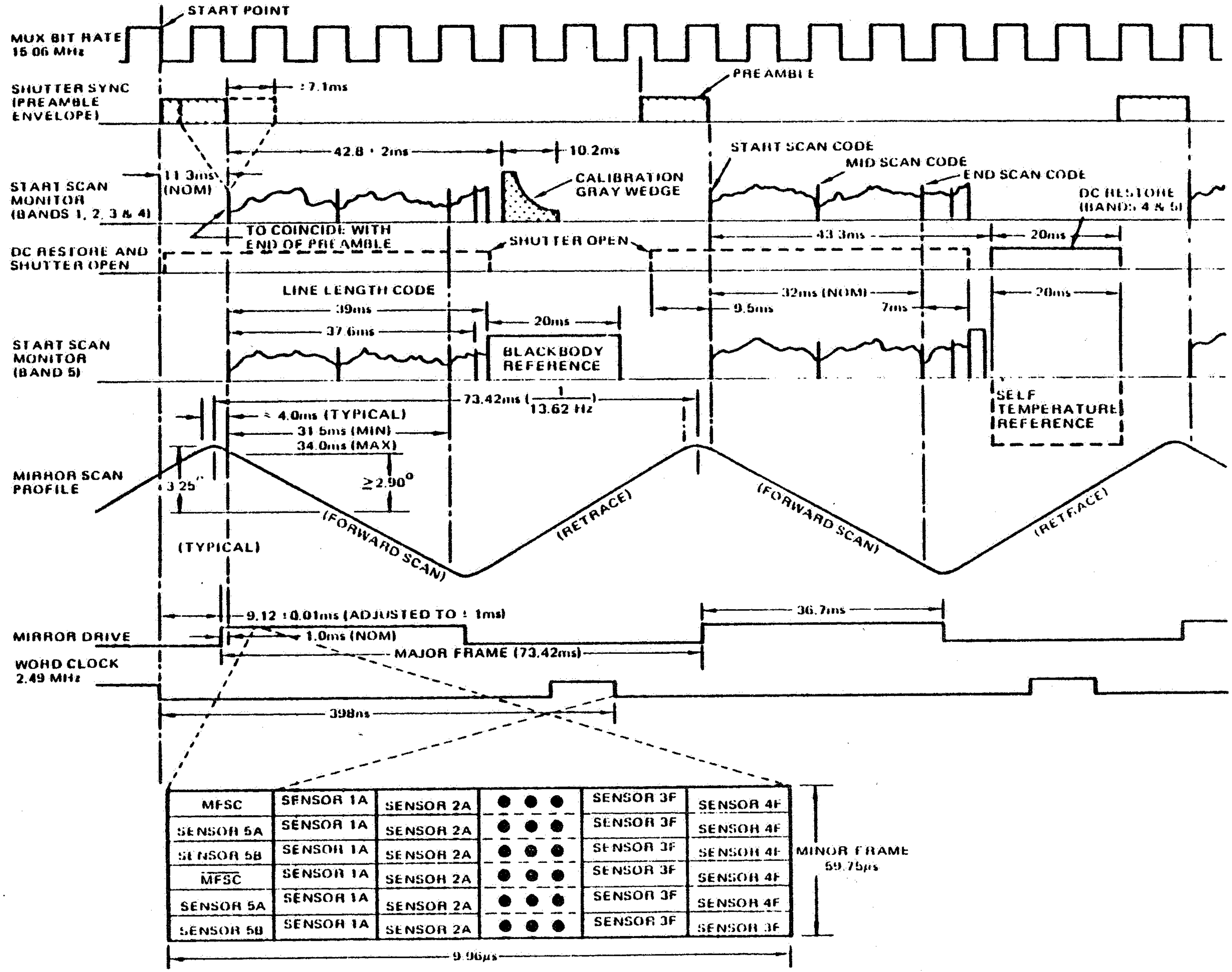

Figure 2-6. System Timing Format

2.6.2 BAND 8 CALIBRATION

Power from the scene being scanned enters through the telescope, passes through the relay optics, and is refocused on the detector, arriving there as a hollow cone of radiation, the central portion being obscured by the telescope secondary mirror. The range of scene radiant power to be observed by the scanner is that corresponding to a temperature range of 260°K to 340°K (+8°F to +152°F). Between scans, the rotating shutter cuts off the telescope path and interposes one of two reference devices, each on alternate between-scan periods as shown in Figure 2-6. One of these is a grooved and blackened surface on the shutter (occurs on the same sweep as the calibration wedge of bands 4 through 7), which approximates a blackbody radiator at shutter temperature. The other is a mirror which causes the detector to view itself; i.e., its own cooled region of very low radiant power. These two reference devices are called the internal blackbody reference and cold reference respectively. While the mirror is in position, the mirror and relay optics will provide a small amount of ambient temperature radiant power, which constitutes the actual cold reference level, since the cooled detector region emits negligible power in comparison. The cold reference level is less than the coldest scene level.

2.6.3 SUN CALIBRATION

Once in each orbit, the scanner is so positioned that the sun calibrate mirror reflects a sample of sunlight into the scanner optics system. During the scan trace interval, the sunlight sample is deflected across the fiber optics array. The sun calibrate mirror is a four-faceted mirror having angles so selected that the sunlight sampling occurs just before the spacecraft crosses the northern terminator (18 degrees before the terminator). At this time, competing light from the earth scene is negligible. The sunlight sampling appears as a one or two millisecond pulse in the video data for each channel of bands 4 through 7, and serves as a primary standard by which changes in the calibration lamp function can be evaluated.

SECTION 3

PRE-LAUNCH TESTING

SECTION 3
PRE-LAUNCH TESTING

3.1 INTEGRATING SPHERE TEST

The primary standard for MSS radiometric calibration is the integrating sphere. Component and pre and post TV system tests were performed using this instrument at various intensities. Through the use of this sensor video data and the calibration wedge data, the response curves of each sensor (bands 4 through 7) is determined.

The integrating sphere does not have a flat spectral response. Therefore, it is spectrally calibrated against a known standard periodically. The results of the last calibration (August 1975) are presented in Appendix D.

3.2 AMBIENT AND THERMAL VACUUM TESTING

The secondary standard sources employed for Landsat C MSS calibration checks during spacecraft level testing consisted of two identical GFE collimators, one for ambient testing, the other for vacuum thermal testing. The collimators were residual units from the Landsat 1 and 2 four-band MSS programs modified to provide IR scene and reference blackbodies for band 8 stimulation. A hot wire target was also included for determination of relative alignment between the band 7 fiber optics and band 8 relay optics. The gain stability of each sensor channel was monitored utilizing the selectable neutral density filters and flat (open) target of the collimator for bands 4 through 7 and by varying the scene temperature from 260°K to 340°K for band 8. System modulation transfer functions were monitored utilizing the 225 foot-bar visible collimator pattern for bands 4 through 7 and the 780 foot-bar infrared pattern for band 8. Scan repeatability was determined from word count location of preselected collimator signal threshold crossings relative to scan line start with the collimator folding mirror set to produce the signal pulse near mid scan. The chevron pattern for the visible channels was utilized to monitor cross axis jitter. The collimator flooding lamp which produces a wide angular range of illumination but reduced level control was used to simulate approximate real scene conditions including effects of high illumination levels on photomultiplier response in bands 4 through 6.

The 24 visible sensors (bands 4 through 7) were tested under ambient and vacuum/thermal environments. The two infrared sensors (band 8) were tested only under the vacuum/thermal environment since the risk of cooler contamination at cryo levels under ambient conditions was considered too great at the spacecraft test level. A space background simulator (SBS) was used to provide radiative cooling of the band 8 detectors during vacuum/thermal testing.

3.3 SPECIAL TESTS

Special testing of the Landsat C MSS was performed where required to evaluate potential problem areas. A "view-of-the-world" test which comprised operating the MSS to view local landscapes was performed to establish the extent of multiplexer input level sensitivity under real scene conditions. A number of scan monitor pulse amplitude measurements were also performed to assure amplitude stability after a scan monitor assembly realignment was necessitated by a loss of mid scan code at low temperatures.

3.4 SIGNAL-TO-NOISE

The mean quantum level signal at 50 percent neutral density filter and the signal-to-noise ratio for bands 4 through 7 are summarized in Appendices E and F for linear low and compressed low modes of operation. The data are from the electrical systems test, three typical simulated orbits from the three spacecraft temperature plateaus during thermal and the pre and post vacuum thermal confidence tests.

The mean signal and NEΔT for band 8 sensors 25 and 26 during the initial detector cooldown and the second detector cooldown are presented in Appendix G for gain step four. The second outgas period and subsequent detector cooldown to less than 100^{O}K yielded a significant increase in channel gain (34%) indicating that a multi-cycle outgas period may be required to achieve satisfactory results.

3.5 SYSTEM MODULATION TRANSFER FUNCTION

3.5.1 MTF FOR GROUND EQUIVALENT 225-FOOT BAR TARGET

The MSS MTF (modulation transfer function) for a 225-foot bar target was measured during the electrical systems test using collimator 4 and in thermal vacuum using collimator 3. The values for bands 4 through 7 are presented in Appendix H and are within the specified value of 35%. The variation in the data between ambient and vacuum thermal is attributed to the difference in reticles and focusing of the two collimators employed.

3.5.2 MTF FOR GROUND EQUIVALENT 780-FOOT BAR TARGET

The MSS IR MTF for band 8 sensors 25 and 26 was calibrated from data accumulated during the thermal vacuum test. Appendix I shows the average of the IR MTF values measured in the MSS prime configuration for sensors 25 and 26 at each of the three spacecraft thermal plateaus. All of the measurements were obtained after the second outgas and detector cooldown cycle was completed and a second stage temperature of 94 to 95^{O}K. All values were greater than the 35% specified, and there was no temperature or system configuration dependence observed.

SECTION 4

PRE-LAUNCH CALIBRATION

SECTION 4

PRE-LAUNCH CALIBRATION

Radiometric calibration parameters are developed for the MSS prior to vehicle launch. These calibration parameters are derived from data generated during preflight radiometric testing. An integrating sphere is used for radiometric testing of the optical bands (4, 5, 6 and 7) and a full aperture infrared source (FAIRS) is used to test band 8 (thermal IR).

4.1 RADIOMETRIC CALIBRATION - OPTICAL BANDS

The optical bands (4, 5, 6 and 7) of the MSS are calibrated by using the MSS as a transfer device between the light integrating sphere and the internal radiance source. The known radiance values from the integrating sphere and their corresponding sensor output voltages are used to establish each sensor's linear transformation equation.

This paragraph describes the calibration process in a step-by-step summary form described below.

- Equivalent Radiance - The MSS is calibrated to an equivalent spectrally flat radiant emittance which must be determined independently for each sensor since the spectral response differs for each sensor within a band.

- Calibration Wedge Words - The calibration wedge words to be used during in-flight video data calibration are used throughout the pre-launch calibration process.

- Adjusted Video Levels - Adjusted video levels are developed to minimize the effects of detector instability during the time required to acquire the test data.

- Calibration Wedge Radiance Values - These values are used to derive the calibration coefficients.

- Calibration Coefficients - These coefficients are linear regression coefficients used to describe the MSS sensors during in-flight video data calibration.
- Sensor Transformation Equation - This equation is a first order polynomial which defines the radiant emittance versus output voltage for each sensor.
- Calibration Algorithm - This algorithm is used to map each of the six sensors within a band to a common straight line.

The subsequent paragraphs are expanded descriptions of each of the steps of the calibration process.

4.1.1 EQUIVALENT RADIANCE

The MSS is calibrated to a spectrally flat radiant emittance approximating the sun's emittance over the optical band. The light integrating sphere uses tungsten lamps which are not spectrally flat. (Reference Appendix D, Spectral Radiant Emittance of 30-inch Spherical Integrator.) The equivalent spectrally flat radiance of the light integrating sphere must, therefore, be determined. This must be determined independently for each sensor since the spectral response differs for each sensor within a band.

The equivalent spectrally flat radiance of the integrating sphere for any sensor may be determined from:

$$E_s = BW \frac{\int E_s(\lambda) R(\lambda) d\lambda}{\int R(\lambda) d\lambda}$$

Where: E_s = Equivalent spectrally flat radiance emittance ($mW/cm^2 \cdot sr$)

BW = Bandwidth of sensor

$E_c(\lambda)$ = Spectral radiance emittance of the integration sphere ($mW/cm^2 \cdot \mu \cdot sr$)

$R(\lambda)$ = Relative sensor spectral response (dimensionless)

The spectral response characteristics of each Landsats 2 and 3 MSS sensor is presented in Appendices Band C. These curves were used in the above equation to determine the equivalent spectrally flat radiance of the integrating sphere for each sensor (Appendices J and K).

4.1.2 CALIBRATION WEDGE WORDS

Six calibration samples are used for the calibration of an MSS sensor. The sampled calibration wedge word counts are the same for each of the six sensors within a band. Since significant differences exist between bands, a set of six sample word counts is chosen for each band.

The selection of the six calibration wedge words to be sampled is based on prelaunch test data and historical experience from previous spacecraft. The primary factors considered in the selection are listed below.

- Temperature Effects - Sensor gain and offset are a function of temperature.
- Aging Experience - Landsats 1 and 2 sensors have experienced long term drift effects, particularly noted for Landsat 1, sensor 13.
- Hysterisis - Sensor (PMTs) gain increases as a direct function of incident radiance. The time constant for this effect is approximately 15 seconds.
- Vacuum - Sensor gain and offset shift somewhat when the MSS is introduced to the vacuum conditions of space.

- <u>Quantization</u> - Samples are selected, as nearly as possible, in the center of a "flat region" of the quantized calibration wedge (Figure 4-1). Word counts are reference to the first sample on the leading edge greater than level 32 as indicated in Figure 4-1.

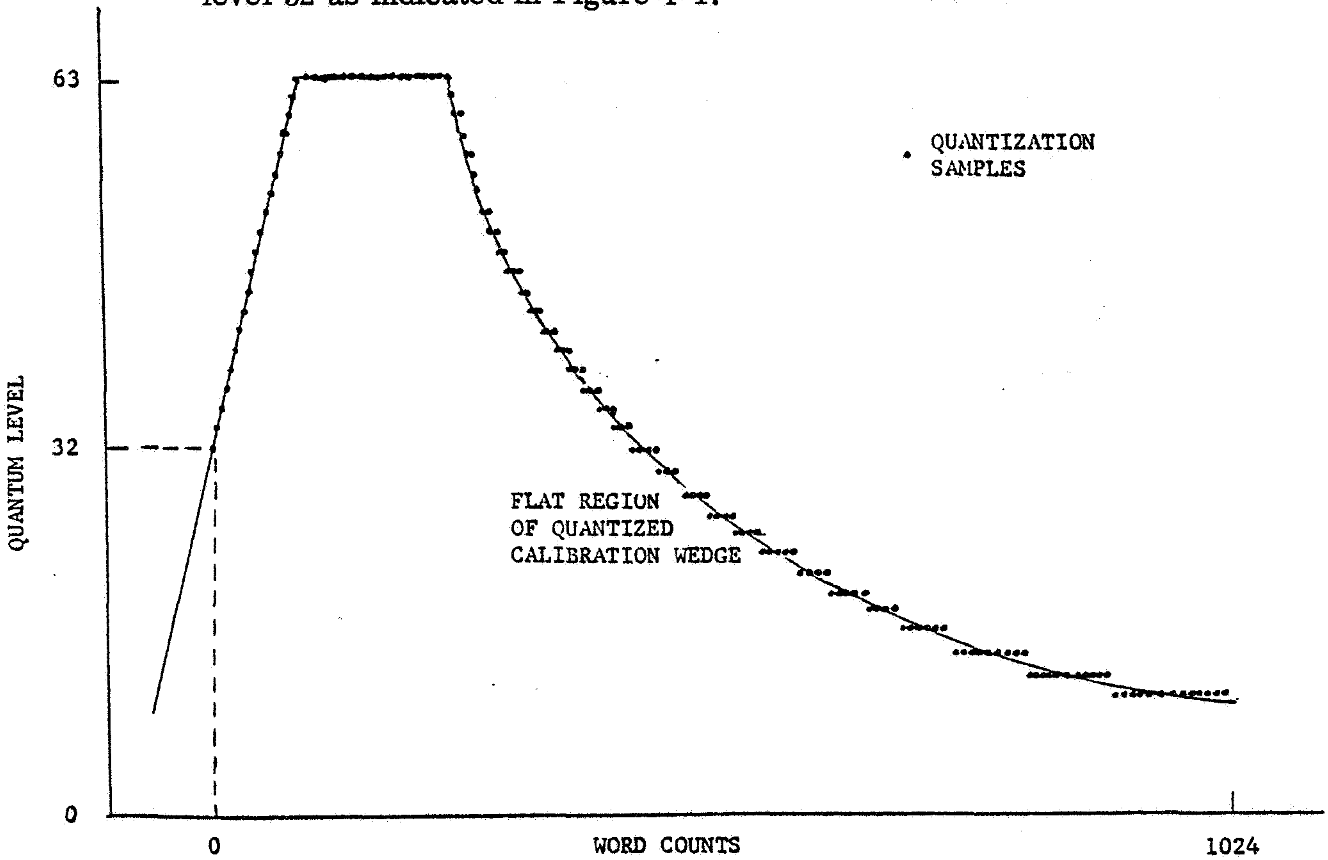

Figure 4-1. Calibration Wedge

All of the above effects, with the exception of aging, are predictable from pre-launch test data.

The six sampled calibration wedge words for bands 4, 5, 6 and 7 for low gain and for bands 4 and 5 for high gain are shown in Table 4-1.

4.1.3 ADJUSTED VIDEO LEVELS

The raw data acquired from light integrating sphere tests is not used directly for the calculation of radiometric calibration coefficients. It must first be adjusted

Table 4-1. Calibration Wedge Words

Landsat 1 (Low Gain)	1	2	3	4	5	6
Band 4	280	300	510*	550*	700*	800*
Band 5	380	410	610*	640*	740*	820*
Band 6	360	390	450	670	700	750
Band 7	250	270	300	500	530	560

*Also high gain

Landsat 2 (Low Gain)	1	2	3	4	5	6
Band 4	300	340	440	490	600	730
Band 5	460	490	580	630	730	870
Band 6	440	470	560	600	700	780
Band 7	250	270	300	340	400	500

Landsat 2 (High Gain)	1	2	3	4	5	6
Band 4	560	600	630	710	810	930
Band 5	700	730	770	820	860	950

Landsat 3 (Low Gain)	1	2	3	4	5	6
Band 4	260	270	280	290	730	740
Band 5	350	360	370	380	840	850
Band 6	330	340	350	360	840	850
Band 7	220	230	240	250	490	500

Landsat 3 (High Gain)	1	2	3	4	5	6
Band 4	460	470	480	490	750	760
Band 5	570	580	590	600	860	870

to minimize the effects of sensor instability (see preceding paragraph) during the time required to perform an MSS radiometric test.

Adjusted video levels are determined by comparing the sensor calibration wedge for each data point (radiance level) and adjusting the video levels to compensate for sensor gain and offset changes. Specifically, the adjusted video quantum levels are calculated from a linear regression fit between the calibration wedge corresponding to each integrating sphere data point and the mean calibration wedge.

$$\bar{Q}_i = 1/N \sum_{j=1}^{N} Q_{ij}$$

Where: Q_i = Mean cal wedge quantums level at the $i^{\underline{th}}$ word count

Q_{ij} = Cal word quantum level at the $i^{\underline{th}}$ word count and the $j^{\underline{th}}$ sphere radiance level

N = Number of radiance level data points

$$K_4 = M \sum_{i=1}^{M} \bar{Q}_i - \left(\sum_{i=1}^{M} \bar{Q}_i \right)^2$$

$$F_i = \left[\sum_{i=1}^{M} Q_i^{\,2} - \bar{Q}_i \sum_{i=1}^{M} Q_i \right] / K_4$$

$$G_i = \left[M\bar{Q}_i - \sum_{i=1}^{M} \bar{Q}_i \right] / K4$$

Where: M = Number of cal wedge word counts = 6

$$VA_j = \left[V_j - \sum_{i=1}^{M} Q_{ij} F_i \right] / \sum_{i=1}^{M} Q_{ij} G_i$$

VA_j = Adjusted video level corresponding to the j^{th} sphere radiance level.

V_j = Video level (raw data point) at the j^{th} sphere radiance level. These adjusted video quantum levels are used in the derivation of the MSS radiometric calibration coefficients.

4.1.4 CALIBRATION WEDGE RADIANCE VALUES

Radiance values at the i^{th} calibration wedge word count are computed from the adjusted video quantum levels and the integrating sphere radiance values. These radiance values are assumed to be fixed (an assumption proven by experience) for all in-flight video data calibration.

The calibration wedge radiance values are determined from:

$$R_i = \left[\bar{Q}_i - \sum_{j=1}^{N} A_j VA_j \right] / \sum_{j=1}^{N} B_j VA_j$$

$$A_j = \left[\sum_{j=1}^{N} R_j^2 - R_j \sum_{j=1}^{N} R_j \right] / K_5$$

$$B_j = \left[NR_j - \sum_{j=1}^{N} R_j \right] / K_5$$

$$K_5 = N \sum_{j=1}^{N} R_j^2 - \left(\sum_{j=1}^{N} R_j \right)^2$$

Where: R_j = Radiance of integrating sphere

R_i = Radiance of internal calibration system at the i^{th} cal wedge word count

N = Number of integrating sphere radiance level

The calibration wedge radiance values, while required for the development of calibration coefficients, are not available because the calibration process has been computerized, and intermediate steps are not outputted by the computer.

4.1.5 CALIBRATION COEFFICIENTS

The first order linear regression coefficients (calibration coefficients) are a function of the radiance values corresponding to the six samples extracted from the calibration wedge.

$$C_i = \left[\sum_{i=1}^{6} R_i^2 - Ri \sum_{i=1}^{6} R_i \right] / K_1$$

$$D_i = \left[6 R_i - \sum_{i=1}^{6} R_i \right] / K_1$$

$$K_1 = 6 \sum_{i=1}^{6} R_i^2 - \left(\sum_{i=1}^{6} R_i \right)^2$$

Where: R_i = Radiance corresponding to the sampled calibration wedge voltage

C_i = Regression coefficient

D_i = Regression coefficient

The C_i coefficient is associated with the offset (intercept) and the D_i coefficient is associated with the gain (slope) of the first order polynomial which describes each sensor.

Appendices L, M, and N contain the calibration coefficients for the three Landsats.

4.1.6 SENSOR TRANSFORMATION EQUATION

The transformation relation between apparent scene radiance and sensor voltage output is a first order polynomial. The MSS sensors are quite linear, so that a first order polynomial provides an accurate characterization:

$$V_o = bR + a$$

Where:

V_o = Sensor Output Voltage

a = 0th Order Coefficient (Offset)

b = 1st Order Coefficient (Gain)

R = Apparent Scene Radiance

The parameters a and b are determined from the calibration wedge complex voltages and their corresponding radiance values:

$$a = \sum_{i=1}^{6} C_i Q_i$$

$$b = \sum_{i=1}^{6} D_i Q_i$$

Where:

Q_i = Sampled Calibration Wedge Voltage

C_i = Regression Coefficient

D_i = Regression Coefficient

The C_i and D_i regression (calibration) coefficients are functions of the radiance of the MSS internal calibration system, which is assumed constant throughout the life of the MSS. Thus, each sensor of the MSS is fully described by the above transformation relation employing the calibration coefficients along with the six calibration wedge samples.

4.1.7 CALIBRATION ALGORITHM

The six sensors in each of the four MSS optical bands each have different gains and offsets (Figure 4-2). Obviously, these differing sensor gains and offsets would produce intolerable striping in film products. The sensors are, therefore, mapped to a common "calibrated curve" to eliminate striping. Values of calibrated R_{max} and R_{min} are chosen to eliminate high and low level striping. The mapping algorithm is:

$$V_C = \frac{V_{max}}{R_{max} - R_{min}} (R - R_{min})$$

Where:

V_C = Calibrated Pixel Value

V_{max} = Maximum Pixel Value
(127 for decompressed data and 63 for linear data)

R = Apparent Scene Radiance

The minimum (R_{min}) and maximum (R_{max}) of incident radiance are derived from the sensors in each band.

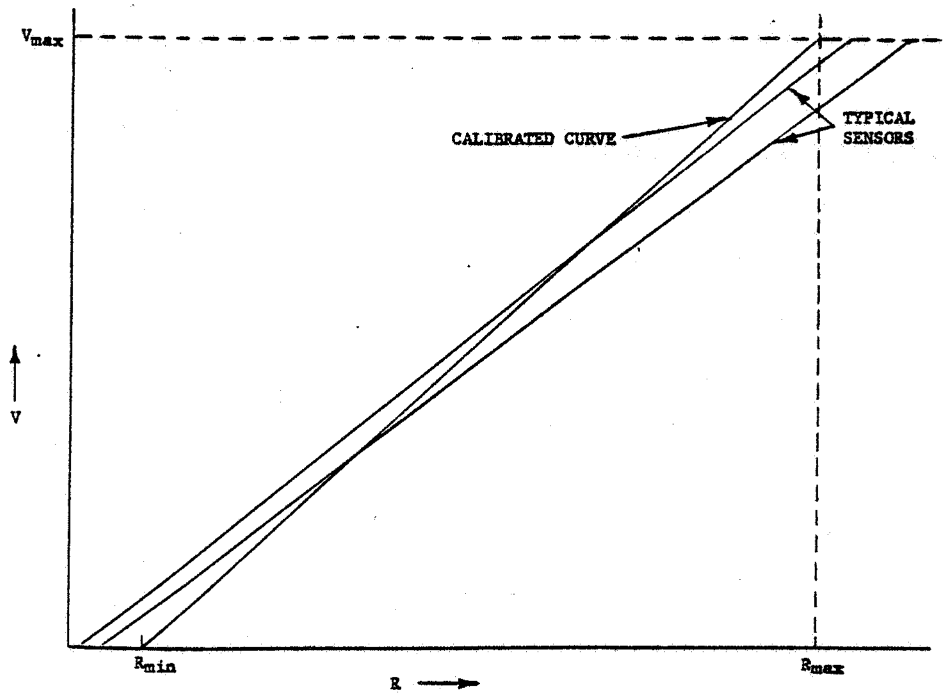

Figure 4-2. MSS Sensor Gains and Offsets

R_{max} = Radiance Value slightly less than the lowest value of Incident Radiance at which a sensor within the Band Reach Saturation

R_{min} = Radiance Value slightly higher than the highest value of Incident radiance at which sensor within the Band Reach Zero Output.

From the sensor transformation relation of paragraph 4. 1. 6:

$$V_o = bR + a$$

solved for scene radiance:

$$R = \frac{1}{b} (V_o - a)$$

and substituted into the mapping algorithm.

$$V_c = \frac{V_{max}}{R_{max} - R_{min}} \left[\frac{V_o - a}{b} - R_{min} \right]$$

The above algorithm maps the six MSS sensors in a given band to a straight line which is definited by the points (R_{min}, 0) and (R_{max}, V_{max}). The values of R_{min} and R_{max} for all optical bands of the three Landsat vehicles are given in Table 4-2.

To simplify the above algorithm and reduce the number of repetitive calculations, the calibration algorithm has been modified to:

$$V_c = \frac{V_{max}}{b'} (V_o - a')$$

The modified gain and offset may be determined by equating the two calibration algorithms giving:

$$a' = a + R_{min}$$

$$b' = (R_{max} - R_{min}) b$$

Since:

$$a = \Sigma C_i V_i$$

$$b = \Sigma C_i V_i$$

Where:

C_i = Regression Coefficient of Offset

Table 4-2. R_{min} and R_{max} Values

Landsat I

	Low Gain		High Gain	
Band	R_{min}	R_{max}	R_{min}	R_{max}
4	0	2.48	0	0.83
5	0	2.00	0	0.67
6	0	1.76		
7	0	4.60		

Landsat II

	Low Gain (Prior to 7/16/75)		High Gain	
Band	R_{min}	R_{max}	R_{min}	R_{max}
4	0.10	2.10	0.06	0.80
5	0.07	1.56	0.04	0.55
6	0.07	1.40		
7	0.14	4.15		

	Low Gain (After 7/16/75)	
Band	R_{min}	R_{max}
4	0.08	2.63
5	0.06	1.76
6	0.06	1.52
7	0.11	3.91

Landsat III

	Low Gain (Using IATs generated prior to 5/31/78)	
Band	R_{min}	R_{max}
4	0.04	2.20
5	0.03	1.75
6	0.03	1.45
7	0.03	4.41

	Low Gain (Data acquired after 4/24/78 using IATs generated after 5/31/78			High Gain (All dates)	
Band	R_{min}	R_{max}	Band	R_{min}	R_{max}
4	0.04	2.59	4	0.01	0.85
5	0.03	1.79	5	0.01	0.65
6	0.03	1.49			
7	0.03	3.83			

D_i = Regression Coefficient of Gain

Q_i = Calibration Wedge Sample at ith Word Count

$a' = \Sigma\, C_i\, V_i + R_{min}\, \Sigma\, D_i\, V_i$

$b' = (R_{max} - R_{min})\, \Sigma\, D_i\, V_i$

We can define:

$C_i' = C_i + R_{min}\, D_i$

$D_i' = (R_{max} - R_{min})\, D_i$

These are the modified regression coefficients actually used in the present MSS calibration system as listed in Appendices L, M, and N.

4.1.8 DECOMPRESSION TABLES

The outputs of the 24 sensors are quantized into 64 levels in the multiplexer. These 64 quantum levels are evenly spaced across the entire four-volt signal range. For bands 4, 5 and 6, however, linear quantization is not optimum, because the noise in the signal diminishes as the square root of the signal. Therefore, shaping the signal according to a square root law will equalize the noise throughout the range of the signal. Then linear quantization matches the quantization errors to the signal noise.

Decompression tables are derived from curves of multiplexer quantized output versus voltage input. These outputs are tabulated in Table 4-3 for all Landsats for bands 4, 5 and 6 (band 7 is linear).

When data is acquired in the compressed mode on bands 4, 5 and 6, the decompression tables are used to linearize the MSS levels. The output value V_o obtained from this decompression step is then used in the linear calibration algorithm described in paragraph 4.1.7.

4.2 RADIOMETRIC CALIBRATION IR BAND

Because of post-launch problems with the IR detectors, a detailed discussion of the planned band 8 sensor calibration is not included here.

4.3 GEOMETRIC

The registration accuracy between bands and between sensors is a function of the multiplexer sampling sequence, the scan profile, and the fiber optics matrix pattern. The measured fiber optics matrix patterns for Landsats 1, 2 and 3 are contained in Appendices O, P, and Q. Band 8 detector dimensions are given in Appendix R.

Table 4-3. Decompression Tables

Input QL	Output QL Bands 4 and 6 Landsat			Output QL Band 5 Landsat		
	1	2	3	1	2	3
0	0	0	0	0	0	0
1	1	1	1	1	1	1
2	2	1	2	2	2	2
3	2	2	3	2	3	3
4	3	3	4	3	4	4
5	4	4	5	4	5	5
6	5	5	6	5	6	6
7	6	6	6	6	7	7
8	7	7	7	7	8	8
9	8	8	8	8	9	9
10	9	9	9	9	10	10
11	10	10	10	10	11	11
12	11	11	12	11	12	12
13	12	12	13	12	13	13
14	13	13	14	13	14	14
15	14	15	15	14	15	16
16	16	16	17	16	17	17
17	17	17	18	17	18	18
18	18	18	19	18	19	19
19	19	20	20	19	20	21
20	21	22	22	21	22	22
21	22	23	23	22	23	23
22	24	25	25	23	25	25
23	25	26	27	25	26	27
24	27	28	28	27	28	28
25	29	30	30	28	30	30
26	30	32	31	30	32	32
27	32	34	33	32	34	34
28	34	35	35	34	35	36
29	36	37	37	36	37	38
30	38	39	39	38	39	40
31	40	41	41	39	41	41
32	42	43	43	41	42	43
33	43	45	45	43	45	45
34	45	47	47	45	47	47
35	47	49	49	47	49	49
36	49	51	51	49	52	51
37	51	53	53	51	54	53
38	53	55	55	53	56	55
39	56	58	57	54	58	58
40	58	60	60	58	60	60
41	61	63	62	60	63	63
42	63	66	65	63	66	66
43	66	68	68	66	69	69
44	69	71	71	69	72	71
45	72	74	74	71	74	74
46	75	77	77	74	77	77
47	78	80	79	77	80	80
48	81	84	82	80	83	83
49	83	87	85	83	86	86
50	86	90	88	86	89	89
51	89	92	91	88	92	92
52	92	95	94	91	95	95
53	95	98	97	94	98	98
54	98	101	100	97	101	101
55	101	104	103	100	104	104
56	104	108	106	104	107	107
57	106	111	109	107	110	110
58	109	114	112	109	113	113
59	112	117	115	112	116	116
60	115	120	118	115	119	118
61	118	123	121	117	122	121
62	121	125	124	120	125	124
63	124	127	127	122	127	127

4.3.1 INSTANTANEOUS FIELD OF VIEW

The instantaneous field of view of each channel is obtained from the telescope focal lenth, the dimensions of the optical fiber terminations, and Landsat height. For band 8, it is the ratio of the prime and relay optics focal lengths, the detector dimensions, and Landsat height.

Figure 4-3 shows the instantaneous spatial relationships of the fiber optics and thermal detectors view of the ground. However, it is to be noted that this is an instantaneous representation and changes occur due to the multiplexer sampling sequence and mirror velocity.

4.3.2 SENSOR TO SENSOR REGISTRATION

Since the detectors are sampled serially, at a time delta of 0.398 μsec, the resultant ground pattern per band does not consist of six samples, one exactly below the other. The pattern consists of each subsequent detector square, in a band, displaced to the right by the time required to perform two detector samples. This is because the detectors in two adjacent bands are alternately sampled. The sampling sequence is shown in Figure 4-3. The displacements, sensor to sensor, within a band are given in Figure 4-4. All four optical bands have this identical pattern. The band registration of the two band 8 detectors is also shown in this illustration.

4.3.3 BAND-TO-BAND REGISTRATION

Band-to-band registration is shown in Figure 4-5. This figure depicts the change between the instantaneous view and subsequent detector samplings. Only sensor 1 of bands 4 through 7 is shown for clarity. The displacements are shown until all detectors have imaged the same area of Earth as the first sample of sensor 1, band 4. Distances are indicated using the leading edge of this pixel as reference.

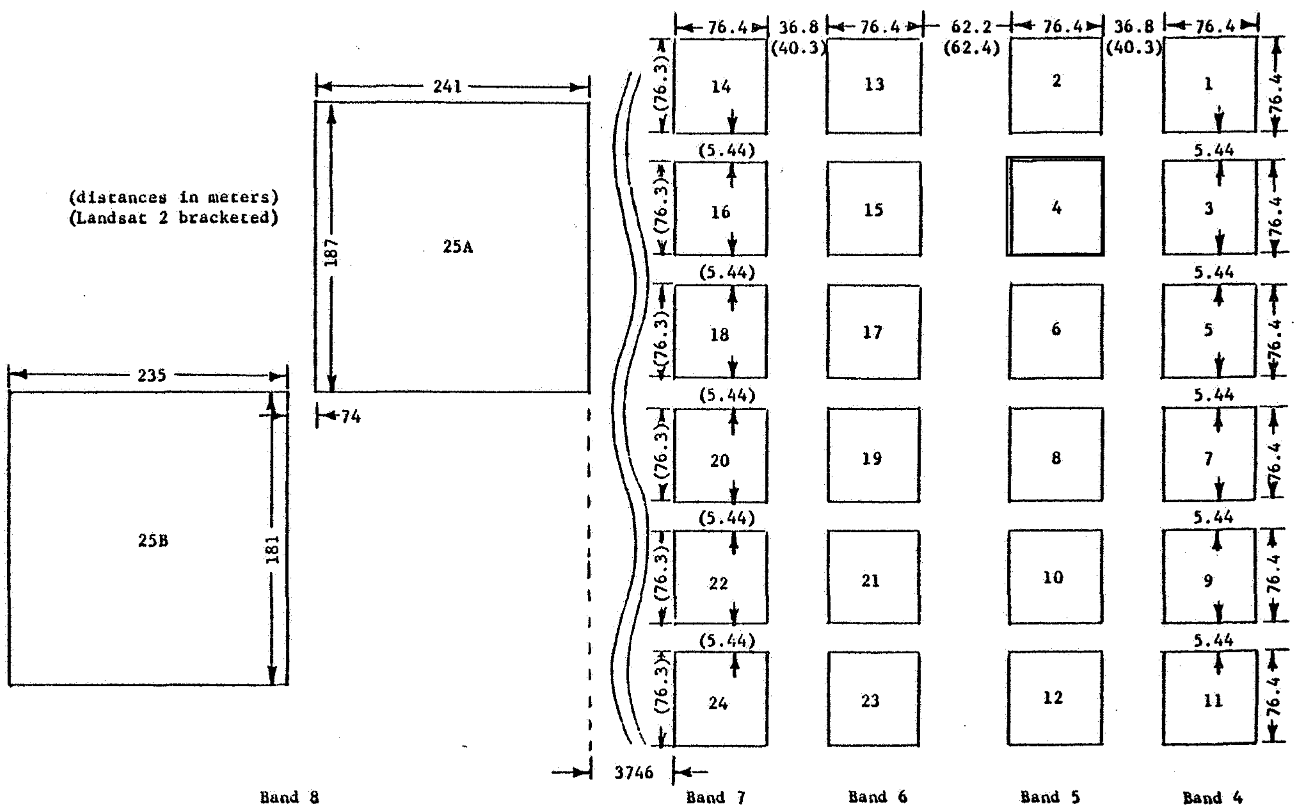

Figure 4-3. Fiber Optics and Thermal Detectors IFOV

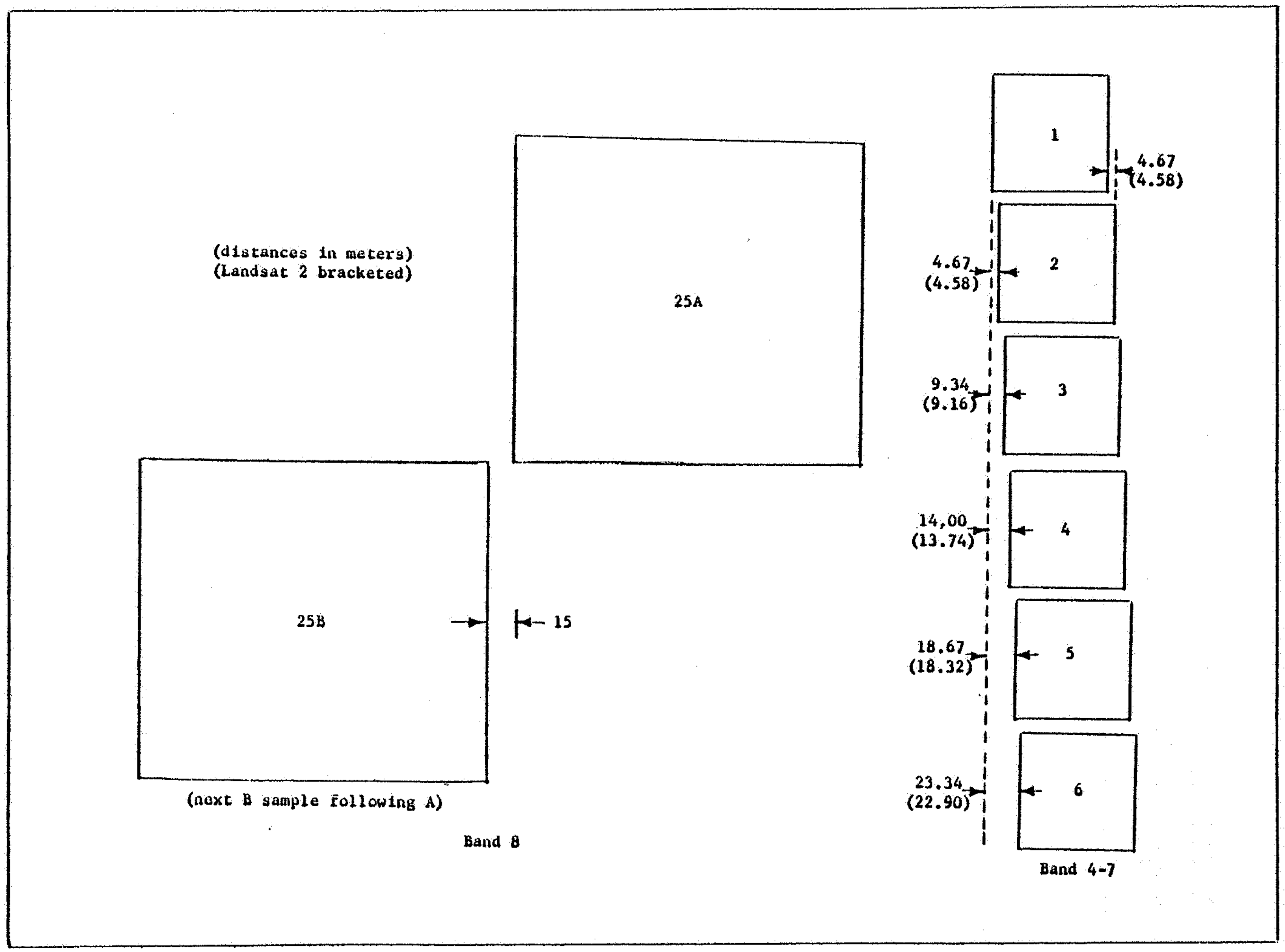

Figure 4-4. Sensor to Sensor Registration

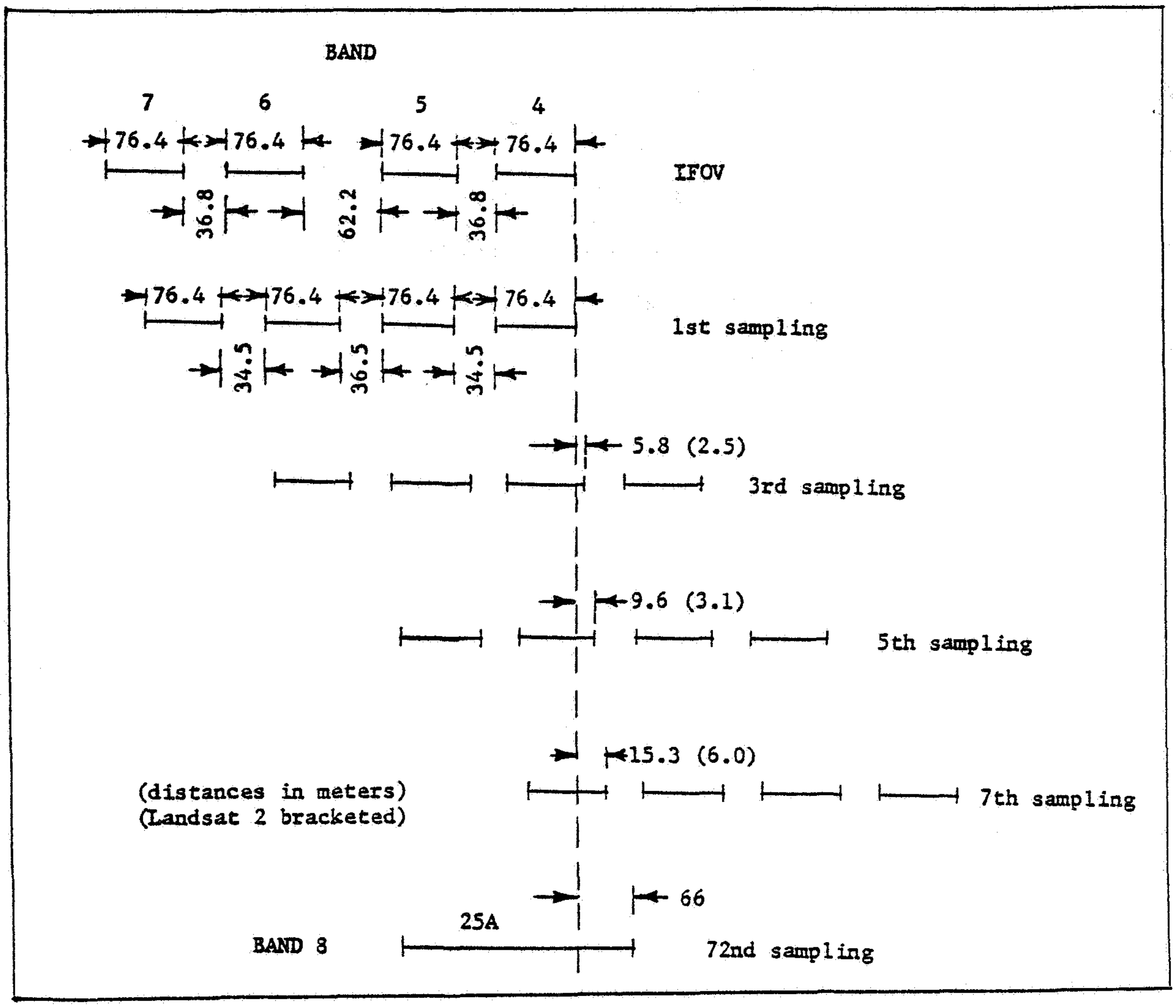

Figure 4-5. Band-to-Band Registration

Note that it takes two complete sample periods (bytes) of 25 words each for band 5 to almost register with band 4. (Landsat 3 band 5 is 5.8 meters ahead of 4 and Landsat 2 band 5 is 2.5 meters ahead of 4.) For band 6 to nearly align with band 4 requires four bytes and band 7, six bytes.

It takes 72 bytes, i.e., 24 band 8 detector A pixels, to reach the first pixel of band 4. The leading edge of the band 8 pixel is ahead of band 4 by 66 meters. Thus the band 4 pixel is near the center of the band 8 pixel at this moment.

4.3.4 SWEEP-TO-SWEEP REGISTRATION

As shown in Figure 4-3, the radiometric IFOV of each fiber optics for Landsat 3 is 76.4 meters square and for Landsat 2, 76.3. When cladding is added and split between two adjacent detectors, the effective along-track dimension for detectors 2, 3, 4 and 5 is 81.8 meters for Landsat 3 and 81.7 meters for Landsat 2. For detectors 1 and 6, the along-track dimension goes to the center line between the sweeps. This is shown in Figure 4-6. The along-track dimension for detectors 1 and 6 is 76.7 meters for Landsat 3 and 76.9 meters for Landsat 2.

The sweep-to-sweep distance was determined by using a ground track velocity of 6546 m/ sec. This velocity was determined from several values from Landsats 1 and 2.

Sweep-to-sweep spacing for this velocity is 480.6 meters. The average along-track dimension for all six pixels in a sweep is 80.1 meters.

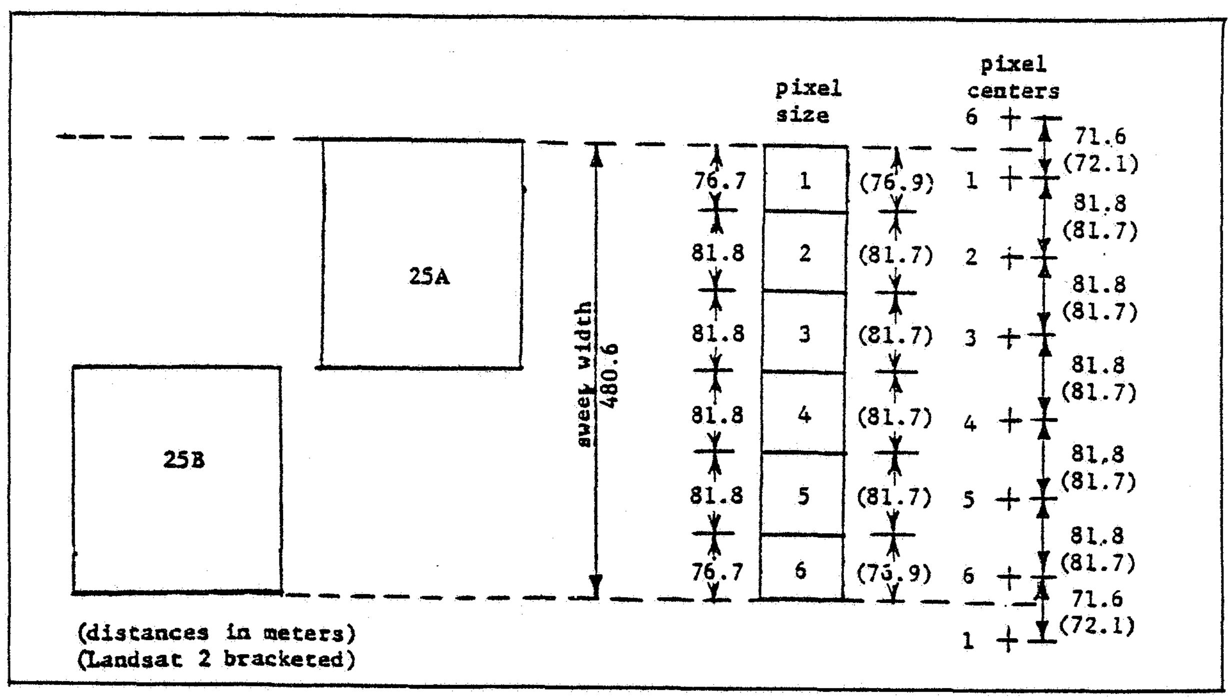

Figure 4-6. Sweep-to-Sweep Registration

The radiometric IFOV of the band 8 detectors underlaps the sweep width. Their effective along-track dimension is one-half the sweep width, i.e., ~240 meters.

4.3.5 PIXEL SIZE SWEEP DIRECTION

Pixel size in the sweep direction depends on the mirror velocity, perspective and sampling frequency. While the radiometric IFOVs are ~76.4 meters, note there is considerable pixel overlap in the sweep direction. The effective pixel size is the amount of ground distance advanced between subsequent detector samplings. This is shown in Figure 4-7. The effective pixel size for Landsat 3 is 58.3 and for Landsat 2, 57.2. These are averages for the total sweep at nominal Landsat height. Pixel size is largest at the center of the sweep and smallest at the ends. (The Landsat 2 center pixel is ~57.8 meters and the end pixel, ~56.4.)

Band 8 effective pixel size in the sweep direction is ~175 meters.

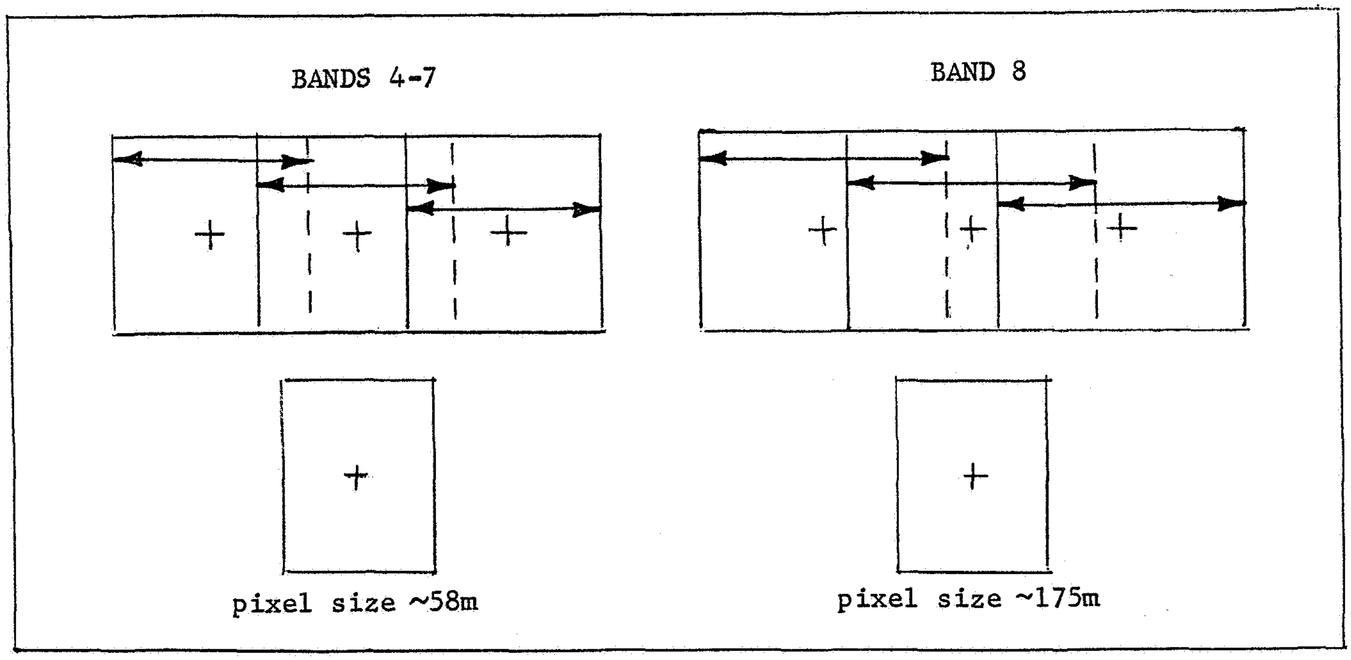

Figure 4-7. Pixel Size Sweep Direction

4.3.6 MIRROR VELOCITY PROFILE

Mirror motion is described in paragraph 2.3. The sinusoidal component caused by the flexure pivot is the primary cause of angular sweep non-linearity. Figure 4-8 shows the relation between the harmonic motion of the "spring" and the scan excursion. Information on mirror velocity profile characteristics are used to improve Landsat image accuracy.

Hughes mirror velocity scan profiles for Landsats 1 and 2 are given in Figure 4-9.

A profile for Landsat 2 using many ground truth points (~240), along with calculated results from mirror parameters was generated. This data is presented in two forms; Figure 4-10 showing the error curve and Figure 4-11 giving the mirror velocity. These curves include the perspective error.

4.3.7 MSS-TO-AMS ALIGNMENT

The attitude measurement sensor (AMS) is an independent component (not used for attitude control purposes) that determines spacecraft pitch and roll attitude. This data is used for image location and correction during ground processing. The AMS detects the radiation level change in the 14-to-16-micron range between the Earth's atmosphere and the spatial background and establishes the spacecraft pitch and roll axis positions relative to the local vertical. After ground compensation of telemetry data for variations due to seasonal radiance and other effects, the pitch and roll attitude can be determined to within about 0.07 degree.

Table 4-4 presents the boresight values to the spacecraft for both the MSS and AMS for all three Landsats.

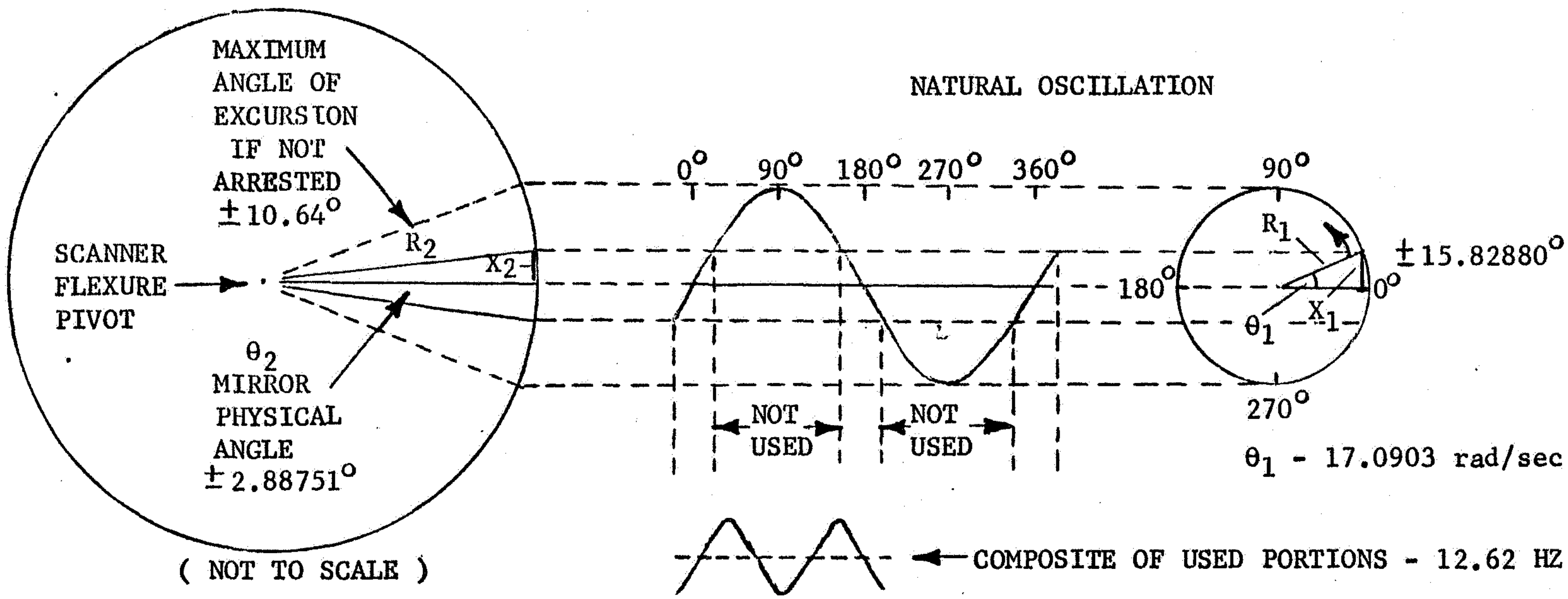

$\sin \theta_2 = \frac{X_2}{R_2}$ $\qquad$ $\sin \theta_1 = \frac{X_1}{R_1}$ $\qquad$ $R_2 = \frac{\sin\theta_1}{\sin\theta_2}$

$X_1 = X_2$ $\qquad$ let $R_1 = 1$ $\qquad$ $R_2 = \frac{\sin 15.82880}{\sin 2.88751}$

$X_1 = R_2 \sin\theta_2$ $\qquad$ $X_1 = \sin\theta_1$ $\qquad$ $R_2 = 5.41464$

$R_2 \sin\theta_2 = \sin\theta_1$ $\qquad$ $\theta_2 = \text{arc sin } .18468 \sin\theta_1$

Figure 4-8. Landsat 2 Scanner Geometric Relationships

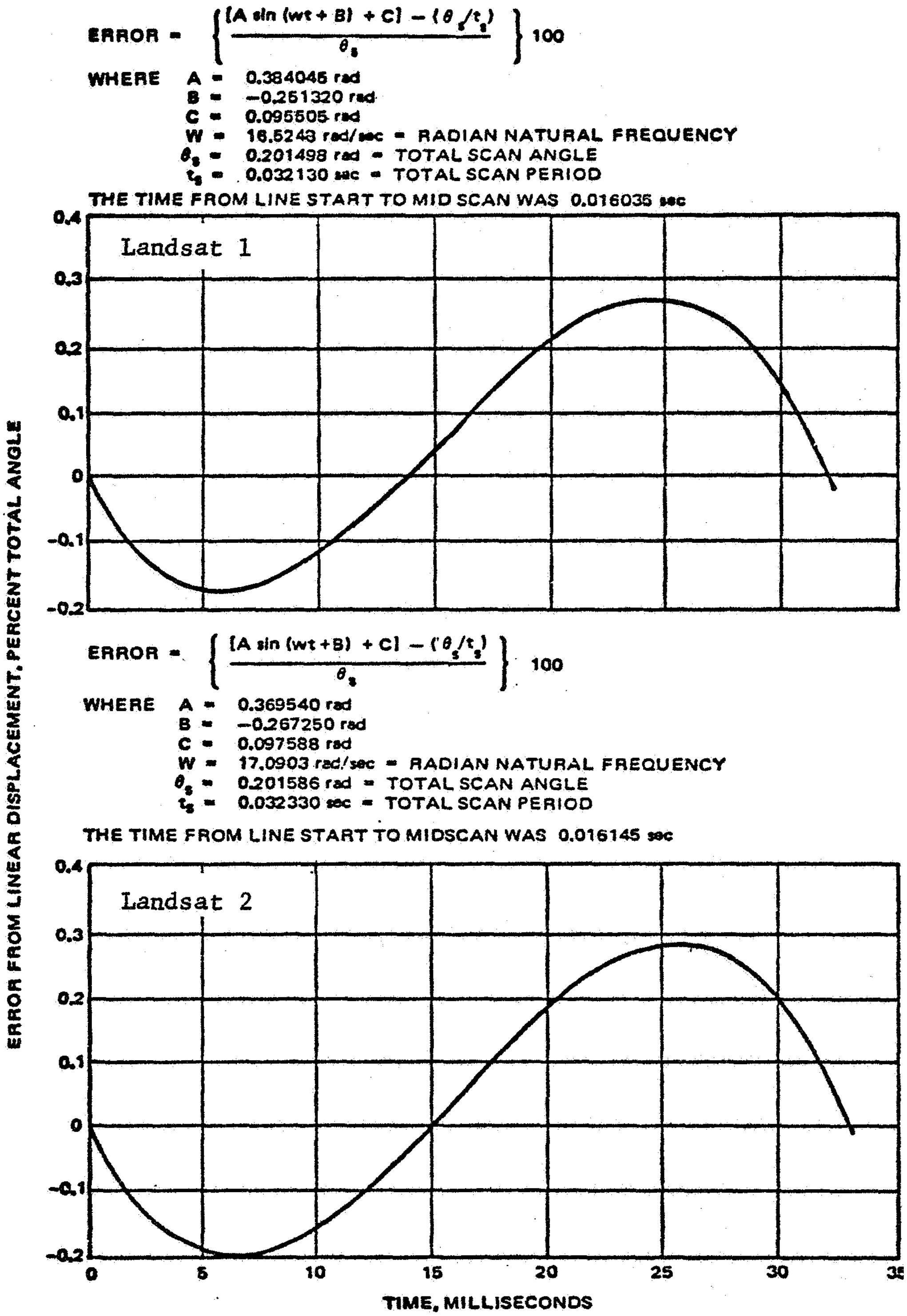

Figure 4-9. Landsats 1 and 2 Mirror Velocity Scan Profiles

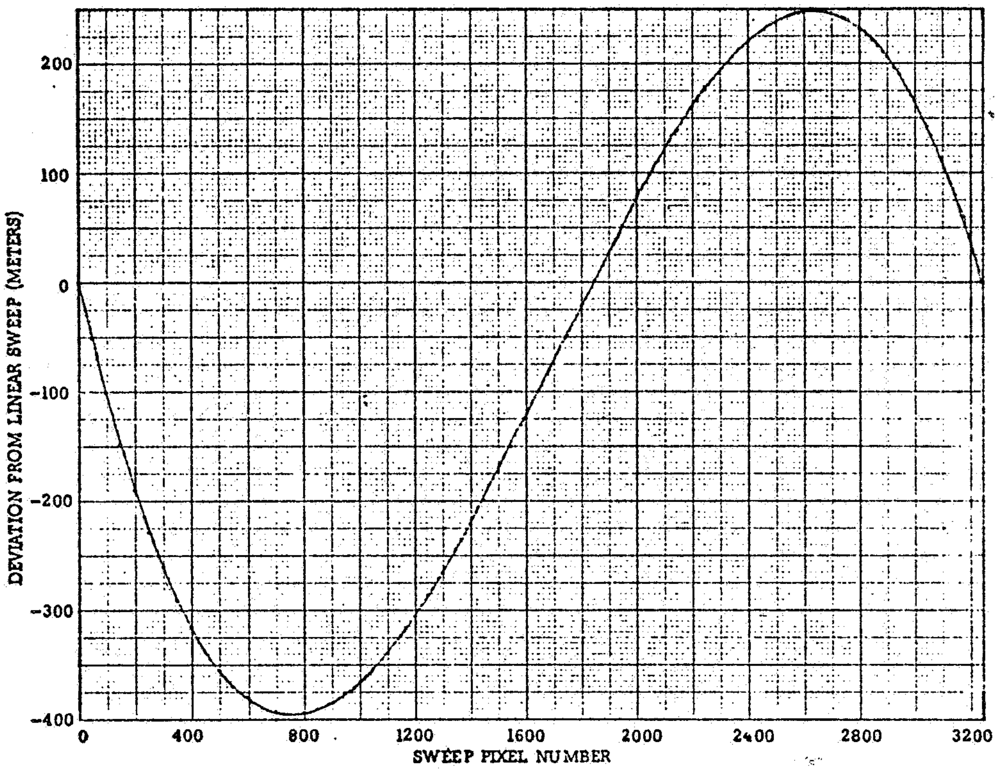

Figure 4-10. Landsat 2 Error Curve

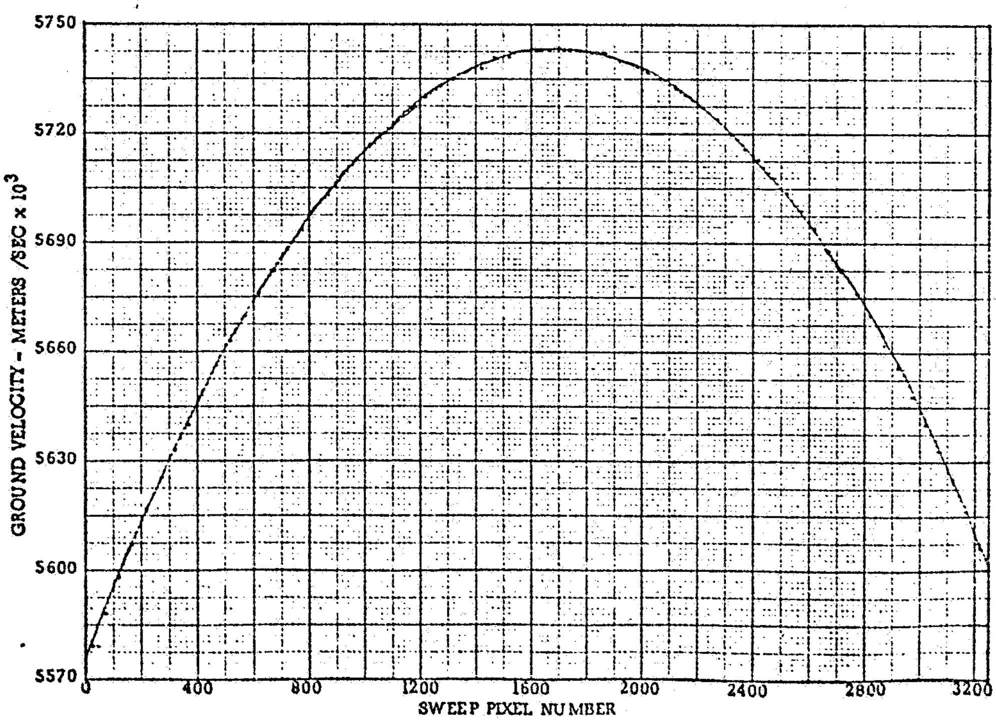

Figure 4-11. Landsat 2 Mirror Velocity

Table 4-4. MSS and AMS Boresight Alignment

	MSS			AMS		
	θx	θy	θz	θx	θy	θz
Landsat 1	-1' 59"	-2' 42"	+12' 19"	-1' 18"	+1' 36"	+8' 36"
Landsat 2	+2' 30"	+1' 19"	-0' 06'	+2' 57"	-0' 43"	-0' 03"
Landsat 3	-1' 56"	+3' 58"	+0' 55"	+0' 41"	-0' 26"	-0' 41"

4.3.8 LINE LENGTH

Pixel line length is determined by pixel sampling rate, angle between start and stop pulses, and mirror velocity.

Ground distance represented by a mirror sweep depends on several factors. The most important of these are scan angle between start and stop pulses and Landsat height. The system was designed for a nominal ground distance of 100 nautical miles (~185Km).

Sweep pixel count variations for the three satellites are presented in Table 4-5.

Table 4-5. MSS Line Length

Landsat 1		Landsat 2		Landsat 3	
Period	Pixels	Period	Pixels	Period	Pixels
Ground test	3221	Ground test	3250	Ground test	3179
72/73	3219	75	3249	9 Mar 78	3187
73/74	3217	76	3248		
74/75	3216	77	3245		
75/76	3217	end 77	3242		
76/77	3215				
77/78	3211				

Nominal ground distance represented by the scan line is given in Table 4-6. Also, included in this table is the full angle between the start and stop pulses and the focal lengths of the telescopes for all three satellites.

Table 4-6. Nominal Ground Distance per Sweep

	Height	Focal Length	Mirror Angle	Ground Distance
Landsat 1	918.6 Km	32.32"	11.545°	185.7 Km
Landsat 2	918.6 Km	32.40"	11.550°	185.8 Km
Landsat 3	918.6 Km	32.465"	11.529°	185.5 Km

SECTION 5

VIDEO DATA PROCESSING

SECTION 5

VIDEO DATA PROCESSING

5.1 RADIOMETRIC

5.1.1 CALIBRATION ALGORITHM

The radiometric calibration algorithm of paragraph 4.1.7 is repeated below for convenience.

$$V_c = \frac{V_{max}}{b'} (V_o - a')$$

$$a' = \sum_{i=1}^{6} C_i' \; Q_i$$

$$b' = \sum_{i=1}^{6} D_i' \; Q_i$$

where:

V_c = Calibrated pixel value

V_{max} = Maximum pixel value (127 for decompressed data and 63 for linearly acquired data)

V_o = Uncalibrated pixel value

b' = Modified gain of sensor

a' = Modified offset of sensor

C_i' = Modified regression coefficient

D_i' = Modified regression coefficient

Q_i = Calibration wedge sample at i^{th} word count.

The above algorithm may be used to calibrate in-flight MSS data and, indeed, was for the first few years of Landsat 1. A modification has recently been added, however, to accomplish calibration updates. The modification is in the form of a set of dated constants. One multiplicative and one additive constant per sensor has been incorporated into the MSS calibration algorithm. The new algorithm is:

$$V_c = \frac{V_{max}}{Mb'} (V_o - a') - A$$

where

M = Multiplicative constant

A = Additive constant

This modification allows occasional calibration updates to occur without change to the primary (C_i and D_i) calibration coefficients.

As the MSS ages, the gain and offsets of the sensors tends to drift. These changes are compensated for by the video data calibration process. However, significant aging drifts may be noted by slightly increased striping in the calibrated imagery. When this increased striping is found, a calibration update is performed using the calibration modifiers (M and A).

5.1.2 NOISE COMPENSATION

Noise from a variety of sources is present in the MSS data. This noise is able to cause significant perturbations in the calculated sensor gain (b) and offset (a). Therefore, the values of "a" and "b" are smoothed according to the following equations. "n" is the number of the estimate and corresponds to the number of calibration wedges that have been processed to the current position in the scene.

$a_s(1) = a(1)$ = value of "a" computed from the first calibration wedge data encountered at scene processing initiation (n = 1).

$$a_s(n) = a_s(n-1) + 1/n\ [a(n) - a_s(n-1)] \text{ for } 1 < n \leqslant 16$$

$$a_s(n) = a_s(n-1) + 1/16\ [a(n) - a_s(n-1)] \text{ for } 16 < n \text{ (calibration wedges)}$$

where $a_s(n)$ = n th estimate of "a"

$a(n)$ = calculation of "a" based solely on the n th set of calibration data received.

Up to and including n = 16, the successive values of a_s are the average of all the computed values of a (n). That is

$$a_s(n) = \frac{a(1) + a(2) + \ldots + a(n).\ n \leqslant 16}{n}$$

Similarly,

$b_s(1) = b(1)$ = value of "b" computed encountered at scene processing initiation.

$$b_s(n) = b_s(n-1) + \frac{1}{n}\ [b(n) - b_s(n-1)] \text{ for } 1 < n \leqslant 16$$

$$b_s(n) = b_s(n-1) + 1/16\ [b(n) - b_s(n-1)] \text{ for } n \geqslant 16$$

The complete radiometric calibration algorithm, using calibration modifiers and smoothed modified gains and offsets, is:

$$V_c = \frac{V_{max}}{Mb_s} (V_o - a_s) - A$$

5.1.3 DECOMPRESSION

Data for bands 4, 5, and 6 are usually acquired in the compressed mode. Decompression is accomplished in digital processing through the use of a table look-up routine. The input byte, value 0-63 is output as 0-127. Two decompression tables are used, one for bands 4 and 6 and the second for band 5. Decompression tables for all Landsats are given in Table 4-3. Bands 7 and 8 are acquired linearly and therefore do not require decompression.

When data is acquired in the compressed mode on bands 4, 5 and 6, the decompression tables are used to linearize the MSS levels. The output value V_o obtained from this decompression step is then used in the linear calibration algorithm decribed in paragraph 4.1.7.

5.1.4 NOMINAL CALIBRATION WEDGE

To further limit the effects of system noise, a nominal calibration wedge has been used. This nominal calibration wedge is the mean value of the calibration wedge, updated periodically. In practice, each calibration wedge sample is compared to the nominal calibration wedge. If the sample does not compare to the nominal wedge within a given window (typically ± 4 quantum levels), it is discarded in favor of the nominal calibration wedge.

A window value of ± 4 quantum levels is adequate to allow normal variations of the MSS sensors, while rejecting large noise excursions in the data.

5.2 GEOMETRIC - SYSTEMATIC

This section discusses errors that exist in the raw data and not the details of correction. These cover the observatory only and do not include any film processing errors.

5.2.1 REGISTRATION

The sensor-to-sensor and band-to-band registration problem is depicted in Figures 5-1 and 5-2. These effects have been described in Section 4.3. To be geometrically correct, the six detectors in a band should be printed with offsets (i.e., in the stepped form as shown) corresponding to the distances travelled between detector samples.

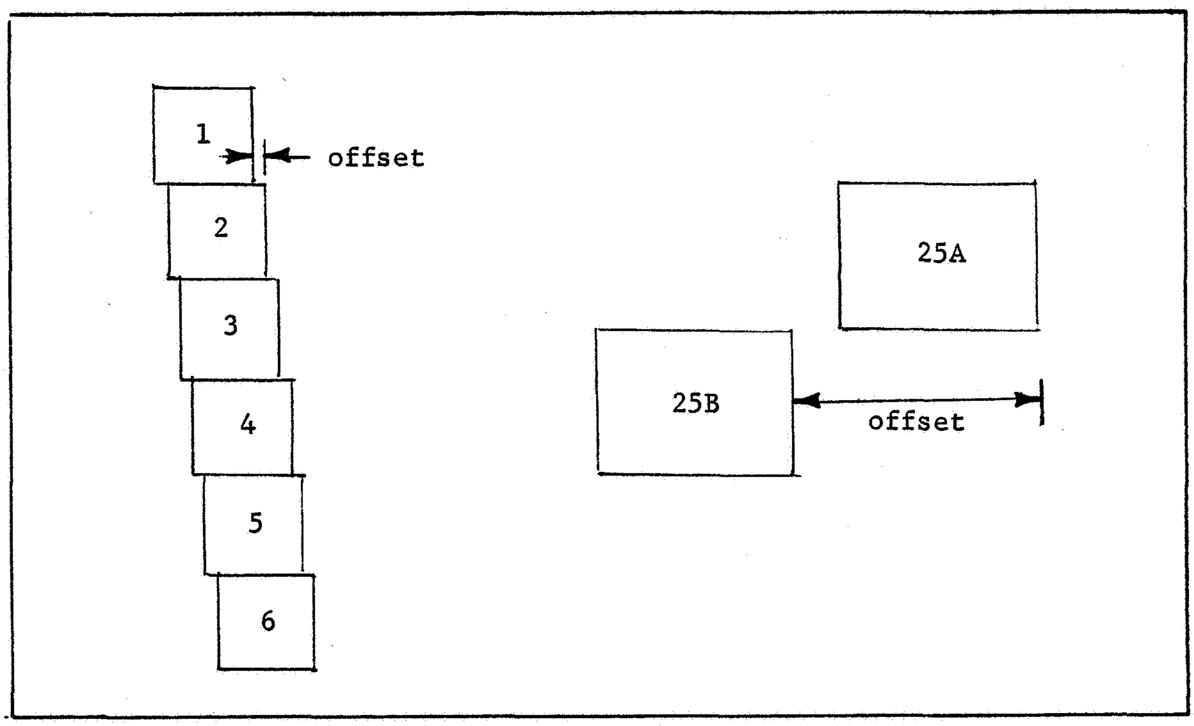

Figure 5-1. Sensor-to-Sensor Registration

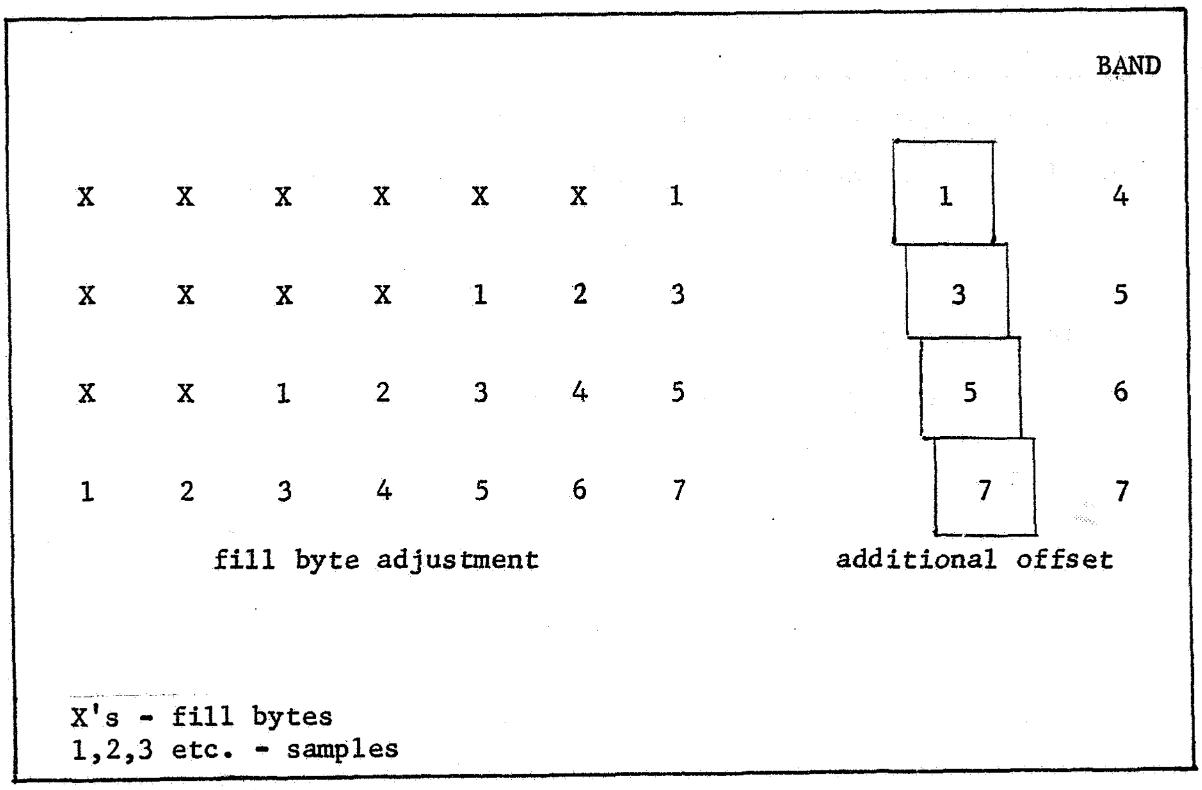

Figure 5-2. Band-to-Band Registration

The major part of the band-to-band registration is the advance of bands 5, 6 and 7 data with respect to band 4 by two, four, or six bytes respectively as shown in Figure 5-2. However, a small residual still exists, as shown, and requires an additional offset to be made.

5.2.2 LINE LENGTH

Changes in line length over a period of time occur due to temperature and aging of the flexure pivot. These cause relatively slow changes and do not affect the pixel count within a scene. Line pixel count within a scene vary due to differences in torquing, mirror position, bumper effects and spacecraft dynamic movements especially in roll. These line pixel count changes within a scene are shown in Figure 5-3.

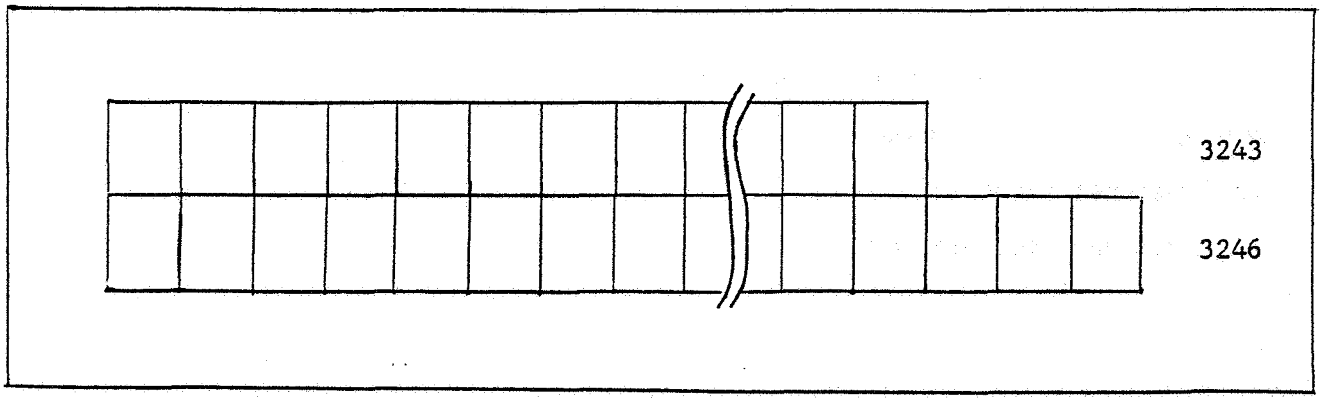

Figure 5-3. Variations in Sweep Pixel Count

Correction can be through the insertion of synthetic bytes (fill pixels). This method of correction is illustrated in Figure 5-4. The fill pixels are inserted uniformily throughout the line to make all lines equal to the multiple of 24 that contains the longest line. The fill pixel is a radiometric copy of the preceding pixel. The varying line pixel count can also be corrected through resampling.

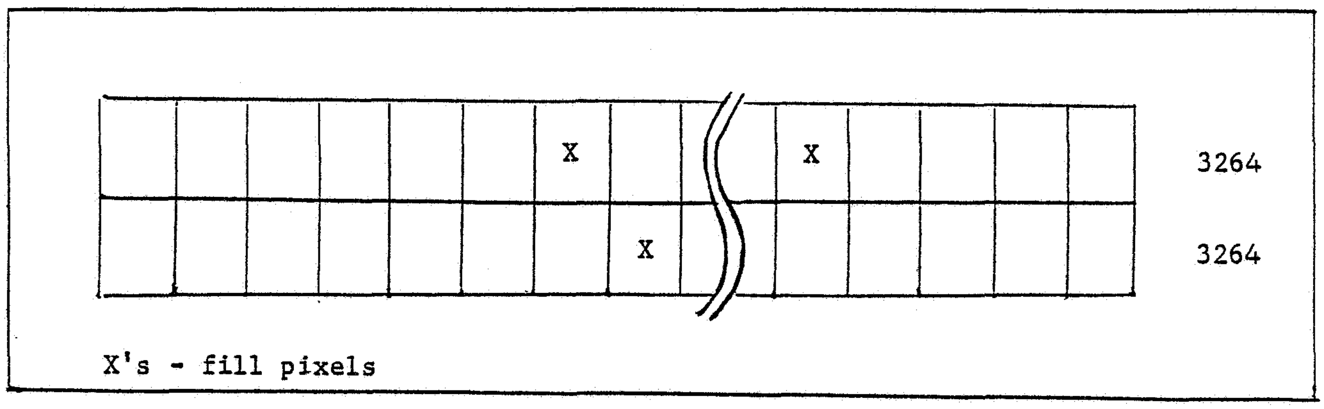

Figure 5-4. Line Length Correction Using Fill Pixels

5.2.3 MIRROR VELOCITY PROFILE

Non-linear mirror velocity is one of the largest systematic sweep errors. If not corrected, this results in a horizontal compression of the scene in the center and an expansion at the right and left edges. Figure 5-5 shows the effect of this error.

An example of the magnitude of this correction are the values from a typical scene. Pixel size at sweep start was 55.6 meters; at maximum near center, 57.2 meters; and at sweep stop, 55.8 meters. (These numbers include the error for perspective which subtracts slightly from the mirror velocity error.)

5.2.4 SCAN LINE SKEW

The along-track displacement of the scan line caused by the spacecraft ground velocity provides the necessary sweep-to-sweep advance. However, this makes a skew in the picture because the scan lines are not normal to the right and left edge of the frame due to the vector addition of the two velocities. Also, because the mirror sweep is not linear, this causes an additional error somewhat like a sine wave. This component rides on the skew line. These effects are shown in Figure 5-6.

5.2.5 EARTH ROTATION SKEW

This systematic error depends on earth rotation at the latitude of interest and spacecraft heading and velocity. Figure 5-7 illustrates this effect. This is the reason for Landsat pictures to be parallelograms rather than rectangles.

5.2.6 PERSPECTIVE

There are two perspective effects in the sweep scan direction.

The major one is the increasing relative ground velocity of the scan the further it is from nadir. This varies as an algorithm of the tangent which increases rapidly for large angles. However, it is very small for the small scan angles used. The effect is an increase in pixel size from nadir as shown in Figure 5-8.

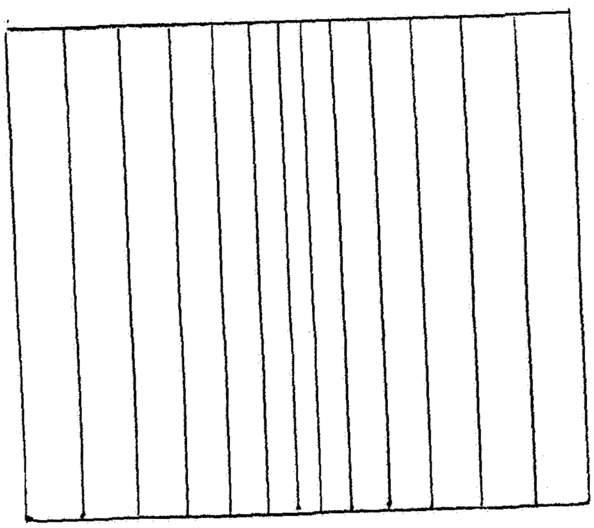

Figure 5-5. Non-linear Sweep Distortion

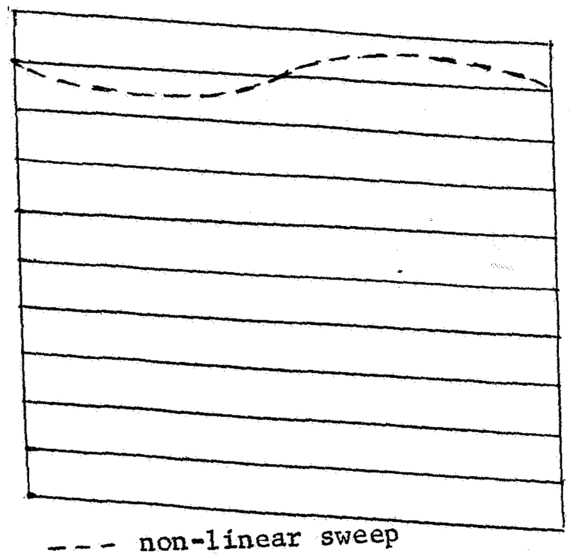

Figure 5-6. Scan Line Skew

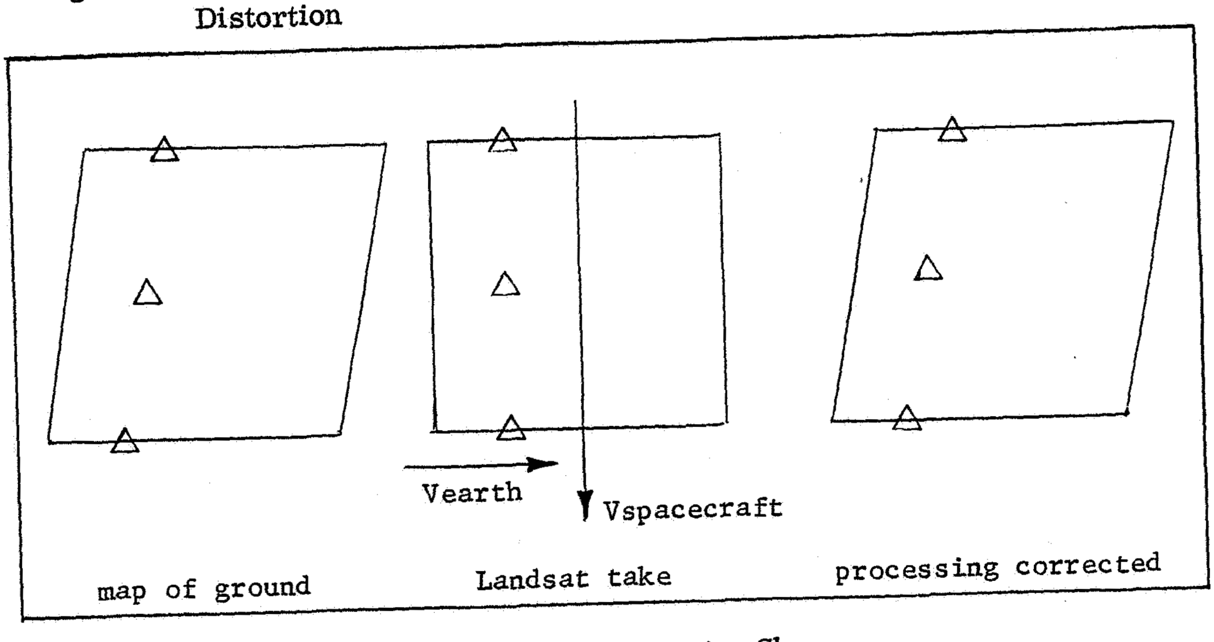

Figure 5-7. Earth Rotation Skew

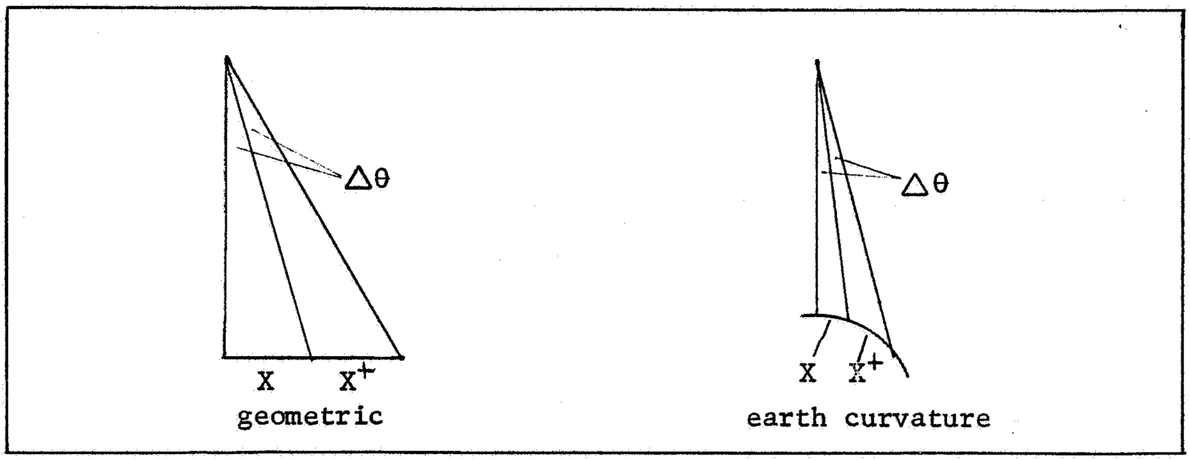

Figure 5-8. Perspective

The second effect is the earth's curvature. This is smaller than the effect above and is almost negligible for the spacecraft/ MSS parameters used. It also causes the pixels to become larger when moving away from nadir with its effect increasing rapidly at the extreme ends of the scan sweep. This effect is also shown in Figure 5-8.

Perspective in the along-track direction, i.e., from the top to bottom of picture, is almost perfect. This occurs because the scene is made up of scan lines of comparatively negligible width. Therefore, for all practical purposes, there is no perspective error in the along track-direction.

5.2.7 ALIGNMENT

MSS alignment deviations from prescribed axis cause constant displacements in X, Y and Z. These effects are shown in Figure 5-9.

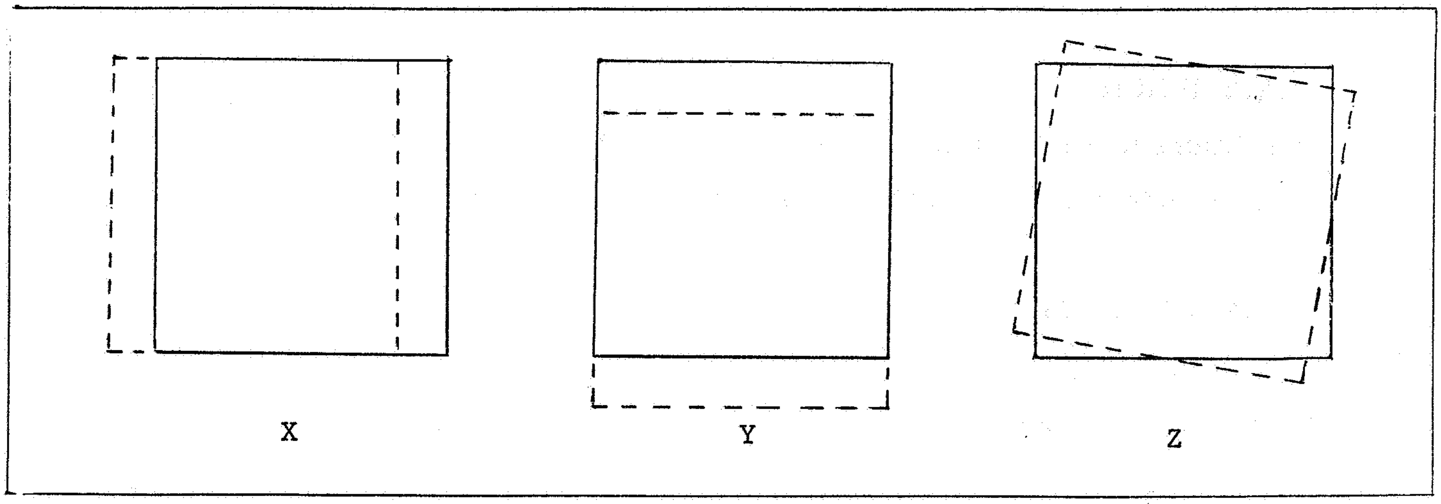

Figure 5-9. Effects of MSS Alignment

5.3 GEOMETRIC ERRORS - DYNAMIC

5.3.1 ATTITUDE CHANGES - PITCH/ROLL/YAW

Spacecraft rates in pitch, roll and yaw are used to correct for the small instabilities in the platform. The effects of these changes on the MSS scene are shown in Figure 5-10.

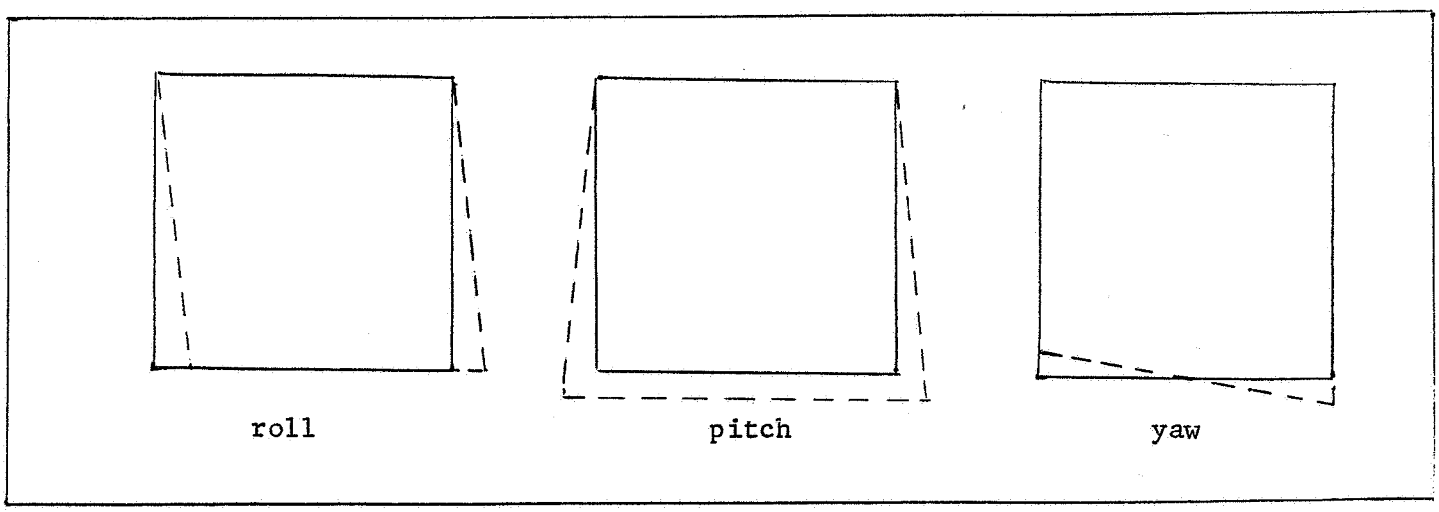

Figure 5-10. Effects of Pitch, Roll and Yaw

5.3.2 HEIGHT

Variations in height within a frame are small, and the effect is slight. It causes a trapezoidal figure if the change is linear.

5.3.3 VELOCITY

This also is a small error. The effect is an expansion or compression of the frame in the along-track direction.

5.4 IMAGE FRAMING

To achieve maximum utility of MSS data, Landsat orbit parameters and data sequences provide systematic and repetitive earth coverage under nearly constant observation conditions.

5.4.1 STANDARD ORBITS

Landsat orbit parameters have been selected to provide repeating orbits every 18 days. Also, the ground tracks of all the Landsat series coincide. The orbit of Landsat 3 is staggered with Landsat 2 so that alternate repeat coverage between the two satellites occurs every nine days. Figure 5-11 shows the ground traces (paths) and the standard reference number for each orbit over the U.S.

5.4.2 STANDARD FRAMES

Picture taking sequences are scheduled so that all images can be registered with one another. This is accomplished by referencing all payload operation to the equator. The equatorial frame is centered on the equator. All other pictures are nominally scheduled at intervals of 25 seconds from this reference frame. Figure 5-11 also shows the picture centers (rows) for each scene over the U.S.

ATTACHED TO INSIDE BACK COVER

Figure 5-11. U. S. Map Keyed to Landsat World Wide Reference System

SECTION 6

POST-LAUNCH CALIBRATION AND EVALUATION

SECTION 6

POST-LAUNCH CALIBRATION AND EVALUATION

6.1 TECHNIQUE FOR GENERATING MIRROR VELOCITY PROFILE

A method to obtain a mirror velocity profile is to identify sweep pixel numbers at known ground distances. This technique was used on Landsat 2. The ground truth used was a matrix of section roads (roads approximately 1 mile apart) with accurate distances being obtained from USGS maps. Interactive processing of the Landsat scene was used to enhance the road signature and enlarge the scene. Sweep pixel numbers were obtained at road intersections. Various algorithms are necessay to make the corrections for Landsat orbit which is oblique to the roads, earth rotation, Landsat height, etc. Once the various corrections are made, mirror velocity and error curves can be obtained from the data.

6.2 POSITIONAL ACCURACY

The geometric accuracy of the processed images using available data averages less than one kilometer. The maximum error is two kilometers. The geometric errors display a small seasonal variation with summer at the positive peak and winter at the negative peak.

This geometric accuracy will be maintained for Landsat 3 images after initial calibration of AMS attitude parameters. It is expected that the same seasonal variation will still exist unless the IR horizon equations are updated or redefined. (See AMS Standard ICD for complete description.)

6.3 RADIOMETRIC CALIBRATION ADJUSTMENT

As discussed in paragraph 5.1.1, MSS calibration can be adjusted using M and A parameters. Analysis of calibrated image data has been used to determine values of M and A for the purpose of minimizing striping. Tables 6-1, 6-2 and 6-3 list the values which have been defined for Landsats 1, 2 and 3 respectively. Note that M and A values are adjusted (at present) only for the normal operating modes, i. e., low gain-compressed for bands 4, 5 and 6 and low gain linear for band 7. All other modes use values M = 1 and A = 0.

Table 6-1. M & A Values for Landsat 1
Detectors 1-18, Low-Compresser
Detectors 19-24, Low-Linear

Detector	M	A
1	1.008	-0.92
2	0.984	0.21
3	0.988	0.24
4	1.016	-0.24
5	0.996	0.57
6	1.004	0.15
7	0.996	-0.06
8	0.984	0.37
9	1.008	-0.32
10	1.004	-0.11
11	1.016	-0.20
12	0.992	0.32
13	0.996	-0.07
14	0.996	-0.05
15	0.996	0.45
16	1.012	0.08
17	1.012	-0.31
18	0.988	-0.11
19	0.948	0.46
20	0.944	0.37
21	1.000	-0.41
22	0.976	-0.41
23	1.080	0.12
24	1.052	-0.12

Table 6-2. M & A Values for Landsat 2
Detectors 1-18, Low-Compresser
Detectors 19-24, Low-Linear

Detector	M	A
1	1.008	-0.21
2	1.004	-0.14
3	1.004	0.16
4	0.996	-0.26
5	1.004	-0.09
6	0.980	0.38
7	1.000	-0.09
8	1.000	-0.02
9	0.996	-0.02
10	0.992	0.14
11	1.004	-0.22
12	1.004	0.17
13	1.000	-0.02
14	1.020	-0.80
15	0.996	0.31
16	0.992	0.15
17	1.000	0.12
18	0.988	0.26
19	1.000	0.06
20	0.996	-0.05
21	1.004	0.08
22	0.992	0.03
23	0.992	0.09
24	1.016	-0.21

Table 6-3. M & A Values for Landsat 3
Detectors 1-18, Low-Compresser
Detectors 19-24, Low-Linear

Detector	Day Since Launch 1 to 49		Day Since Launch 50 +	
	M	A	M	A
1	0.879	0	1.035	0
2	0.883	-0.398	1.039	-0.398
3	0.875	0	1.027	0
4	0.887	0.199	1.047	0.199
5	0.863	0.297	1.016	0.297
6	0.883	-0.098	1.039	-0.098
7	0.871	0.098	0.887	0.098
8	0.867	-0.297	0.887	-0.297
9	0.887	-0.297	0.906	-0.297
10	0.875	0.199	0.891	0.199
11	0.875	-0.199	0.895	-0.199
12	0.855	0.500	0.875	0.500
13	0.883	-0.598	0.910	-0.598
14	0.891	0.398	0.918	0.398
15	0.863	0	0.891	0
16	0.855	0.199	0.883	0.199
17	0.863	-0.098	0.891	-0.098
18	0.887	0.098	0.902	0.098
19	0.965	0.398	0.836	0.398
20	0.969	0	0.840	0
21	1.000	0.199	0.863	0.199
22	0.953	0	0.828	0
23	1.004	-0.199	0.867	-0.199
24	0.980	-0.398	0.848	-0.398

APPENDICES

APPENDIX A

LANDSAT-1 RELATIVE SPECTRAL RESPONSE

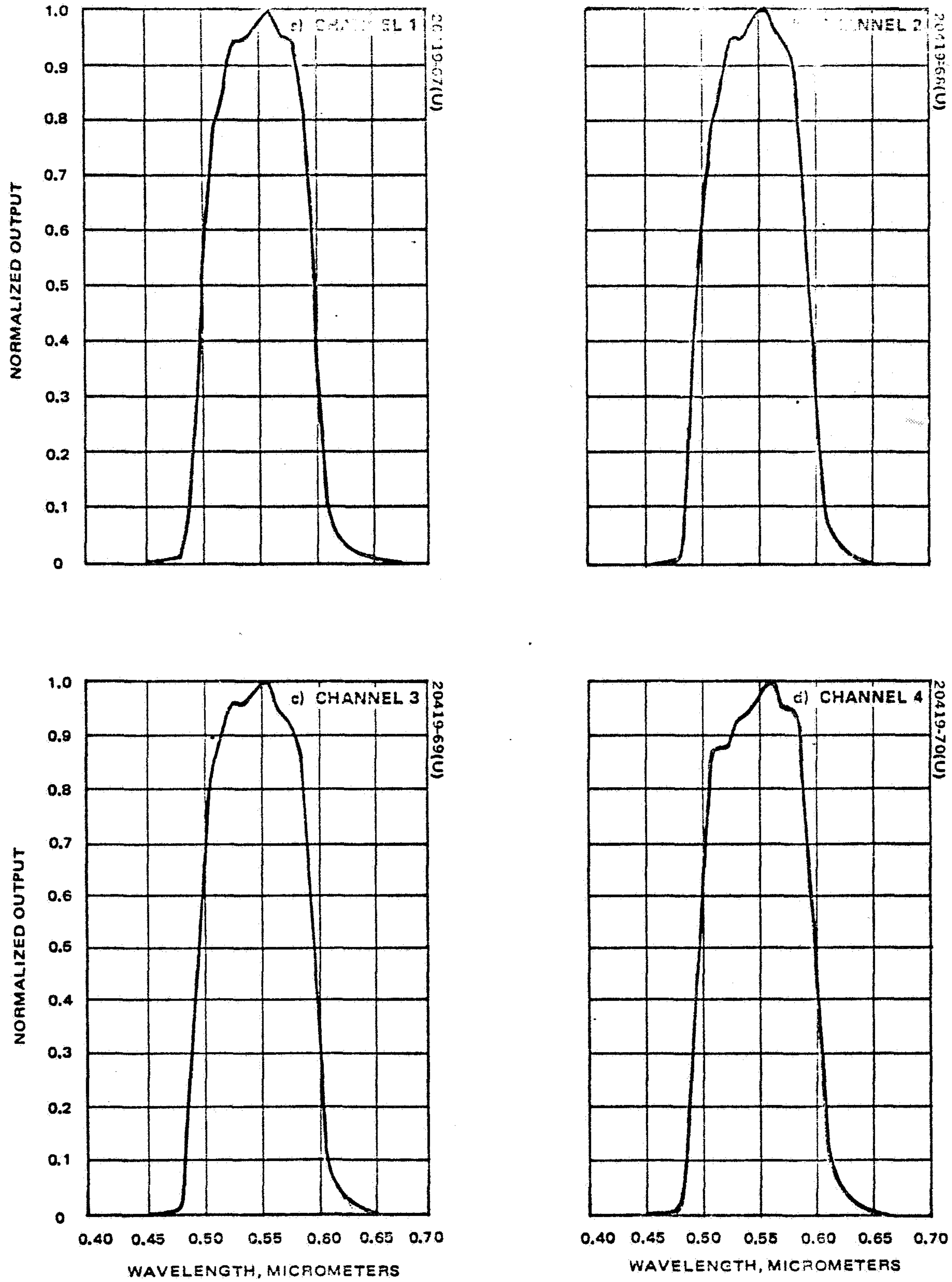

LANDSAT -1 RELATIVE SPECTRAL RESPONSE (Cont'd)

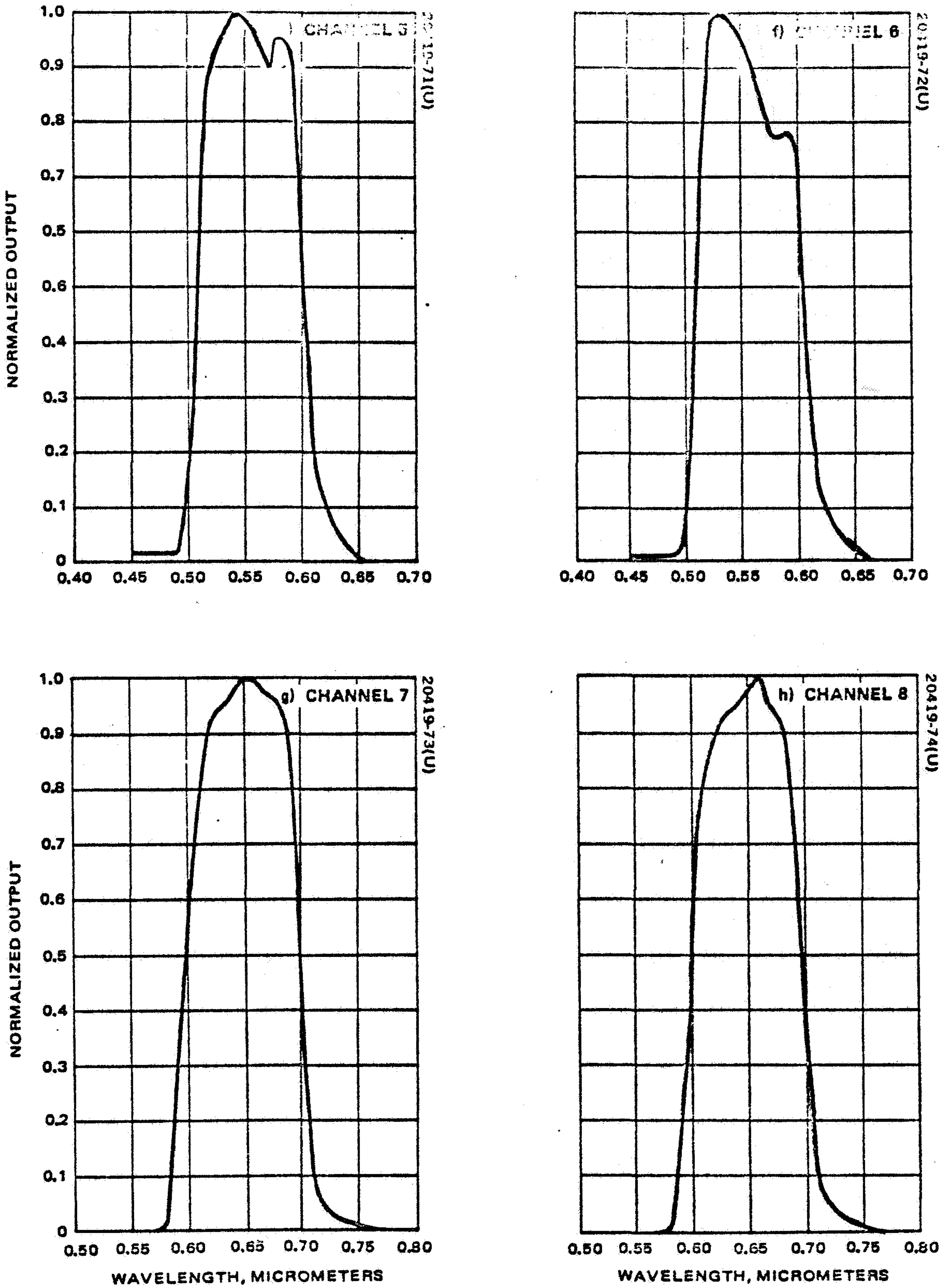

LANDSAT-1 RELATIVE SPECTRAL RESPONSE (Cont'd)

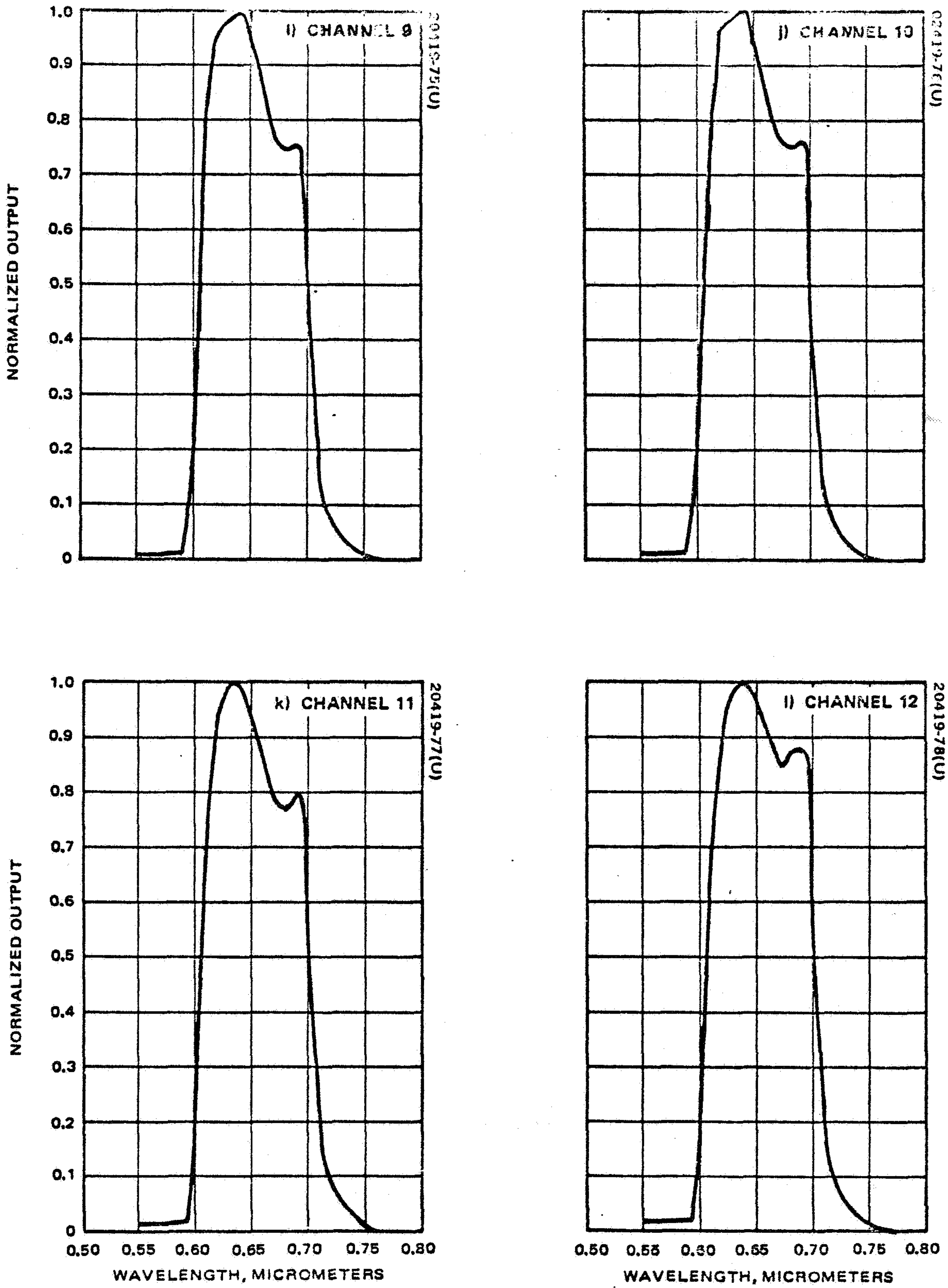

LANDSAT-1 RELATIVE SPECTRAL RESPONSE (Cont'd)

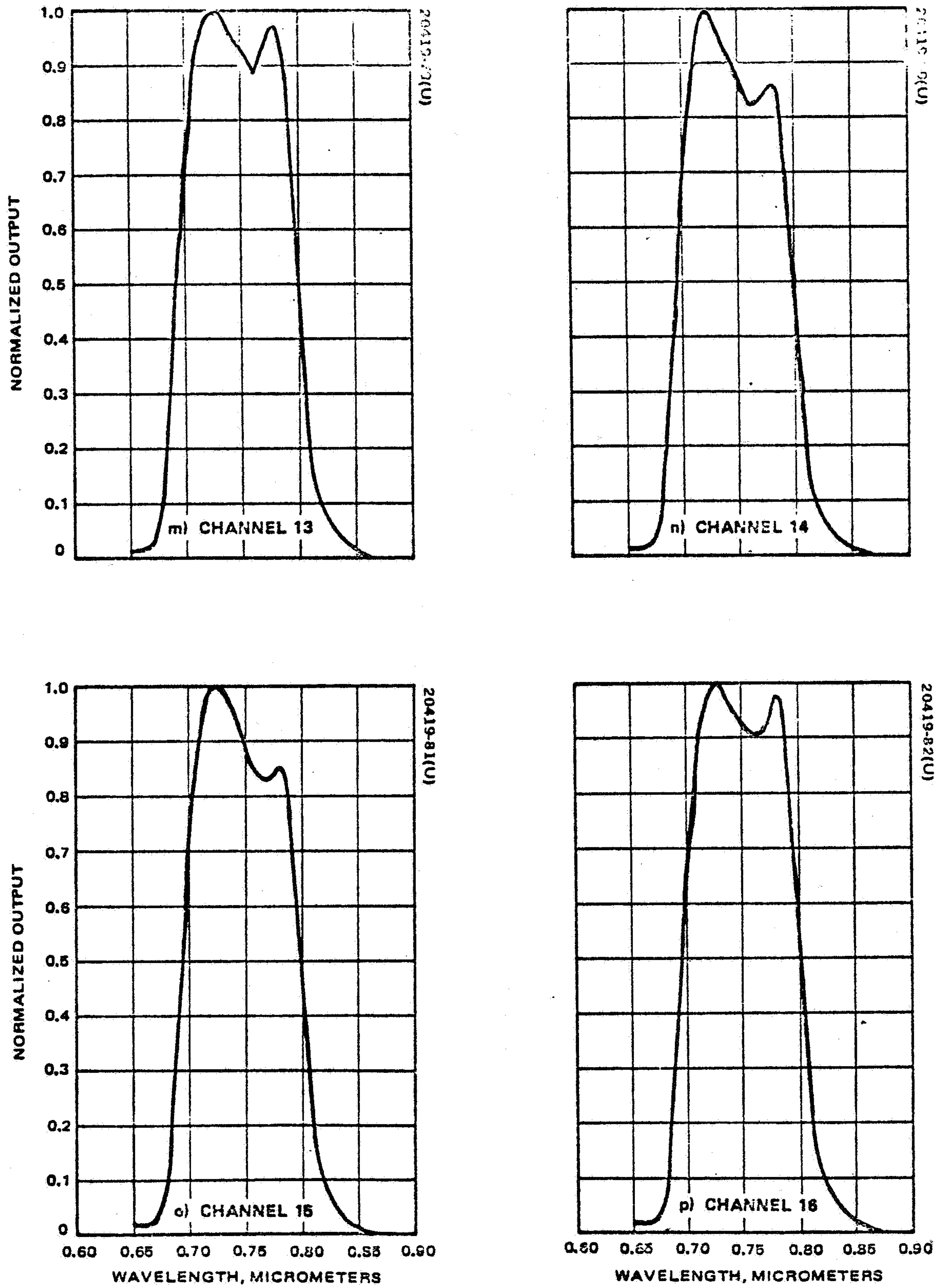

LANDSAT-1 RELATIVE SPECTRAL RESPONSE (Cont'd)

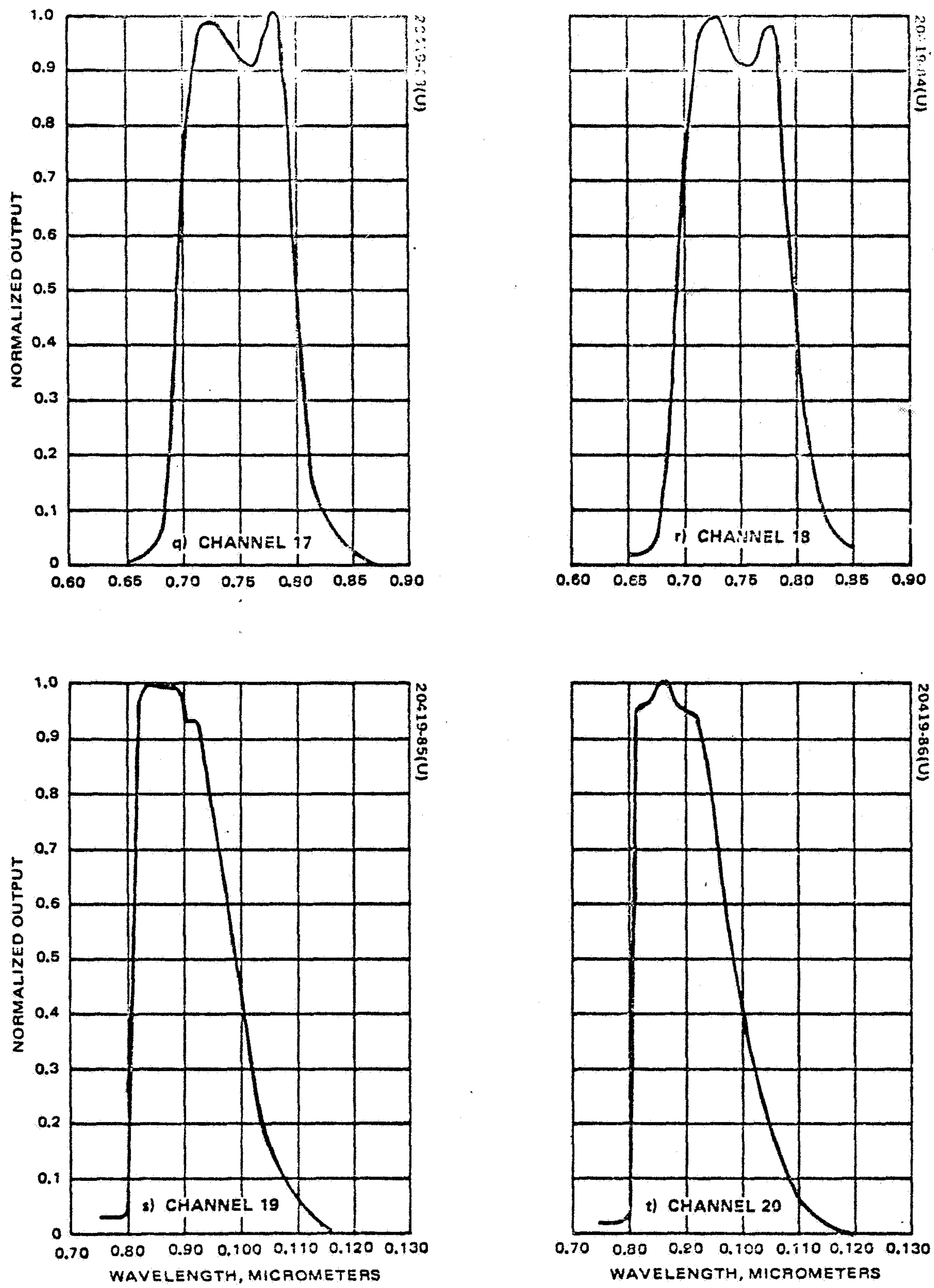

LANDSAT-1 RELATIVE SPECTRAL RESPONSE (Cont'd)

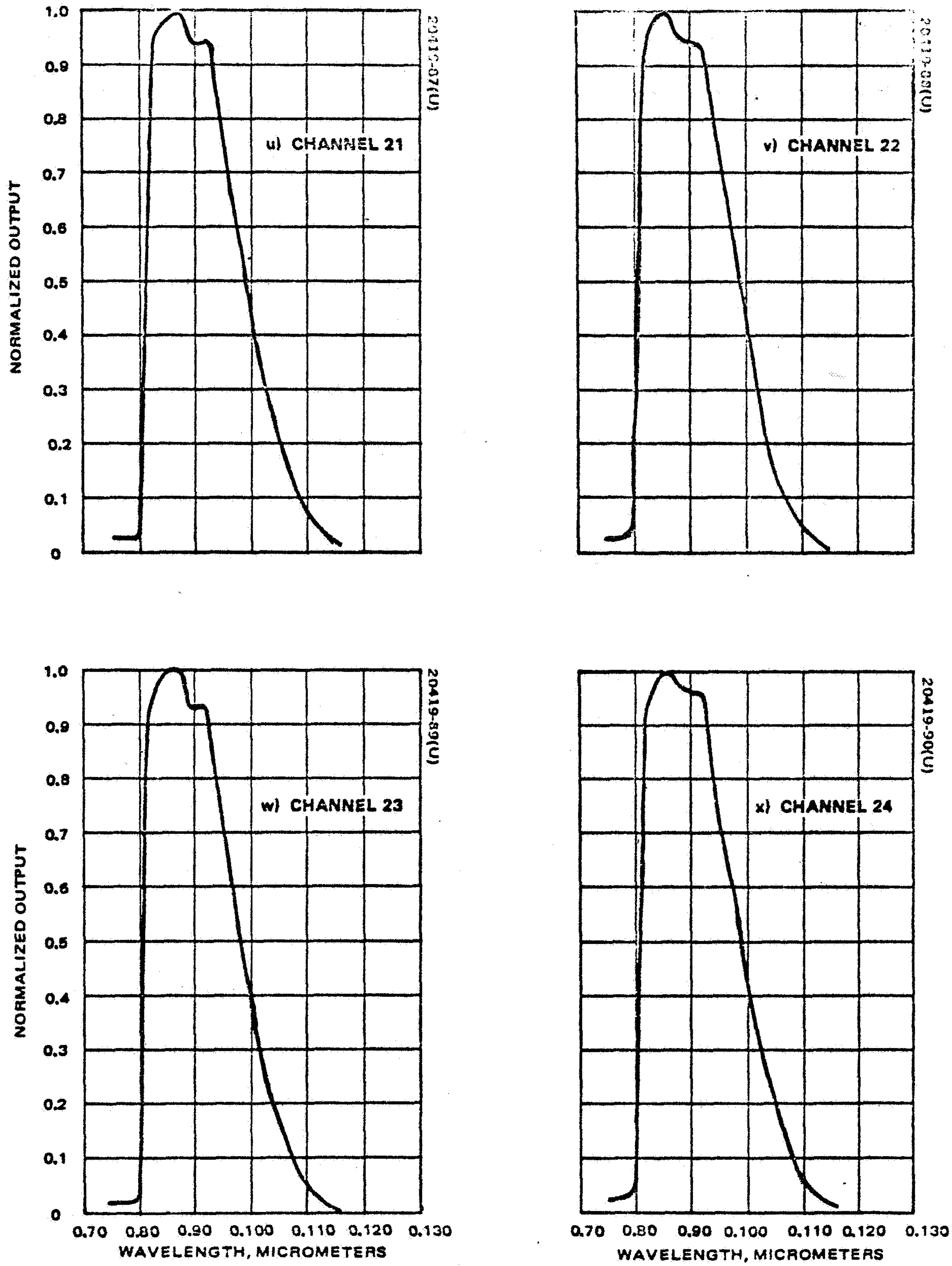

APPENDIX B

LANDSAT-2 RELATIVE SPECTRAL RESPONSE

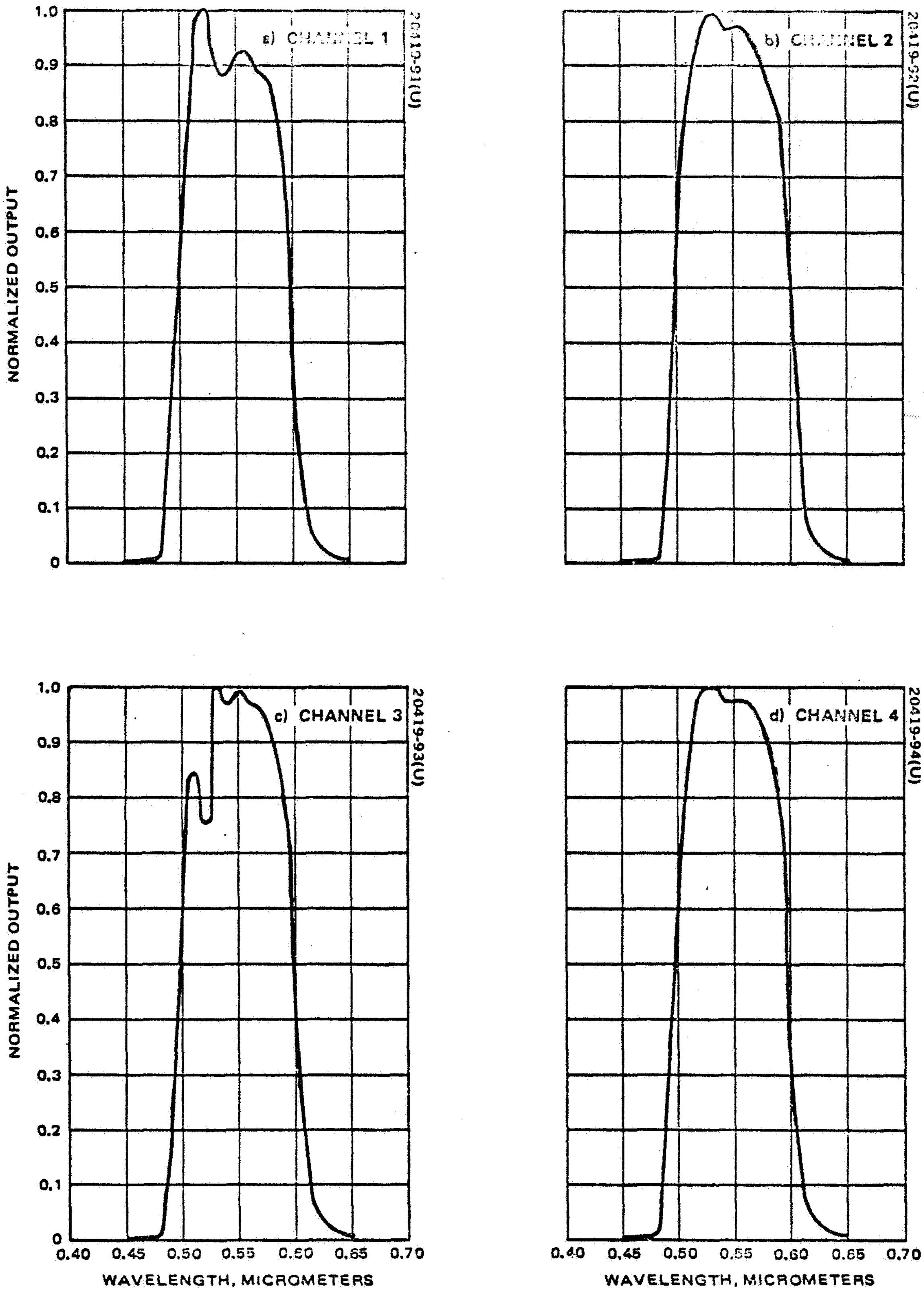

LANDSAT-2 RELATIVE SPECTRAL RESPONSE (Cont'd)

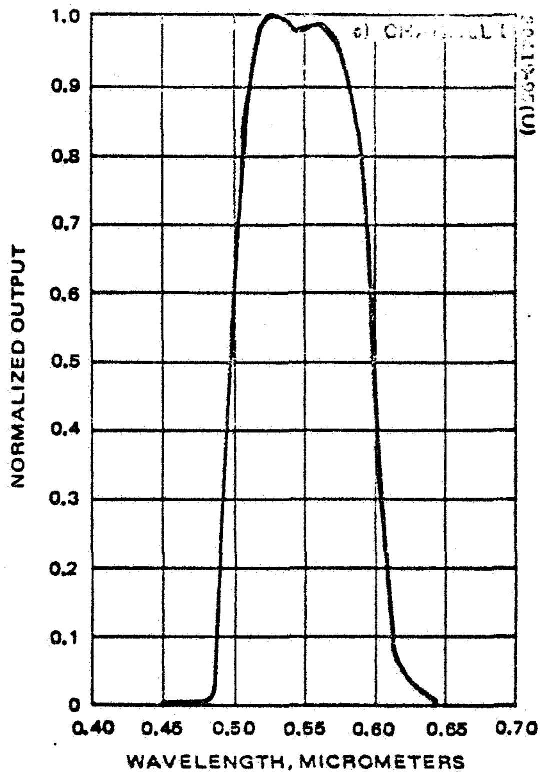

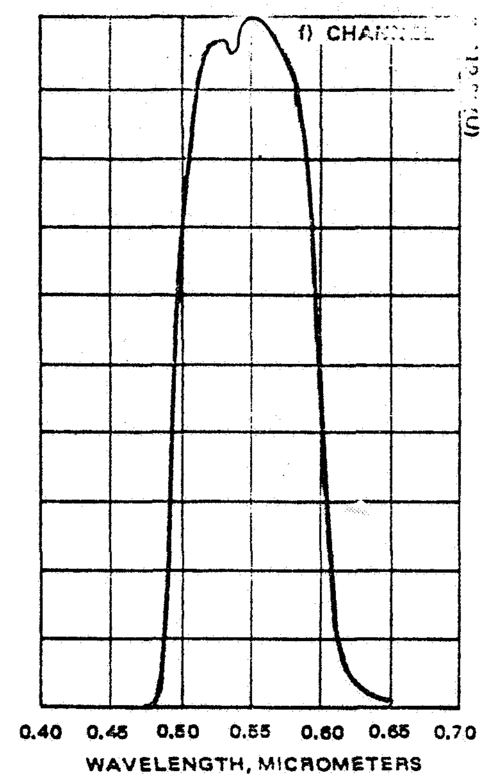

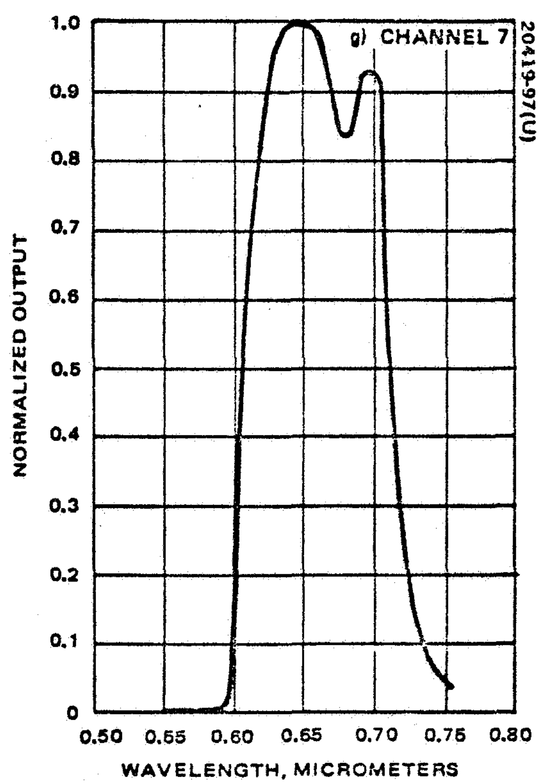

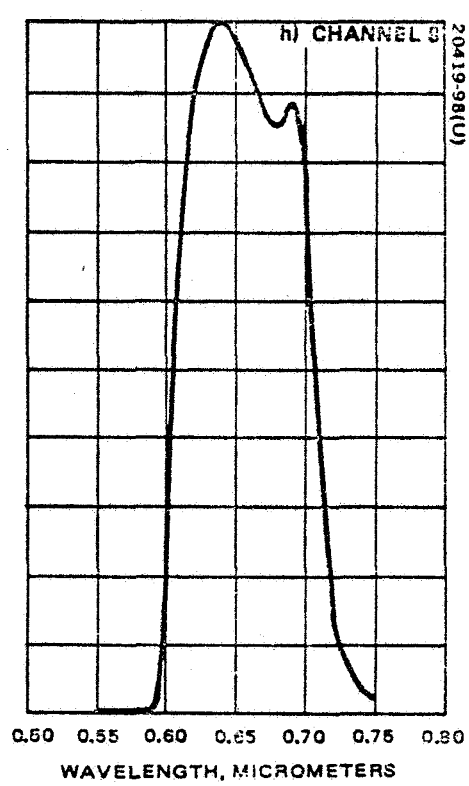

LANDSAT-2 RELATIVE SPECTRAL RESPONSE (Cont'd)

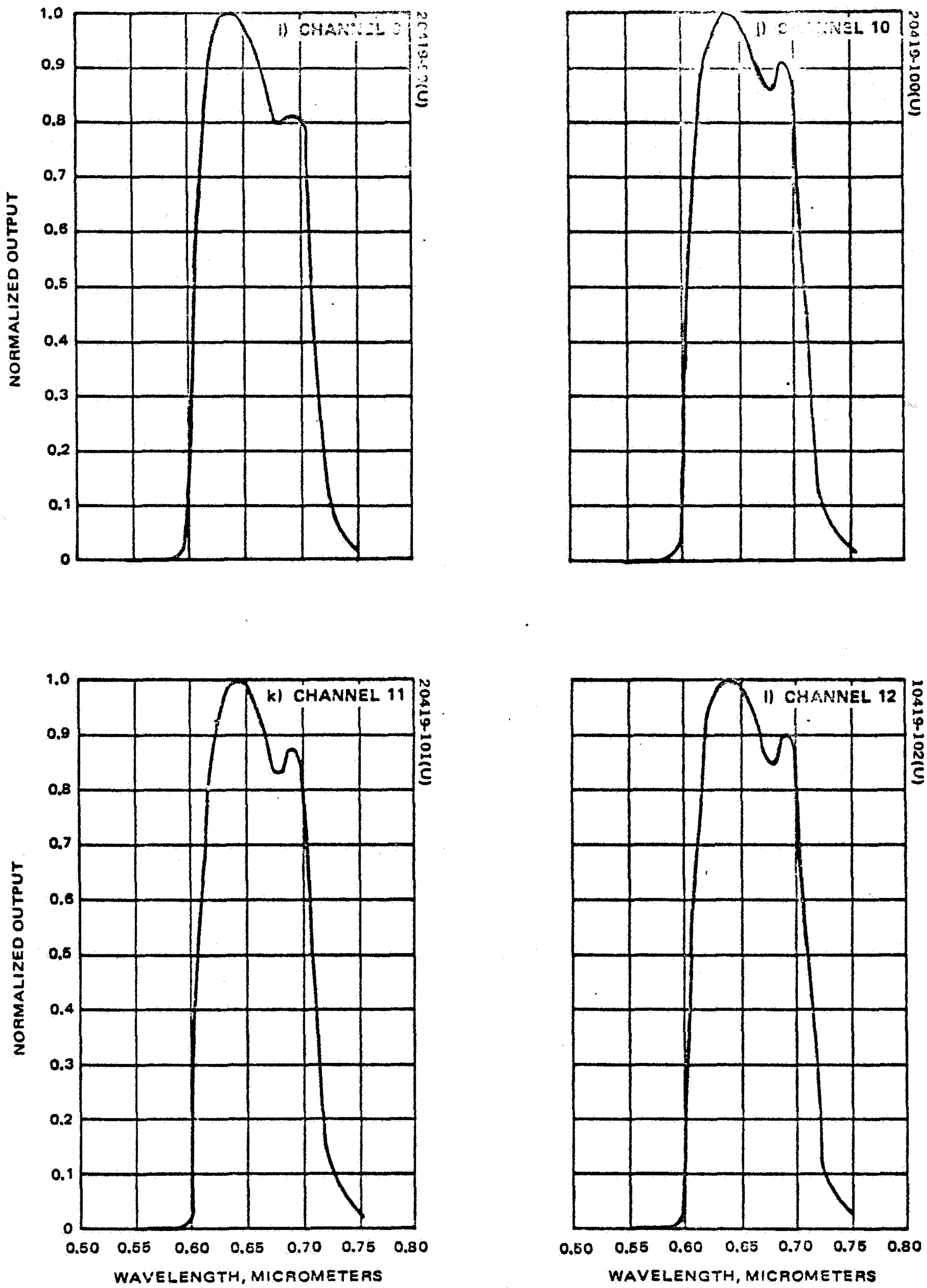

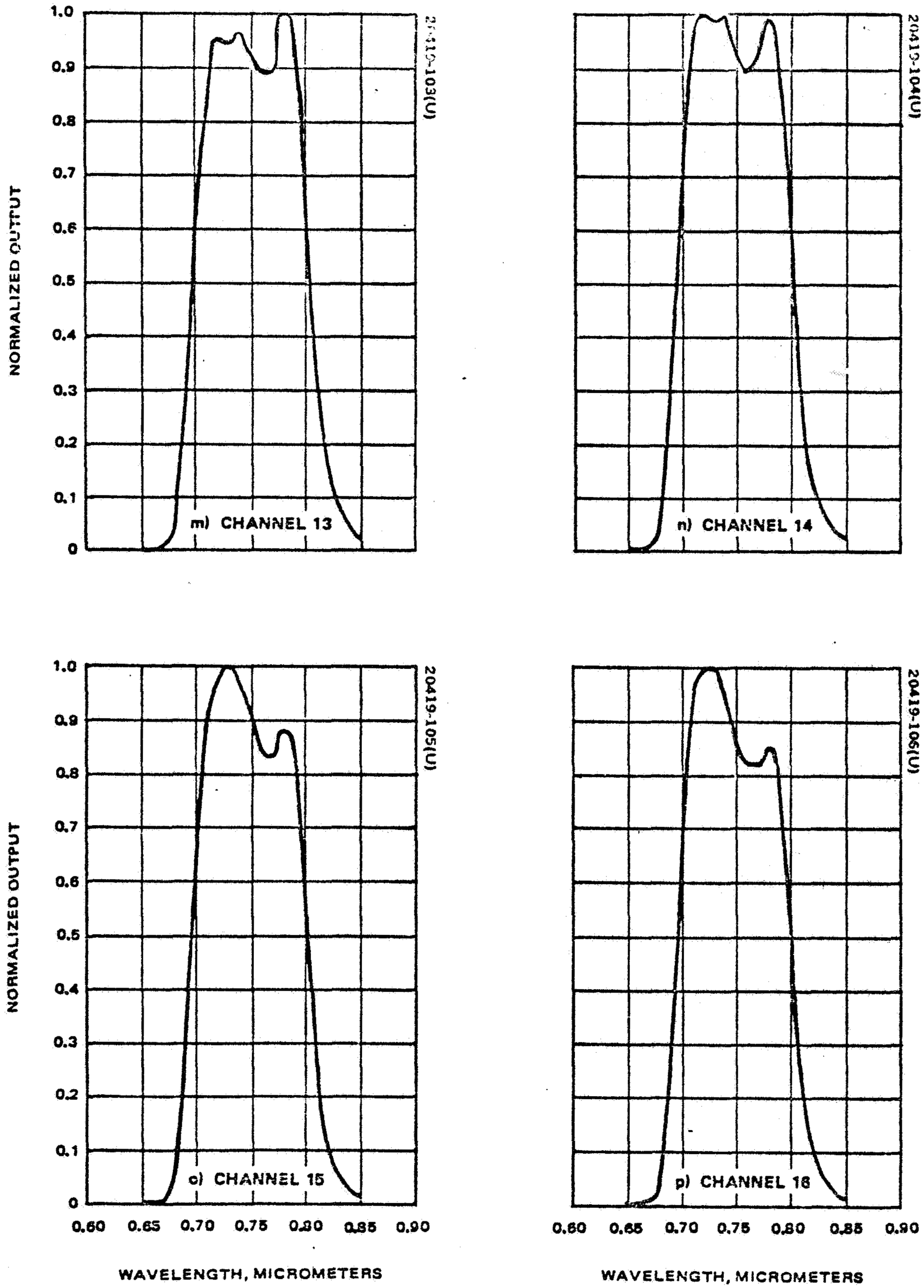
NORMALIZED OUTPUT
1.0
0.9
0.8
0.7
0.6
0.5
0.4
0.3
0.2
0.1
0
m) CHANNEL 13
n) CHANNEL 14
o) CHANNEL 15
p) CHANNEL 16
20419-104(U)
20419-105(U)
20419-106(U)
0.60
0.65
0.70
0.75
0.80
0.85
0.90
WAVELENGTH, MICROMETERS

LANDSAT-2 RELATIVE SPECTRAL RESPONSE (Cont'd)

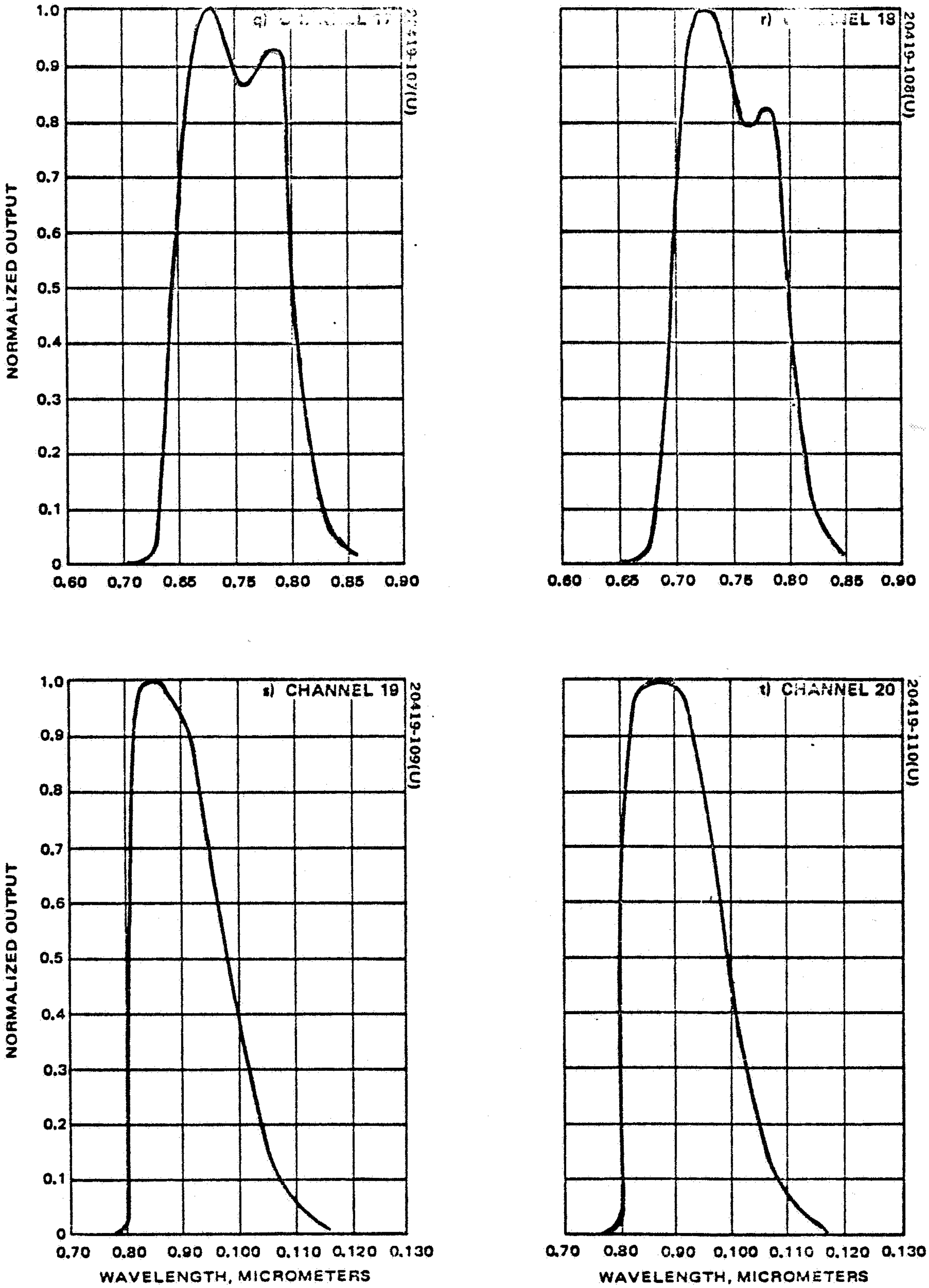

LANDSAT-2 RELATIVE SPECTRAL RESPONSE (Cont'd)

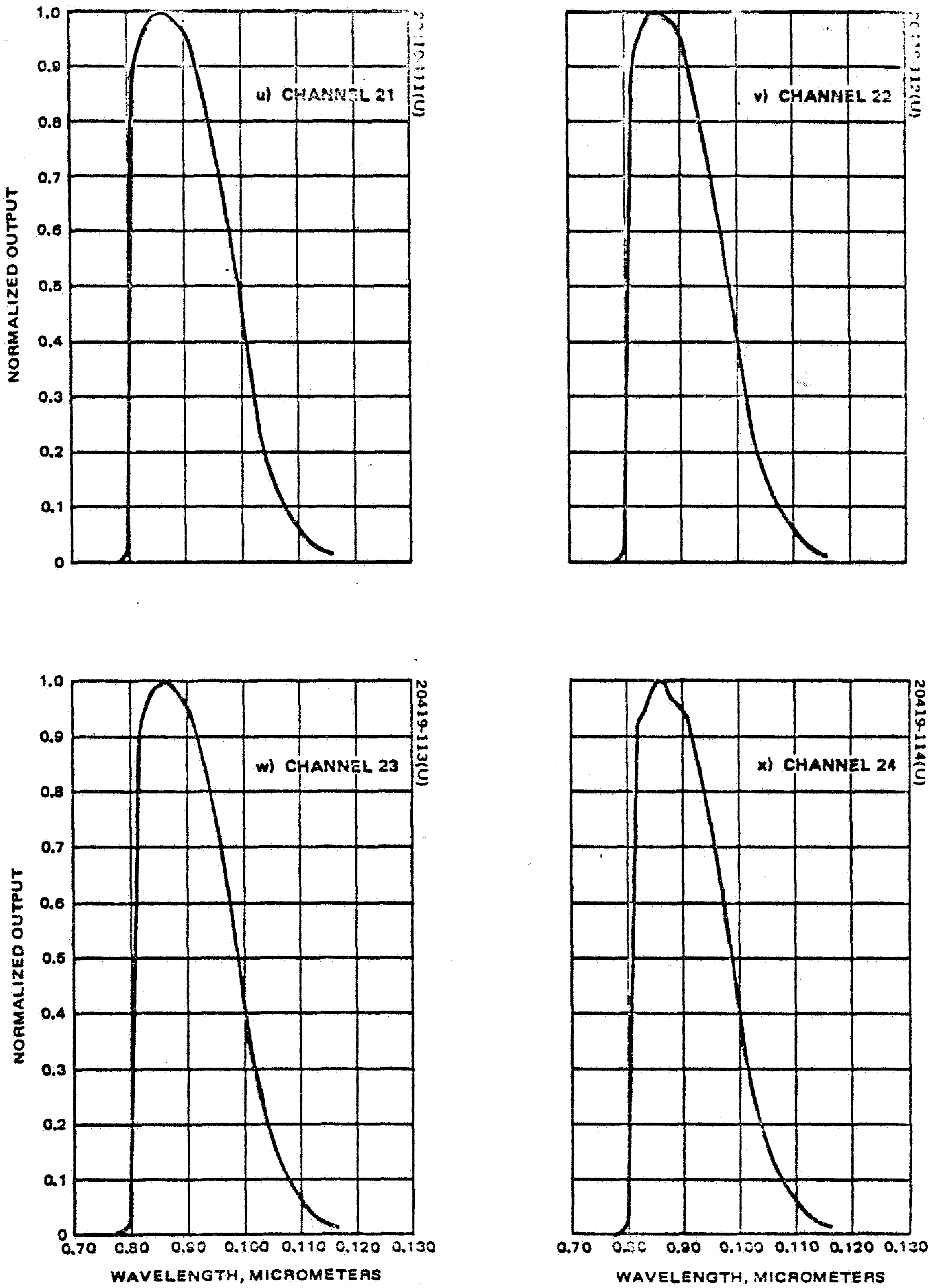

APPENDIX C

LANDSAT-3 RELATIVE SPECTRAL RESPONSE

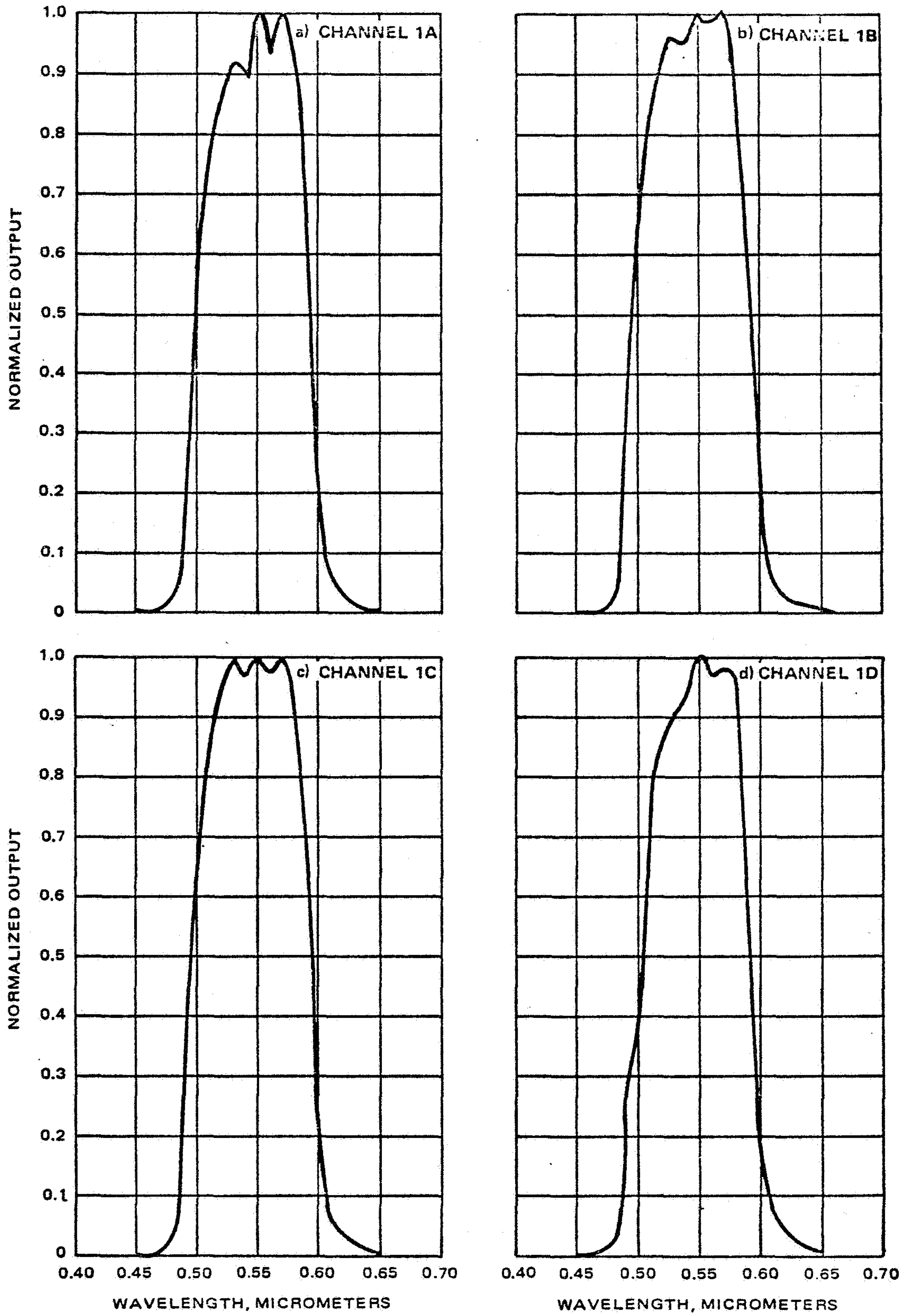

LANDSAT-3 RELATIVE SPECTRAL RESPONSE (Cont'd)

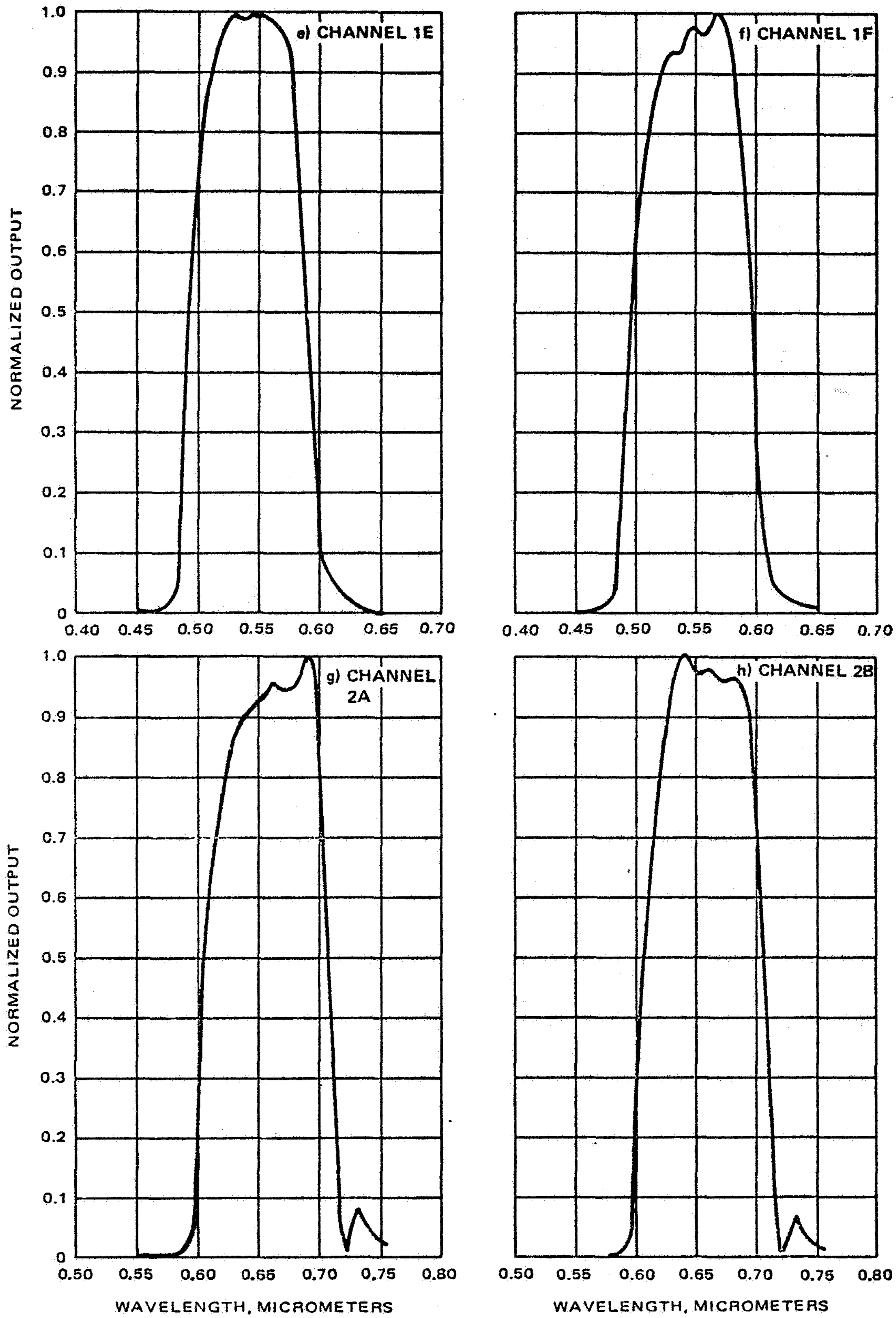

LANDSAT-3 RELATIVE SPECTRAL RESPONSE (Cont'd)

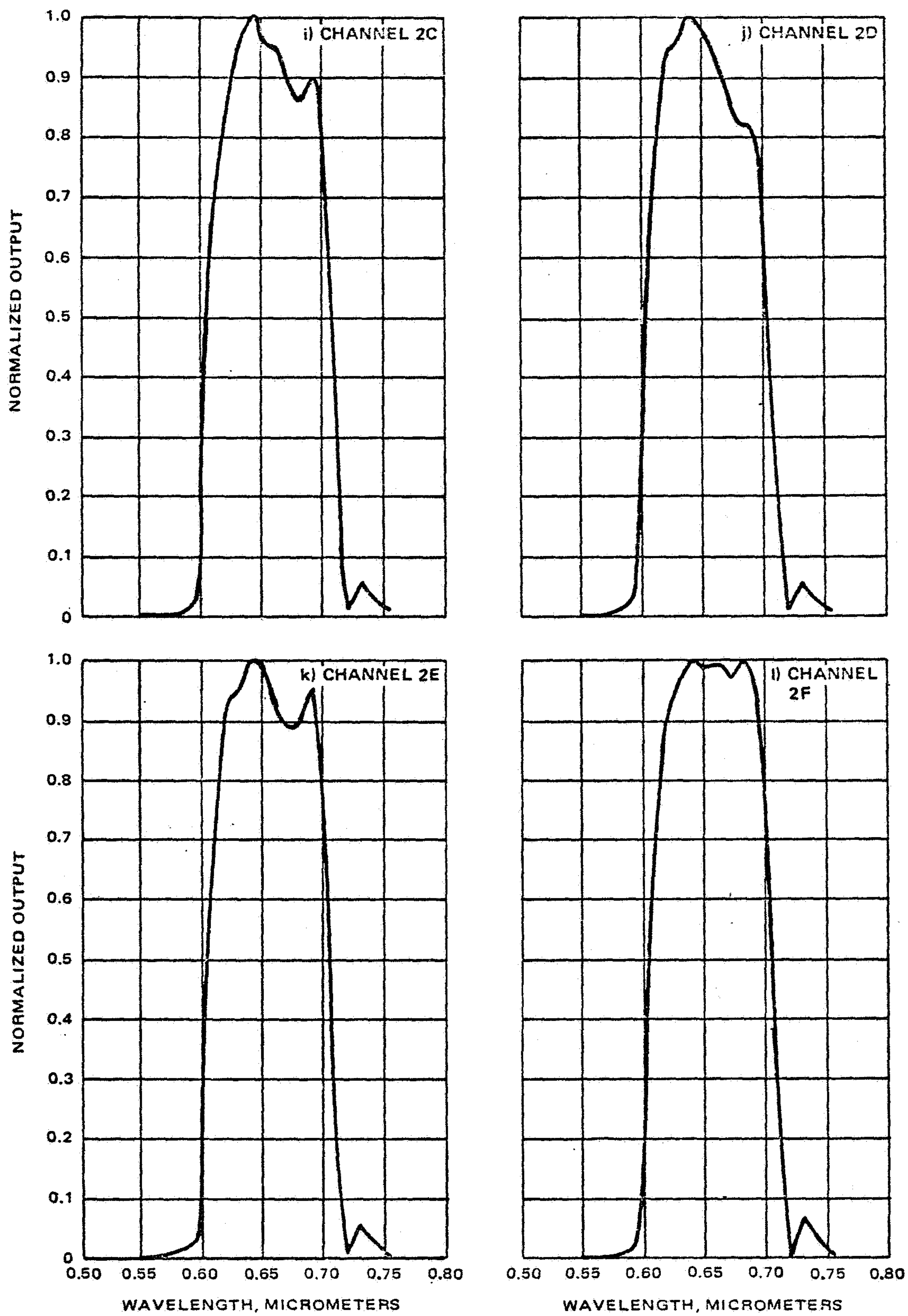

LANDSAT-3 RELATIVE SPECTRAL RESPONSE (Cont'd)

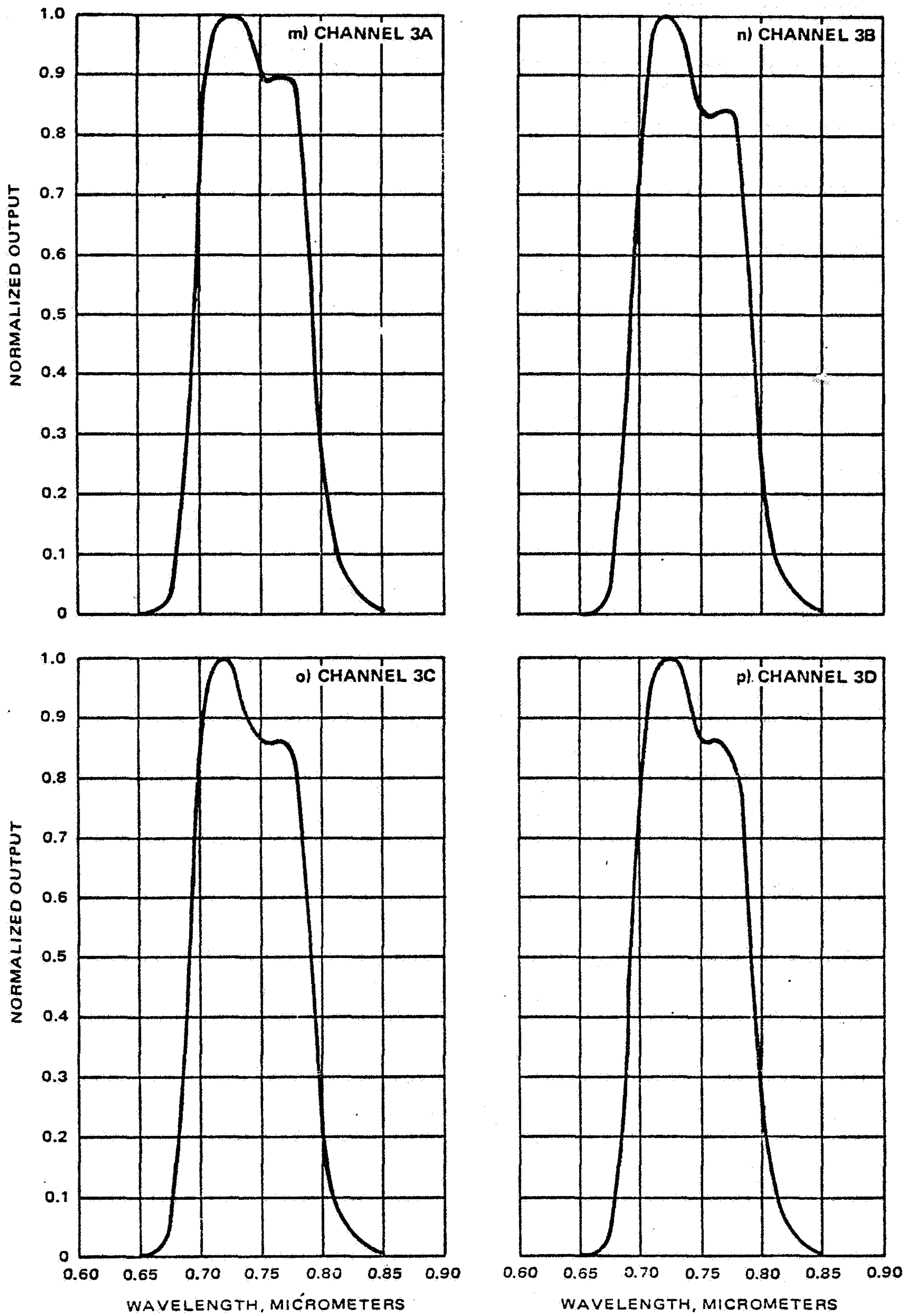

LANDSAT-3 RELATIVE SPECTRAL RESPONSE (Cont'd)

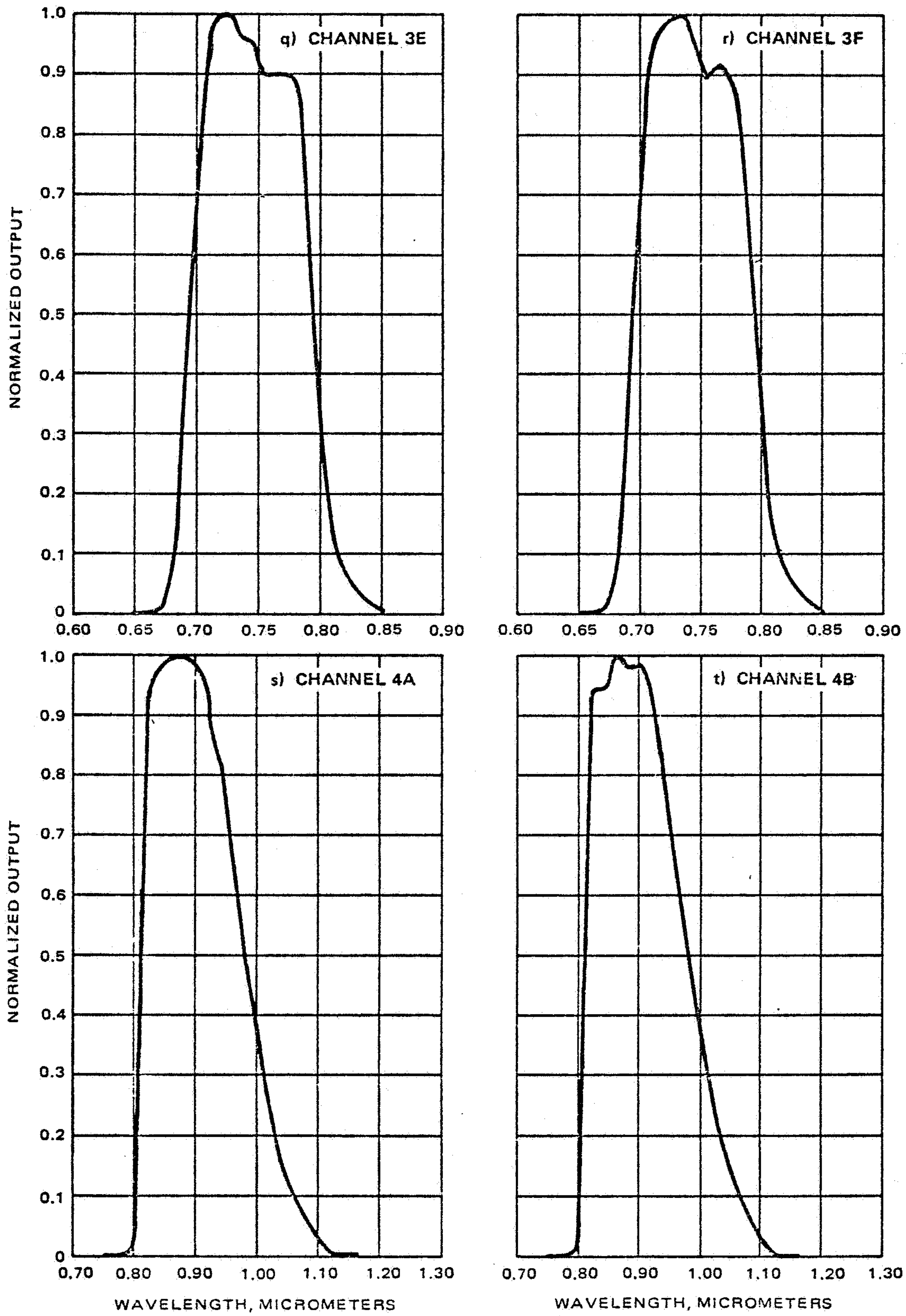

LANDSAT-3 RELATIVE SPECTRAL RESPONSE (Cont'd)

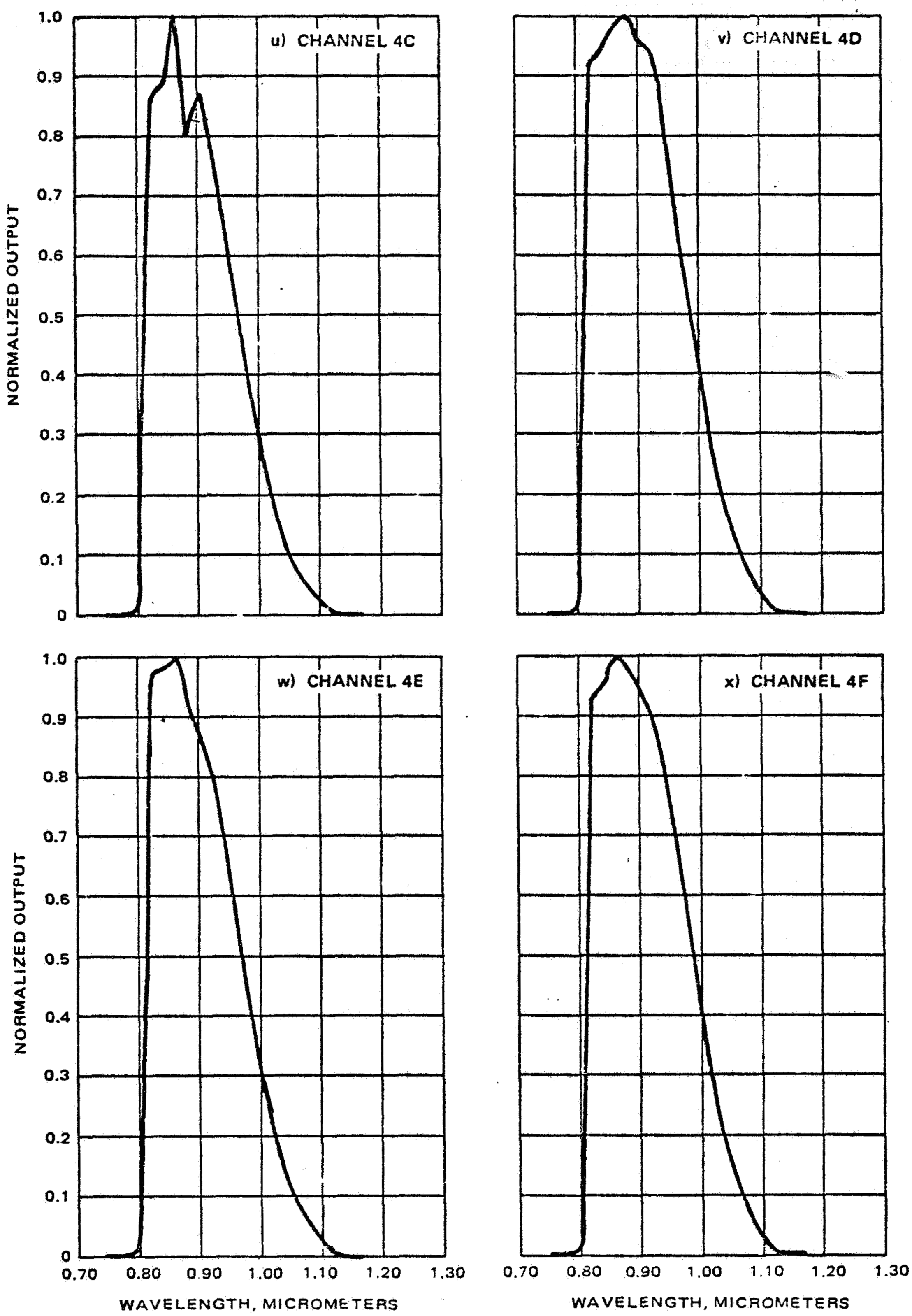

APPENDIX D

SPECTRAL RADIANT EMITTANCE OF 30-INCH SPHERICAL INTEGRATOR
λ IN MILLIMICROMETERS
W_λ IN MILLIWATTS $CM^{-2}\mu^{-1}$

λ	W_λ	$W/m^2\mu$ sr	λ	W_λ	$W/m^2\mu$ sr
320	.423	1.3	1000	166.4	529.7
350	1.51	4.8	1100	155.4	494.7
400	7.34	23.4	1200	136.3	433.9
450	22.2	70.7	1300	122.6	390.2
500	42.6	135.6	1400	97.5	310.4
550	64.4	205.0	1500	80.6	256.6
600	88.2	280.7	1600	70.0	222.8
650	110.0	350.1	1700	64.2	204.4
700	130.5	415.4	1800	51.3	163.3
750	149.8	476.8	1900	33.7	107.3
800	171.7	546.5	2000	27.9	88.8
900	184.3	586.6			

RATIO OF INTENSITY OF N LAMPS
TO 12 LAMPS IN SPHERICAL INTEGRATOR

No. of Lamps	$W_{\lambda N}/W_{\lambda 12}$
12	1.000
11	.9194
10	.8331
9	.7450
8	.6624
7	.5733
6	.4922
5	.4063
4	.3242
3	.2421
2	.1605
1	.0778

Sensor	Elec. Sys. (Task 5.3)		Pre V/T (D0)		VAC 10°C (D22)		VAC 23°C (D13)		VAC 35°C (D16)		Post V/T (D32)	
	Q. L. Signal (50% NDF)	S/N	Q. L. Signal (50% NDF)	S/N	Q. L. Signal (50% NDF)	S/N	Q. L. Signal (50% NDF)	S/N	Q. L. Signal (50% NDF)	S/N	Q. L. Signal (50% NDF)	S/N
1	24.8	55.1	25.6	50.4	26.0	52.2	25.0	49.1	23.5	63.2	24.6	67.3
2	25.1	54.1	25.5	50.8	26.1	54.6	24.7	56.0	23.1	44.9	25.0	51.2
3	25.1	60.9	26.0	53.7	25.8	57.2	24.7	54.3	23.8	54.6	25.7	54.7
4	24.6	50.6	25.4	55.0	26.0	59.4	24.8	58.5	23.4	44.1	24.3	55.3
5	25.8	53.8	26.5	57.3	27.0	57.1	24.9	56.3	24.5	47.2	26.0	61.1
6	25.0	47.0	25.7	48.9	26.1	46.5	25.0	65.8	23.8	58.9	26.0	52.0
7	36.5	73.2	37.8	77.4	40.7	69.2	39.0	72.8	36.8	71.2	37.4	62.9
8	36.2	59.2	37.7	68.0	41.8	69.0	39.3	63.9	36.3	56.8	37.3	64.7
9	33.8	64.3	33.9	54.0	38.0	57.2	35.7	64.5	32.6	52.2	33.0	65.0
10	35.4	61.4	36.6	59.4	40.3	66.4	38.5	55.6	36.0	72.2	36.2	78.5
11	34.2	63.1	35.1	68.5	39.0	59.7	37.1	70.2	34.3	66.0	34.8	57.4
12	36.5	59.6	37.6	56.5	41.6	61.9	39.5	70.9	36.7	65.0	37.3	64.0
13	37.1	-	39.5	49.5	43.8	48.4	40.9	50.6	36.7	45.6	38.7	50.4
14	40.5	43.6	43.0	48.3	46.3	50.4	43.0	49.2	39.6	47.5	41.7	43.3
15	40.6	55.8	43.6	59.7	45.6	59.5	43.4	51.2	40.5	53.9	43.3	54.5
16	38.1	47.6	41.3	52.4	42.0	58.0	40.5	57.6	38.9	49.1	40.6	51.1
17	37.0	61.7	40.0	52.9	43.0	68.7	40.3	63.4	36.9	58.0	39.2	61.8
18	37.0	49.2	38.9	67.7	41.8	63.9	39.6	59.3	36.3	62.1	38.8	68.3
19	39.2	98.9	44.0	105.2	44.5	102.2	43.9	92.4	45.4	113.1	45.4	100.7
20	38.7	83.2	43.1	95.7	43.8	107.6	43.1	103.6	44.8	96.6	44.2	114.3
21	38.9	70.6	43.3	79.1	43.4	82.5	43.5	78.4	45.1	76.3	44.6	72.8
22	38.2	-	42.7	103.9	43.2	117.9	42.8	123.7	44.7	106.1	44.0	135.7
23	37.3	-	42.3	78.4	42.9	87.1	42.5	82.4	44.2	77.2	43.5	86.5
24	33.1	88.3	37.5	75.9	35.3	105.1	32.2	89.8	38.8	122.7	38.4	82.1

All data from prime linear low mode.

APPENDIX E

QUANTUM LEVEL SIGNAL AND SIGNAL-TO-NOISE RATIO AT 50% NDF

Sensor	Elect. Sys. (Task 5.3)		Pre V/T (C0)		VAC 10°C (C27)		VAC 23°C (C14)		VAC 35°C (C16)		Post V/T (C23)	
	Q. L. Signal (50% NDF)	S/N	Q. L. Signal (50% NDF)	S/N	Q. L. Signal (50% NDF)	S/N	Q. L. Signal (50% NDF)	S/N	Q. L. Signal (50% NDF)	S/N	Q. L. Signal (50% NDF)	S/N
1	37.0	62.6	37.0	55.3	37.4	52.0	36.1	71.0	35.2	58.8	36.1	57.4
2	36.2	48.9	36.8	48.8	37.5	45.4	35.9	49.1	34.7	52.0	36.3	52.0
3	33.9	48.3	37.3	47.3	37.1	61.7	35.9	55.2	35.4	52.1	37.1	71.5
4	33.9	57.6	36.9	59.0	37.2	56.0	36.0	71.2	35.0	81.9	36.0	51.4
5	38.0	49.3	37.9	57.1	38.4	47.8	37.1	52.5	36.1	55.2	37.5	44.0
6	36.0	50.8	37.1	52.2	37.5	46.4	36.1	59.7	35.2	60.6	37.2	53.2
7	45.6	56.2	46.2	48.0	48.1	68.5	46.5	58.3	45.5	56.6	45.7	60.2
8	46.1	61.4	46.1	47.3	48.9	62.4	46.6	58.8	45.4	48.2	45.8	58.5
9	43.3	50.9	43.6	49.8	46.3	58.9	44.0	57.0	47.4	65.8	42.8	59.3
10	45.5	59.6	45.4	55.8	48.0	77.0	46.2	54.1	45.0	-	45.1	78.2
11	44.2	61.9	44.5	49.4	47.0	68.2	45.0	-	43.9	64.9	44.2	60.9
12	45.6	53.4	46.1	60.9	48.9	69.2	46.9	64.0	45.5	54.0	45.9	57.9
13	46.4	49.2	47.6	44.3	51.0	49.3	47.4	48.5	45.3	76.0	46.8	51.8
14	47.6	45.2	49.5	46.1	51.5	50.5	49.1	45.6	47.6	45.7	48.8	11.3
15	49.5	47.3	50.5	55.0	51.7	48.6	49.5	52.7	48.2	52.8	49.8	53.2
16	47.1	56.3	48.5	49.7	49.1	54.5	47.8	51.6	46.9	67.8	48.2	57.5
17	42.4	-	47.7	50.8	50.1	58.2	47.2	61.3	45.7	63.1	47.2	52.8
18	41.5	-	47.2	72.0	49.1	67.4	46.8	56.2	45.1	62.2	46.8	56.9
19	39.1	149.6	43.8	97.1	44.6	97.0	44.4	109.3	45.3	152.3	45.1	128.8
20	38.4	80.9	42.9	101.0	43.8	139.7	43.6	91.0	44.8	102.8	43.9	84.9
21	38.8	81.5	43.3	63.7	43.7	66.1	44.0	81.2	45.0	110.9	44.3	81.2
22	38.7	-	42.4	95.0	43.1	119.5	43.3	124.1	44.5	185.2	43.9	138.9
23	38.0	60.9	42.2	78.8	43.2	77.5	42.9	85.1	44.1	117.2	43.4	83.3
24	32.8	119.4	37.2	103.3	37.9	113.1	37.6	81.7	38.4	113.7	38.2	96.0

Data from prime compressed low mode.

APPENDIX F

QUANTUM LEVEL SIGNAL AND SIGNAL-TO-NOISE RATIO AT 50% NDF

APPENDIX G

MEAN SIGNAL AND NEΔT (AT GAINSTEP 4)

Scene Temp °K	VAC 35°C		VAC 20°C		VAC 10°C		Sensor No.
	Mean Sig.	NEΔT	Mean Sig.	NEΔT	Mean Sig.	NEΔT	
Initial Det. Cooldown							
260	0.42	1.14	0.38	1.36	0.41	1.25	25
280	0.82	1.16	0.79	1.27	0.80	1.28	25
300	1.32	1.23	1.26	1.23	1.31	1.17	25
320	1.90	1.30	1.79	1.33	1.87	1.18	25
340	2.46	1.22	2.40	1.28	2.52	1.28	25
260	0.27	1.43	0.25	1.43	0.25	1.78	26
280	0.66	1.66	0.61	1.49	0.62	1.65	26
300	1.11	1.42	1.04	1.44	1.08	1.48	26
320	1.65	1.67	1.52	1.29	1.62	1.49	26
340	2.17	1.42	2.10	-	2.23	1.32	26
2nd Det. Cooldown							
260	0.64	1.08	0.91	1.01	0.22	0.72	25
280	1.18	0.99	1.47	1.08	1.45	0.91	25
300	1.85	1.04	2.16	1.04	2.16	0.96	25
320	2.70	1.05	2.96	0.89	2.99	0.94	25
340	3.63	1.01	3.89	1.01	3.95	0.62	25
260	0.49	1.06	.74	1.00	0.09	0.68	26
280	1.00	0.88	1.24	1.12	1.24	0.94	26
300	1.61	1.08	1.88	1.00	1.88	1.03	26
320	2.41	0.93	2.63	1.13	2.66	1.00	26
340	3.26	1.09	3.49	0.84	3.56	1.13	26

APPENDIX H

MSS MTF FOR 225 FOOT BAR TARGET (BANDS 1 THROUGH 4)

Sensor	Mode	Elec. Systems Task 5.3		VAC 10°C		VAC 35°C		Post V/T	
		PRI	Red	PRI (D25)	Red (B25)	PRI (D18)	Red (B18)	PRI (D32)	Red (B32)
1	LL	0.38	0.40	0.46	0.47	0.46	0.46	0.45	0.47
2	LL	0.42	0.38	0.46	0.47	0.47	0.46	0.44	0.43
3	LL	0.38	0.38	0.46	0.44	0.45	0.46	0.43	0.49
4	LL	0.38	0.40	0.46	0.43	0.46	0.46	0.45	0.43
5	LL	0.41	0.38	0.44	0.49	0.49	0.46	0.42	0.44
6	LL	0.44	0.44	0.44	0.45	0.45	0.42	0.46	0.47
7	LL	0.41	0.38	0.47	0.47	0.50	0.48	0.41	0.46
8	LL	0.38	0.38	0.46	0.48	0.48	0.48	0.43	0.51
9	LL	0.41	0.38	0.47	0.48	0.45	0.48	0.48	0.49
10	LL	0.39	0.36	0.50	0.47	0.43	0.46	0.44	0.45
11	LL	0.39	0.37	0.48	0.47	0.43	0.46	0.44	0.46
12	LL	0.38	0.41	0.48	0.48	0.50	0.47	0.46	0.49
13	LL	0.41	0.41	0.53	0.53	0.55	0.50	0.47	0.52
14	LL	0.38	0.36	0.50	0.43	0.50	0.55	0.43	0.46
15	LL	0.37	0.37	0.48	0.47	0.43	0.48	0.43	0.46
16	LL	0.41	0.41	0.52	0.50	0.51	0.49	0.47	0.48
17	LL	0.39	0.41	0.48	0.46	0.44	0.45	0.44	0.47
18	LL	0.39	0.41	0.45	0.46	0.45	0.43	0.44	0.47
19	LL	0.38	0.35	0.45	0.44	0.48	0.48	0.40	0.42
20	LL	0.41	0.46	0.50	0.54	0.51	0.53	0.48	0.50
21	LL	0.41	0.41	0.45	0.49	0.48	0.46	0.43	0.45
22	LL	0.44	0.46	0.55	0.57	0.54	0.56	0.50	0.53
23	LL	0.51	0.53	0.58	0.60	0.61	0.58	0.53	0.58
24	LL	0.41	0.38	0.45	0.46	0.46	0.46	0.44	0.44

APPENDIX I

MSS BAND 5 IRMTF FOR 780' BAR TARGET

Sensor No.	VAC 10°C	VAC 20°C	VAC 35°C
25	45.2	46.5	46.2
26	45.6	46.6	49.0

APPENDIX J

LANDSAT-2 MSS EQUIVALENT RADIANCE
(MW/CM^2 SR)

Sensor	BULBS							
	1	2	3	4	5	6	9	12
1	0.177	0.361	0.539	0.722	0.907	1.09	1.64	2.19
2	0.176	0.359	0.535	0.717	0.901	1.08	1.63	2.18
3	0.178	0.363	0.540	0.724	0.910	1.09	1.65	2.20
4	0.176	0.359	0.535	0.717	0.902	1.08	1.63	2.18
5	0.176	0.359	0.535	0.716	0.900	1.08	1.63	2.18
6	0.177	0.361	0.538	0.720	0.905	1.09	1.64	2.19
7	0.318	0.649	0.967	1.30	1.63	1.96		
8	0.315	0.643	0.958	1.28	1.61	1.94		
9	0.317	0.646	0.962	1.29	1.62	1.95		
10	0.317	0.646	0.963	1.29	1.62	1.95		
11	0.317	0.647	0.963	1.29	1.62	1.95		
12	0.318	0.648	0.966	1.29	1.63	1.96		
13	0.417	0.850	1.27	1.70	2.13			
14	0.414	0.843	1.26	1.68	2.12			
15	0.412	0.841	1.25	1.68	2.11			
16	0.412	0.841	1.25	1.68	2.11			
17	0.415	0.846	1.26	1.69	2.12			
18	0.412	0.840	1.25	1.68	2.11			
19	1.44	2.94	4.39					
20	1.45	2.95	4.39					
21	1.45	2.95	4.39					
22	1.45	2.95	4.39					
23	1.44	2.95	4.39					
24	1.45	2.95	4.39					

APPENDIX K

LANDSAT-3 MSS EQUIVALENT RADIANCE (MW/CM^2 SR)

Sensor	BULBS							
	1	2	3	4	5	6	9	12
1	0.158	0.327	0.493	0.660	0.827	1.002	1.516	2.035
2	0.155	0.320	0.483	0.647	0.811	0.982	1.486	1.995
3	0.157	0.323	0.488	0.653	0.819	0.992	1.501	2.015
4	0.158	0.327	0.493	0.660	0.827	1.002	1.517	2.036
5	0.152	0.313	0.473	0.633	0.793	0.961	1.454	1.952
6	0.158	0.326	0.492	0.659	0.826	1.001	1.515	2.033
7	0.279	0.575	0.868	1.162	1.456	1.764		
8	0.277	0.571	0.862	1.154	1.446	1.752		
9	0.277	0.572	0.863	1.156	1.448	1.755		
10	0.273	0.564	0.851	1.140	1.428	1.730		
11	0.276	0.569	0.858	1.149	1.440	1.744		
12	0.276	0.570	0.860	1.151	1.443	1.748		
13	0.366	0.755	1.139	1.525	1.912			
14	0.372	0.768	1.159	1.552	1.945			
15	0.363	0.749	1.129	1.512	1.895			
16	0.365	0.752	1.135	1.520	1.905			
17	0.361	0.745	1.124	1.505	1.886			
18	0.367	0.756	1.141	1.528	1.914			
19	1.333	2.751	4.150					
20	1.332	2.748	4.145					
21	1.336	2.756	4.157					
22	1.333	2.749	4.147					
23	1.336	2.756	4.157					
24	1.332	2.748	4.145					

LOW GAIN DECOMPRESSED

Sensor	D_1	C_1	D_2	C_2	D_3	C_3	D_4	C_4	D_5	C_5	D_6	C_6
Band 4												
1	1.036133	- .108398	.854736	- .065918	- .247559	.191650	- .352783	.216309	- .601807	.274658	- .688477	.294922
2	1.047363	- .188477	.862793	- .114258	- .251709	.332764	- .357422	.375244	- .606934	.475342	- .694092	.510254
3	1.116943	- .140137	.913574	- .084961	- .273926	.237061	- .383301	.266602	- .640869	.336426	- .732178	.361328
4	1.009521	- .131592	.826172	- .077393	- .250244	.240479	- .348877	.269775	- .578613	.337646	- .657471	.360840
5	1.096191	- .140869	.894043	- .083740	- .273193	.246582	- .378906	.276611	- .625732	.346436	- .712158	.370850
6	1.114258	- .171387	.914551	- .102539	- .272217	.305664	- .382568	.343750	- .641846	.433105	- .731934	.464111
Band 5												
7	1.062500	- .108154	.754639	- .044922	- .293701	.170654	- .366943	.185791	- .537109	.220703	- .619385	.237793
8	1.057373	.211914	.765137	.093750	- .283936	- .330322	- .361572	- .361572	- .543701	- .435303	- .633057	- .471436
9	1.049805	- .195068	.750488	- .082764	- .287354	.307129	- .361328	.334717	- .533691	.399658	- .617432	.431152
10	1.077393	- .163818	.777100	- .071533	- .291016	.255859	- .369141	.279297	- .552246	.335937	- .641846	.363525
11	1.041992	- .125000	.744873	- .053711	- .284668	.192383	- .358154	.209961	- .530029	.250977	- .613770	.271240
12	1.092285	- .212646	.784180	- .093506	- .296143	.324219	- .374268	.354492	- .557861	.425293	- .647705	.460205
Band 6												
13	1.118652	.629883	.769043	.247070	.240479	- .331787	- .647949	-1.305176	- .703125	-1.365723	- .777100	-1.446777
14	1.104980	- .008057	.773437	- .003174	.259521	.003906	- .647705	.017090	- .706055	.018066	- .784424	.019043
15	1.146484	- .170654	.805664	- .070313	.273926	.085938	- .673828	.364746	- .735107	.382812	- .817383	.406982
16	1.285645	.382812	.902100	.153320	.30443	- .204590	- .755615	- .839355	- .823242	- .879883	- .913574	- .934082
17	1.256104	- .166016	.873535	- .064697	.284668	.091064	- .733643	.360840	- .797607	.377930	- .882812	.400391
18	1.157227	- .175049	.808594	- .070068	.270752	.092529	- .677490	.379639	- .737793	.397949	- .818848	.422607
Band 7												
19	1.533203	- .180664	1.105713	- .083984	.583496	.034180	- .984863	.389893	-1.079834	.411377	-1.157471	.428955
20	1.715088	- .184326	1.236816	- .086426	.652832	.032959	-1.101562	.392090	-1.207764	.413818	-1.294922	.431641
21	1.628174	- .181885	1.169189	- .083496	.610840	.035645	-1.043701	.389893	-1.142090	.411133	-1.222656	.428223
22	1.874512	- .177490	1.369141	- .084717	.743652	.030029	-1.212646	.389160	-1.336426	.411865	-1.438477	.430664
23	1.934570	- .171631	1.399902	- .078125	.744385	.036377	-1.245605	.384521	-1.366943	.405518	-1.466309	.423096
24	1.704102	- .170898	1.218018	- .074707	.629395	.041748	-1.090088	.382568	-1.189941	.402344	-1.271484	.418701

APPENDIX L

LANDSAT-1 Ci's AND Di's - 9/5/75

HIGH GAIN DECOMPRESSED

Sensor	D_1	C_1	D_2	C_2	D_3	C_3	D_4	C_4	D_5	C_5	D_6	C_6
Band 4												
1	.000000	.000000	.000000	.000000	1.712646	- .410889	.911133	- .086914	- .981689	.678467	-1.642578	.945557
2	.000000	.000000	.000000	.000000	1.689697	- .525391	.898193	- .113037	- .967773	.859131	-1.620117	1.198730
3	.000000	.000000	.000000	.000000	1.855469	- .408936	.987061	- .103027	-1.058350	.617187	-1.783936	.872803
4	.000000	.000000	.000000	.000000	1.625488	- .282715	.855957	- .058350	- .932861	.462891	-1.548584	.642578
5	.000000	.000000	.000000	.000000	1.839844	- .386963	.972656	- .092529	-1.052002	.594971	-1.760498	.835693
6	.000000	.000000	.000000	.000000	1.757324	- .354492	.930664	- .076660	-1.007080	.574707	-1.681152	.801270
Band 5												
7	.000000	.000000	.000000	.000000	1.911377	- .573730	1.039062	- .200195	- .985352	.666504	-1.965088	1.085937
8	.000000	.000000	.000000	.000000	1.863281	-1.101318	1.022461	- .377441	- .958008	1.327637	-1.927490	2.162354
9	.000000	.000000	.000000	.000000	1.852783	- .517578	1.010742	- .179443	- .954102	.610352	-1.908936	.993652
10	.000000	.000000	.000000	.000000	1.929688	- .952881	1.057129	- .328125	- .992432	1.139893	-1.994385	1.857178
11	.000000	.000000	.000000	.000000	1.883301	- .509277	1.029297	- .180420	- .968506	.588379	-1.944092	.964111
12	.000000	.000000	.000000	.000000	1.875244	- .440918	1.027832	- .156982	- .963135	.510010	-1.940186	.837646

LANDSAT-1 Ci's AND Di's - 9/5/75 (Cont'd)

HIGH GAIN DECOMPRESSED

Sensor	D_1	C_1	D_2	C_2	D_3	C_3	D_4	C_4	D_5	C_5	D_6	C_6
Band 4												
1	.930420	- .229248	.518555	- .053955	.272461	.050781	- .231934	.265625	- .612793	.427734	- .875732	.539795
2	1.061279	- .229248	.585205	- .051514	.311523	.050537	- .260254	.263916	- .697998	.427246	- .999023	.539795
3	.822266	- .225586	.496826	- .070313	.246094	.049072	- .200928	.262695	- .566406	.437256	- .797119	.547363
4	.867920	- .220459	.528320	- .069092	.264404	.048584	- .212402	.261475	- .600098	.434814	- .847412	.545166
5	.919189	- .222900	.526611	- .056396	.286133	.045410	- .225586	.262451	- .630859	.434326	- .874756	.537598
6	.892334	- .225098	.511475	- .057861	.268799	.048584	- .218262	.262695	- .609619	.434570	- .843994	.537598
Band 5												
7	1.280273	- .454102	.762451	- .202881	.225342	.057373	- .295654	.310059	- .728271	.520020	-1.243408	.769775
8	1.460693	- .449219	.905518	- .215088	.304443	.038330	- .424805	.345947	- .824707	.514648	-1.420410	.765869
9	1.158203	- .482422	.685303	- .217285	.218750	.043945	- .297363	.333496	- .633301	.521729	-1.130859	.800781
10	1.156738	- .444824	.703857	- .205322	.216553	.052246	- .303467	.327148	- .638184	.504395	-1.134521	.766846
11	1.137939	- .450195	.690918	- .207764	.208252	.053711	- .286865	.322266	- .634521	.510742	-1.114990	.771484
12	1.321289	- .502197	.709527	- .233398	.200439	.065186	- .447266	.393311	- .651855	.496826	-1.212402	.780762

APPENDIX M

LANDSAT-2 Ci's AND Di's - 9/5/75

LOW GAIN DECOMPRESSED

Sensor	D_1	C_1	D_2	C_2	D_3	C_3	D_4	C_4	D_5	C_5	D_6	C_6
Band 4												
1	1.124023	- .120850	.710205	- .046143	.031738	.076416	- .238770	.125244	- .658203	.201172	- .968018	.257324
2	1.268066	- .158691	.786377	- .057861	.040283	.098145	- .269287	.163086	- .734131	.260498	-1.090332	.334961
3	1.088379	- .174561	.720459	- .077148	.045166	.101562	- .212646	.169922	- .654053	.266865	- .986572	.375000
4	1.113770	- .168213	.760010	- .078613	.050537	.100342	- .211426	.166992	- .684082	.286621	-1.027832	.373779
5	1.145996	- .194092	.736572	- .078369	.051025	.114990	- .224121	.192871	- .680176	.322021	-1.028076	.420410
6	1.114502	- .151123	.723877	- .062256	.039307	.093018	- .229248	.154053	- .661865	.252441	- .985596	.326172
Band 5												
7	1.049561	- .053711	.735107	- .025635	.073975	.032715	- .256592	.062256	- .656494	.097656	- .944824	.123291
8	1.221924	- .089600	.872559	- .045898	.036621	.058594	- .276367	.098145	- .761963	.158936	-1.090820	.200195
9	.979004	- .088379	.697754	- .045898	.080566	.047119	- .230713	.094482	- .615479	.152832	- .910400	.197266
10	.978027	- .083740	.706299	- .042480	.074219	.052002	- .237305	.077881	- .614502	.155273	- .832520	.198730
11	.938721	- .094727	.672607	- .048828	.065918	.055176	- .231689	.106445	- .586914	.167725	- .858643	.214600
12	.975586	- .149902	.689941	- .074707	.058105	.090332	- .238037	.168213	- .604980	.264648	- .879883	.336670
Band 6												
13	1.194580	- .176758	.831787	- .090332	.018555	.103027	- .278809	.174316	- .753662	.287354	-1.011475	.348877
14	1.132324	- .106934	.766602	- .051758	.022949	.060059	- .251953	.101807	- .713379	.171387	- .955811	.207764
15	1.133545	- .135010	.787598	- .069824	.025146	.072998	- .240723	.123047	- .728271	.214844	- .976807	.261719
16	1.043213	- .103027	.740967	- .055176	.020752	.058594	- .219727	.096680	- .675293	.168701	- .908936	.205811
17	1.046875	- .120605	.750244	- .065430	.011230	.072021	- .224609	.115967	- .673340	.199463	- .909180	.243652
18	1.156250	- .064941	.782959	- .031006	.014160	.038574	- .255127	.062988	- .724854	.105713	- .973145	.128418
Band 7												
19	1.763672	- .473877	1.112793	- .219971	.352539	.075928	- .383057	.363281	-1.077881	.634277	-1.767334	.903320
20	1.740234	- .709473	1.126709	- .353760	.383301	.076416	- .348389	.500244	-1.077148	.922363	-1.823730	1.354980
21	1.468262	- .490479	.944336	- .245361	.330078	.041504	- .266113	.321045	- .898926	.616943	-1.576660	.934570
22	1.533936	- .644775	1.005615	- .333008	.340576	.059570	- .281494	.427490	- .953857	.824463	-1.644287	1.232422
23	1.455811	- .363525	.942383	- .180176	.322998	.039795	- .280762	.256104	- .9[illegible]0635	.477295	-1.539063	.704834
24	1.612305	- .535400	1.044922	- .263916	.352539	.066895	- .296143	.377686	-1.002197	.713867	-1.714844	1.056885

LANDSAT-2 Ci's AND Di's - 9/5/75 (Cont'd)

LOW GAIN DECOMPRESSED

Sensor	C_1	D_1	C_2	D_2	C_3	D_3	C_4	D_4	C_5	D_5	C_6	D_6
Band 4												
1	-.0767775	.4723176	-.0297305	.3810391	.0098215	.3043025	.0426518	.2406069	.5257815	-.6967356	.5282528	-.7015303
2	-.0688948	.5421933	-.0289396	.4502282	.006029	.3697398	.0432885	.2839802	.5232090	-.8206558	.5253074	-.8254856
3	-.0680994	.5391159	-.0283859	.4479179	.0056697	.3697128	.0433705	.2831367	.5220696	-.8161466	.5253748	-.8237367
4	-.0694699	.5232948	-.0276320	.4305792	.0056610	.3567997	.0428468	.2743931	.5232083	-.7901211	.5253854	-.7949454
5	-.0730701	.5379394	-.0257085	.4316658	.0056528	.3612949	.0401899	.2837979	.5251247	-.8043351	.5278108	-.8103626
6	-.0701149	.5332242	-.0313050	.4458256	.0034703	.3675127	.0441144	.2759836	.5255005	-.8080823	.5283341	-.8144636
Band 5												
7	-.0664185	.4239522	-.0319113	.3611877	.0000549	.3030453	.0357996	.2380303	.5301728	-.6611714	.5323017	-.6650435
8	-.0653869	.4469336	-.0308140	.3803463	.0030491	.3151260	.0374251	.2489183	.5265592	-.6931506	.5291672	-.6981735
9	-.0667386	.4494866	-.0305869	.3798666	.0024194	.3163037	.0361514	.2513433	.5280644	-.6959720	.5306900	-.7010281
10	-.0666878	.4740652	-.0299929	.3995185	.0037218	.3310263	.0359411	.2655722	.5270723	-.7321719	.5299460	-.7380098
11	-.0673617	.4348123	-.0305733	.3664612	.0028745	.3043171	.0377464	.2395270	.5271589	-.6697750	.5301554	-.6753424
12	-.0699236	.4842626	-.0318142	.4062586	.0031512	.3346899	.0348883	.2697292	.5304310	-.7445675	.5332669	-.7503722
Band 6												
13	-.0616200	.4306502	-.0262348	.3638981	.0107761	.2940791	.0417079	.2357278	.5164130	-.6597773	.5189577	-.6645777
14	-.0638097	.4412859	-.0292337	.3750842	.0075691	.3046191	.0382028	.2459655	.5223855	-.6810840	.5248854	-.6858705
15	-.0616950	.4869490	-.0258545	.4105244	.0114960	.3308796	.0367988	.2769251	.5182062	-.7496077	.5210494	-.7556702
16	-.0647359	.4808173	-.0261992	.4007441	.0105595	.3243656	.0378577	.2676444	.5198331	-.7338221	.5226855	-.7397490
17	-.0626419	.4440771	-.0262266	.3735555	.0093932	.3045745	.0406043	.2441314	.5181369	-.6806540	.5207343	-.6856842
18	-.0630136	.4686363	-.0264008	.3939321	.0114837	.3166329	.0359997	.2666110	.5196000	-.7201201	.5223307	-.7256918
Band 7												
19	-.1806238	1.0235090	-.0610395	.6710796	.0326245	.3950394	.1039723	.1847678	.5494111	-1.1279964	.5556555	-1.1463995
20	-.1754252	.9497854	-.0541723	.6131391	.0360079	.3627625	.1018317	.1800079	.5435621	-1.0464153	.5481956	-1.0592794
21	-.1793272	.8628369	-.0612958	.5684921	.0338047	.3313305	.1013777	.1628175	.5491753	-.9538993	.5562648	-.9715794
22	-.1753371	.9447533	-.0535507	.6083295	.0330526	.3690969	.0984407	.1884683	.5455005	-1.0464935	.5518939	-1.0641546
23	-.1771896	.9123761	-.0574325	.5946172	.0349436	.3495100	.1015812	.1724302	.5458690	-1.0061617	.5521286	-1.0227709
24	-.1685808	.9417751	-.0552244	.6233358	.0370401	.3641466	.0980132	.1928612	.5406870	-1.0506973	.5480649	-1.0714226

APPENDIX N

LANDSAT-3 Ci's AND Di's

LOW GAIN DECOMPRESSED (REDUNDANT)

Sensor	C_1	D_1	C_2	D_2	C_3	D_3	C_4	D_4	C_5	D_5	C_6	D_6
Band 4												
1	-.0653040	.5299023	-.0303710	.4501010	.0080946	.3622324	.0410394	.2869754	.5228905	-.8137369	.5236509	-.8154740
2	-.0696180	.6419095	-.0265303	.5248527	.0157743	.4099249	.0470070	.3250757	.5153868	-.9473580	.5179805	-.9544045
3	-.0693147	.6248142	-.0266218	.5117750	.0153450	.4006587	.0473021	.3160448	.5163795	-.9259433	.5169105	-.9273491
4	-.0680177	.5861695	-.0273127	.4845008	.0141871	.3808470	.0483096	.2956194	.5153330	-.8708618	.5175001	-.8762743
5	-.0624810	.5686969	-.0304062	.4890941	.0100128	.3887823	.0440330	.3043512	.5177952	-.8714289	.5210456	-.8794958
6	-.0718671	.5994462	-.0296285	.4932985	.0134995	.3849160	.0477877	.2987484	.5183212	-.8837227	.5218878	-.8926857
Band 5												
7	-.0643714	.4723024	-.0308923	.4038624	.0016121	.3374150	.0319987	.2752966	.5290603	-.7408277	.5325925	-.7480484
8	-.0649660	.4885893	-.0297243	.4142529	-.0001997	.3519760	.0328531	.2822567	.5294791	-.7652905	.5325578	-.7717845
9	-.0616248	.4748171	-.0284130	.4057406	-.0002100	.3470820	.0334639	.2770444	.5266215	-.7486603	.5301619	-.7560238
10	-.0625337	.5010741	-.0269510	.4232839	.0005158	.3632363	.0341775	.2896457	.5258210	-.7851779	.5289699	-.7920620
11	-.0630814	.4529950	-.0302777	.3883157	.0017994	.3250692	.0353298	.2589571	.5262250	-.7089429	.5300041	-.7163941
12	-.0648832	.5167198	-.0308791	.4408373	-.0014489	.3751617	.0326984	.2989594	.5309092	-.8128330	.5336032	0.8188450
Band 6												
13	-.0690129	.4695074	-.0225671	.3769806	.0101778	.3117482	.0380133	.2562960	.5203142	-.7045167	.5230744	-.7100152
14	-.0731553	.4828908	-.0264157	.3887787	.0053608	.3247954	.0389436	.2571751	.5263024	-.7241404	.5289637	-.7294991
15	-.0684409	.5256839	-.0194130	.4160612	.0070146	.3569709	.0324482	.3001031	.5228025	-.7962947	.5255883	-.8025234
16	-.0686144	.5125976	-.0224700	.4120644	.0081211	.3454168	.0307514	.2961132	.5247762	-.7801998	.5274347	-.7859916
17	-.0700477	.4805364	-.0225494	.3841134	.0092982	.3194620	.0373304	.2625557	.5216049	-.7205338	.5243634	-.7261335
18	-.0681912	.5133887	-.0176684	.4029480	.0043852	.3547397	.0332994	.2915347	.5227301	-.7783396	.5254439	-.7842718
Band 7												
19	-.1878476	1.0406342	-.0635388	.6757420	.0323838	.3941724	.1009163	.1930022	.5555465	-1.1415100	.5625404	-1.1620398
20	-.1840709	1.0456924	-.0606173	.6776266	.0329570	.3986439	.1032429	.1890918	.5503362	-1.1438761	.5581520	-1.1671782
21	-.1844870	.9315912	-.0618314	.6061936	.0331551	.3541990	.1004704	.1756154	.5523141	-1.0231009	.5603791	-1.0444975
22	-.1769628	1.0484238	-.0566286	.6812810	.0317375	.4116743	.0980960	.2092108	.5463923	-1.1585560	.5573654	-1.1920347
23	-.1816075	1.0537081	-.0597251	.6849521	.0325594	.4057435	.1000325	.2016020	.5497301	-1.1589622	.5590112	-1.1870432
24	-.1771373	1.1781120	-.0531871	.7533719	.0300429	.4681709	.0955325	.2437551	.5497310	-1.3127165	.5549976	-1.3306923

APPENDIX N

LANDSAT-3 Ci's AND Di's (Cont'd)

HIGH GAIN DECOMPRESSED

Sensor	C_1	D_1	C_2	D_2	C_3	D_3	C_4	D_4	C_5	D_5	C_6	D_6
Band 4												
1	-.1390668	.5247137	-.0915327	.4431337	-.0417495	.3576929	.0075287	.2731203	.6269886	-.7900258	.6378295	-.8086318
2	-.1385278	.6272712	-.0835882	.5143536	-.0434456	.4318466	-.0006716	.3439335	.6284384	-.9490855	.6377941	-.9683148
3	-.1389027	.6284514	-.0810795	.5095294	-.0447175	.4347455	-.0001633	.3431122	.6282305	-.9492778	.6366310	-.9665548
4	-.1364253	.5970588	-.0799507	.4858097	-.0421927	.4114310	-.0015217	.3313130	.6251735	-.9032097	.6349147	-.9223989
5	-.1444781	.6181401	-.0938253	.5175102	-.0431162	.4167681	.0022107	.3267191	.6329890	-.9264259	.6462187	-.9527088
6	-.1395825	.6087410	-.0846178	.4994858	-.0479243	.4265492	-.0002923	.3318703	.6316776	-.9243167	.6407375	-.9423251
Band 5												
7	-.1560426	.5518665	-.0992072	.4546716	-.0453791	.3626205	.0067823	.2734180	.6431835	-.8148912	.6506611	-.8276793
8	-.1613963	.5910916	-.1034963	.4867696	-.0455884	.3824342	.0065343	.2885204	.6481347	-.8674901	.6558121	-.8813231
9	-.1629270	.5953695	-.1018216	.4849899	-.0455539	.3833493	.0036108	.2945392	.6469432	-.8675578	.6597456	-.8906841
10	-.1576287	.6206412	-.1000667	.5104772	-.0430135	.4012881	.0077498	.3041369	.6414458	-.9086376	.6515092	-.9278972
11	-.1550148	.5584256	-.1017851	.4660206	-.0433260	.3645390	.0105744	.2709705	.6399757	-.8216435	.6495750	-.8383080
12	-.1636969	.6360582	-.1031114	.5194108	-.0441277	.4058478	.0069403	.3075250	.6479717	-.9266692	.6560216	-.9421678

APPENDIX N
LANDSAT-3 Ci's AND Di's (Cont'd)

APPENDIX O
Fiber Matrix Pattern (Landsat 1)

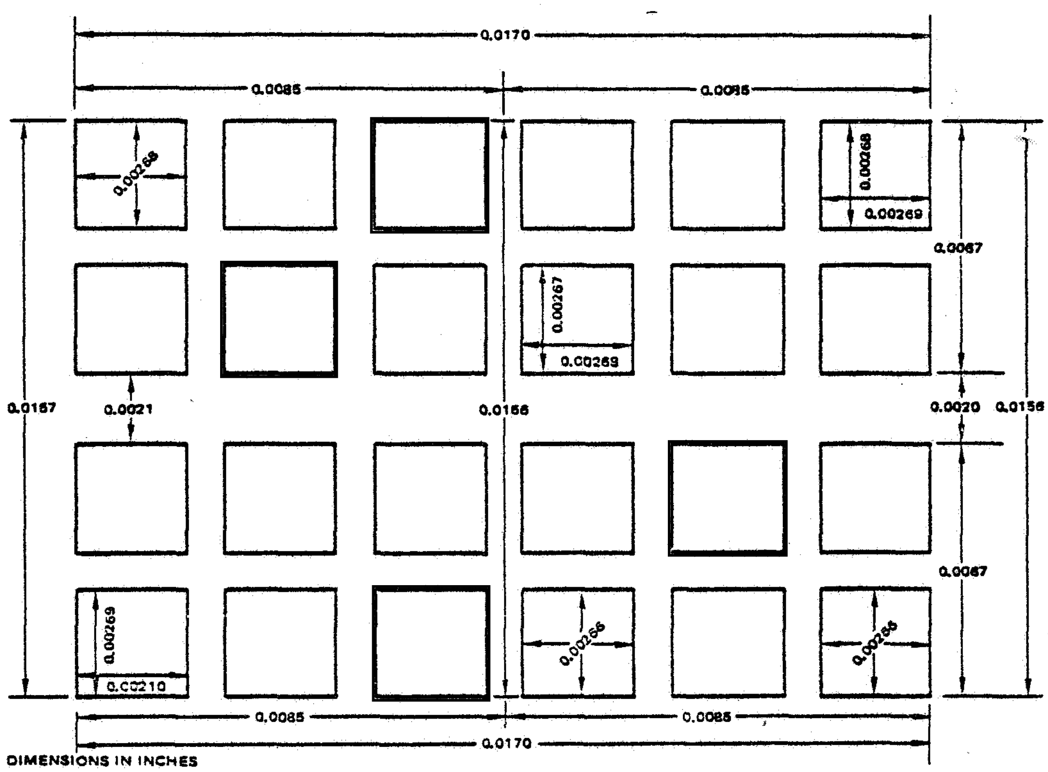

APPENDIX P
Fiber Matrix Pattern (Landsat 2)

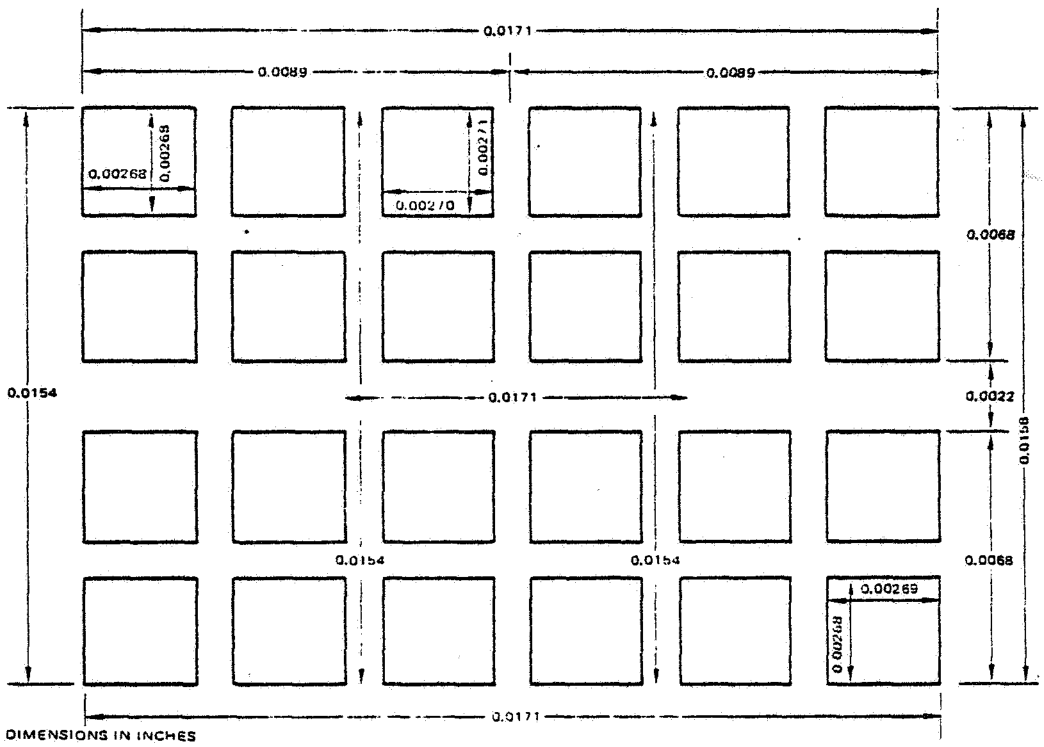

APPENDIX Q
Fiber Matrix Pattern (Landsat 3)

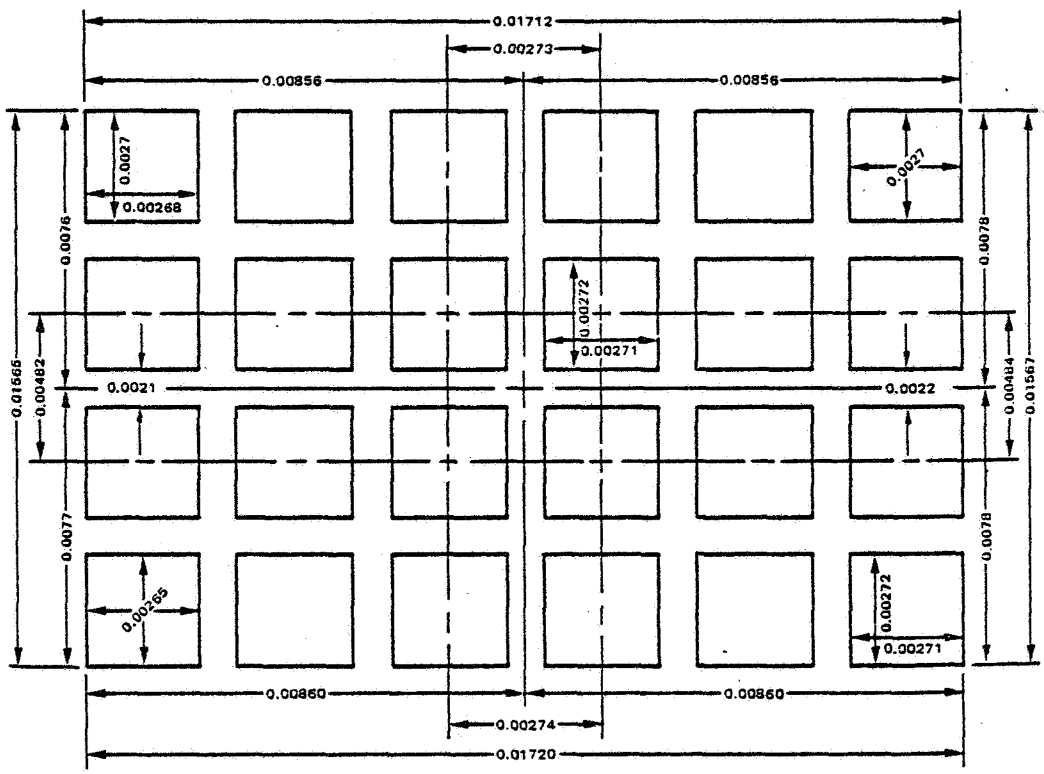

DIMENSIONS IN INCHES

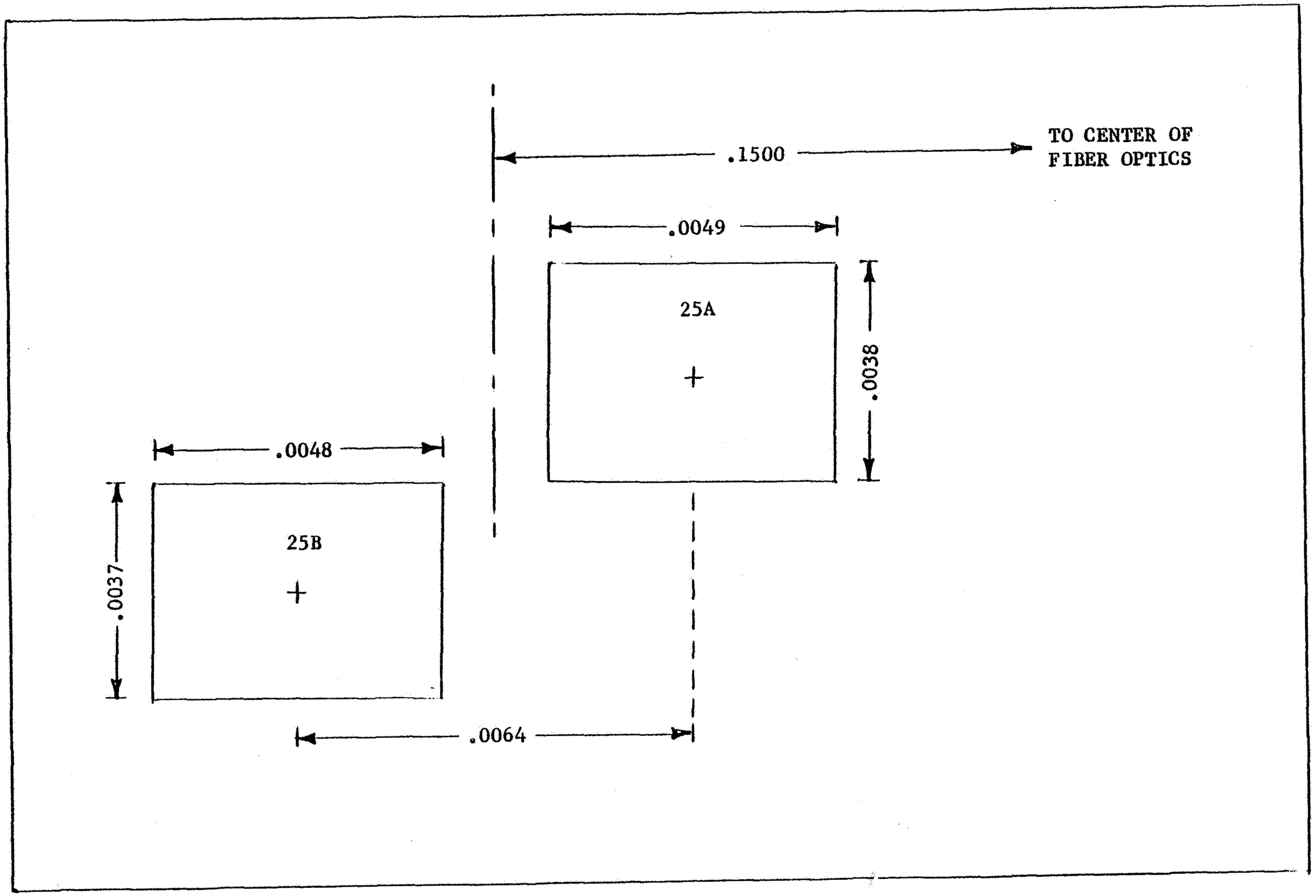

APPENDIX R
Band 8 Detector Dimensions